University of Southampton

Faculty of Engineering and Physical Sciences
School of Physics and Astronomy

Holographic Descriptions of Multi-Scale, Strongly Coupled Gauge Dynamics

by

Anja Alfano

MSc (Hons)

ORCiD: 0000-0003-0413-5917

A thesis for the degree of
Doctor of Philosophy

February 2026

University of Southampton

Abstract

Faculty of Engineering and Physical Sciences
School of Physics and Astronomy

Doctor of Philosophy

Holographic Descriptions of Multi-Scale, Strongly Coupled Gauge Dynamics

by Anja Alfano

This thesis employs the dynamic AdS/QCD framework to investigate non-perturbative dynamics in strongly coupled gauge theories. We first study the approach to the conformal window, demonstrating that walking theories can exhibit low-energy properties which mimic those of infrared-conformal theories over a wide range of scales, posing a significant challenge for their unambiguous identification in lattice simulations. We then explore mass generation hierarchies in theories with matter in multiple representations. We begin with a theory with fundamental and two-index symmetric representation fermions, for which we predict a significant hierarchy in the meson spectra, with the higher-representation states becoming up to an order of magnitude more massive than their fundamental counterparts. We continue our exploration of mass hierarchies by analysing the separation between confinement and chiral symmetry breaking in a theory with adjoint fermions. We show that while a pure adjoint theory tightly couples these phenomena, the introduction of fundamental flavours can catalyse chiral symmetry breaking at a scale much lower than confinement, dramatically amplifying the hierarchy. Finally, we apply our model to survey the landscape of strongly-coupled dark sectors, systematically mapping the light mesonic spectrum across the N_c-N_f plane to identify distinct phenomenological regions and their implications for dark matter relic density generation. Collectively, these studies provide a set of holographic predictions for lattice gauge theory and demonstrate the framework's utility for model-building in areas such as dark matter phenomenology and the generation of fermion mass hierarchies.

Contents

List of Figures **ix**

List of Tables **xiii**

Declaration of Authorship **xv**

Acknowledgements **xvii**

I Foundations **1**

1 Introduction **3**

2 Non-Abelian Gauge Theories **7**
2.1 QCD Lagrangian 8
2.2 Renormalization, Divergence and Scale Evolution 11
2.3 Beta Function and the Running of the Coupling 12
2.3.1 Walking Behaviour and the Conformal Window 14
2.4 The Anomalous Mass Dimension 17
2.5 Chiral Symmetry Breaking 18
2.5.1 Spontaneous Symmetry Breaking 18
2.5.2 Goldstone's Theorem 20
2.6 Confinement 21
2.7 Confinement as Motivation for String Theory 22

3 Strings **25**
3.1 Classical String Dynamics in String Theory 25
3.1.1 Mode Expansions 28
3.2 Quantization of the Bosonic String 30
3.2.1 Physical State Constraints and Emergent Spectra 31
3.3 Superstring Theory 34
3.4 The GSO Projection 38
3.5 D-Branes 40
3.5.1 The Dirac-Born-Infeld Action 42

4 Gauge/Gravity Duality **45**
4.1 The AdS/CFT Conjecture 45
4.1.1 Motivating the Conjecture 45
Open String Perspective (lambda « 1): 45

Closed String Perspective (lambda » 1): 46
4.1.2 Maldacena's Conjecture 47
4.1.3 Symmetry Matching 48
4.2 Formalizing the Correspondence 49
4.2.1 Parameter Matching and Correspondence Forms 49
4.2.2 Conformal Boundary and Holographic Principle 49
4.2.3 Field-Operator Dictionary 50
4.2.4 Bulk Dynamics and Stability 50
4.3 D3/D7 Probe Brane Setup 51
4.3.1 Fundamental Matter via Probe Branes 51
4.3.2 Embedding Geometry and Chiral Symmetry 52
4.3.3 Meson Spectroscopy From Brane Fluctuations 52

5 Holographic QCD **55**
5.1 Top-Down Approaches 56
5.1.1 D3/D7 System: Fundamental Matter From Strings 56
5.1.2 Embedding Dynamics and Chiral Symmetry 56
5.1.3 Holographic Renormalization and Condensate 58
5.1.4 Constable-Myers and Dilaton Flow 58
5.2 Bottom-Up Approaches 60
5.2.1 Confinement Mechanisms 60
5.3 Dynamic AdS/QCD Model 61
5.3.1 The Running Mass and the Anomalous Dimension 62
5.3.2 Vacuum Structure and Chiral Symmetry Breaking 63
5.3.3 Meson Spectroscopy and Decay Constants 64
Scaling of Physical Observables 66

II Research **69**

6 Scale Separation, Strong Coupling UV Phases, and the Identification of the Edge of the Conformal Window **71**
6.1 The Holographic Model 73
6.2 Approaching the edge of the Conformal Window from above 75
6.3 Approaching the edge of the Conformal Window from below 76
6.4 Discussion 78

7 Mass Hierarchies in Gauge Theory With Two Index Symmetric Representation Matter **81**
7.1 The Holographic Model 83
7.2 Nc and NfF Dependence In the Massless Theory 84
7.2.1 Nc=5 Theory 84
7.2.2 Other Nc 88
7.3 A Massive Theory 92
7.4 Conclusions 92

8 Holography for QCD(Adj) and QCD(Adj)+F **95**
8.1 Holography for QCD(Adj) 95

8.1.1 The Gauge Theories . . . 97
8.1.2 Confinement in Compact SU(2)(Adj) Gauge Theory . . . 98
8.1.2.1 Summary of the SU(2)(Adj) theory on R3 x S1 . . . 98
8.1.2.2 From Weak to Strong Coupling with Holography . . . 100
8.1.2.3 The SU(Nc) Theory . . . 105
8.1.3 Comparison of Instabilities . . . 105
8.2 Holography of QCD(Adj) + Fundamentals . . . 107
8.2.1 The Holographic Model . . . 108
8.2.2 Nc and NfF Dependence In The Massless Theory . . . 108
8.2.2.1 Nc=5 Theory . . . 108
8.2.2.2 Other Nc . . . 111
8.2.3 Conclusions . . . 112

9 Surveying the Theory Space of Pion Dark Matter 115
9.1 Introduction . . . 115
9.2 The Holographic Model . . . 118
9.3 Mass spectrum . . . 119
9.3.1 Nc=3 results . . . 119
9.3.2 Nc Dependence . . . 124
9.4 Comparison to Lattice Data . . . 124
9.5 Phenomenology . . . 127
9.5.1 Region 1: only light pi . . . 128
9.5.2 Region 2: light pi, sigma . . . 129
9.5.3 Region 3: walking dilaton sigma . . . 130
9.5.4 Region 4: light pi, rho . . . 130
9.5.5 Region 5: light rho, sigma . . . 131
9.5.6 Region 6: dilaton sigma, light rho . . . 131
9.5.7 Region 9: light glueballs . . . 131
9.6 Other Strongly Coupled Possibilities . . . 132
9.6.1 Glueball Dark Matter in Pure Yang-Mills or Heavy Quark Theories . . . 132
9.6.2 Unparticles . . . 132
9.6.3 sigma Dark Matter . . . 132
9.6.3.1 Nf=1 + NX Theories . . . 133
9.6.3.2 Chirally Gauged Nf=2 + NX Theories . . . 133
9.7 Conclusions . . . 134

10 Conclusion 137

References 141

List of Figures

2.1 Interaction vertices for three- and four-gluon interactions 9
2.2 The beta function $\beta(\alpha_s)$ and its corresponding running $\alpha_s(\mu)$ for 3 distinct cases. (a) has $\beta_0 > 0$ and $\beta_1 > 0$ (asymptotic freedom). (b) has $\beta_0 > 0$ and $\beta 1 < 0$ (walking theory with NTIR fixed point). (c) has $\beta_0 < 0$ and $\beta_1 < 0$ (IR freedom). Note that (b) shows the running of the coupling as a function of $\ln \mu$. 14
2.3 Plot of $\alpha_s(\mu)$ for the case $\alpha_s^* > \alpha_s^\chi$. The critical coupling is met at the scale, Λ_χ, triggering χSB and generating a dynamic mass for the quarks of order this scale. Below Λ_χ, the quarks decouple and the theory then runs into the IR as '$N_f = 0$'. The scale Λ_1 can be seen as the UV boundary of the walking regime and is dictated by the scale generated by the one-loop running. 15
2.4 Phase diagram for theories with fermions in the fundamental representation (grey), two-index antisymmetric (red), two-index symmetric (blue), and adjoint representation (green) as a function of the N_f and N_c. The shaded areas depict the corresponding conformal windows. For each colour, starting from the bottom, the dashed curve denotes the existence of a Banks-Zaks fixed point. Below this there is only a trivial UV fixed point, above it, there are walking regimes. Crossing the lower solid curve into the shaded region, χSB is lost. Crossing the upper solid curve, asymptotic freedom is lost. 16
2.5 (a) The potential with global minimum occurring at $|\phi| = 0$ exhibiting a global $U(1)$ symmetry. (b) The old minimum becomes an unstable extremum of the potential. The new global minimum is a set of solutions at fixed $|\phi| \neq 0$ – there is a non-zero vacuum expectation value of the field ϕ. 19

3.1 D-branes as hypersurfaces anchoring open strings: (A) stretched between distinct branes, (B) on a single brane, (C) with one Dirichlet endpoint. 41

5.1 String configurations in D3/D7 system: (a) 3-3 strings (adjoint gluons), (b) 3-7 strings (fundamental quarks), (c) 7-7 strings (mesonic operators) 56
5.2 10D spacetime diagram of the D3/D7 probe brane setup. As seen in the right hand diagram, The D7 brane may have either $L = const$ or $L = L(\rho)$. 57
5.3 Dynamic AdS/QCD embeddings: $L(\rho) \to 0$ in UV with IR mass generation . . 64

6.1 The beta function plot taken from Hasenfratz, 2023; our fit is overlaid in red. The resulting $\alpha(\mu)$, on integrating up the beta function, is plotted below, showing an IR fixed point at $\alpha = 15/4\pi$. We show UV boundary conditions that approach the fixed point from above and below. 72
6.2 The vacuum solutions ϕ for $k = 3, 1.8, 1.4$ with the scale of $r_{\min}$ scaled to one in each case. The red part of each solution shows the r range where the BF bound is broken at $\phi = 0$. 75

6.3 Mass ratio as a function of k for the four values of x along with a 10% area (blue box) under the minimum BF-bound violating value of $k = 0.84$. Curves pass through a mass ratio of 35 at: $k = 1.099$ for $x = 0.8$, $k = 1.088$ for $x = 0.85$, $k = 1.076$ for $x = 0.9$ and $k = 1.058$ for $x = 0.95$. The blue shaded region below the critical k value shows where the critical coupling lies within 10% above the fixed point value. 76

7.1 SU(5) gauge theory with $N_f^F = 15$: The running of Δm^2 for the two index symmeric 15 dimensional rep. (blue), fundamental (red) and for the fundamentals with the higher dim rep. decoupled below the scale where it is on mass shell (green). The energy scales are given in units of the ρ-meson mass in the 15 sector. BF bound violation occurs at 14.2 for the 15 and -2.3 for the fundamental with the 15 decoupled. 85

7.2 SU(5) gauge theory with $N_f^F = 15$: The $L_R(\rho)$ functions for the 15 (blue) and 5 (green) representations with $m_{IR,S} \approx 0.29$ and $m_{IR,F} \approx 0.027$ respectively in units of the ρ-meson mass in the 15 sector. 85

7.3 Mass spectra for the SU(5) theory, ρ-mesons in blue (symmetric) and dark yellow (fundamental), σ-mesons in green (symmetric) and orange (fundamental), axials in purple (symmetric) and brown (fundamental). The pions in both sectors are massless at zero fermion mass. 86

7.4 Decay constants for the SU(5) theory, ρ-mesons in blue (symmetric) and dark yellow (fundamental), σ-mesons in green (symmetric) and orange (fundamental), axials in purple (symmetric) and brown (fundamental) and pions in cyan (symmetric) and light yellow (fundamental). 87

7.5 The spectra and decay constants of the SU(N_c) gauge theory with one two index symmetric rep. matter field and N_f^F fundamentals for $N_c = 3, 4, 6, 7$. ρ-mesons in blue (symmetric) and dark yellow (fundamental), σ-mesons in green (symmetric) and orange (fundamental), axials in purple (symmetric) and brown (fundamental) and pions in cyan (symmetric) and light yellow (fundamental). . 89

7.6 Meson masses for the SU(3) theory with a factor of 2 removed in (7.1): ρ-mesons in blue (symmetric) and dark yellow (fundamental), σ-mesons in green (symmetric) and orange (fundamental), axials in purple (symmetric) and brown (fundamental) and pions in cyan (symmetric) and light yellow (fundamental). 90

7.7 The running of Δm^2 vs $\ln \mu$, for theories with N_f^F multiples of 4 that give the largest spectral gaps, for the two index symmetric rep. (blue), fundamental (red) and for the fundamentals with the higher dim. rep. decoupled below the scale where it is on mass shell (green). The energy scales are given in units of the ρ-meson mass in the 15 sector. 91

7.8 Mass spectra for the SU(3) theory with $N_f = 8$ and non-zero UV mass. ρ-mesons in blue (symmetric) and dark yellow (fundamental), σ-mesons in green (symmetric) and orange (fundamental), axials in purple (symmetric) and brown (fundamental) and pions in cyan (symmetric) and light yellow (fundamental). . 92

7.9 Decay constants for the SU(3) theory with $N_f = 8$ and non-zero UV mass. ρ-mesons in blue (symmetric) and dark yellow (fundamental), σ-mesons in green (symmetric) and orange (fundamental), axials in purple (symmetric) and brown (fundamental) and pions in cyan (symmetric) and light yellow (fundamental). . 92

8.1 Left: The blue line is the numerical result for the vacuum solution $I(\rho)$. The grey line represents the function $y = x^3$ which sets the IR boundary. Right: The blue line shows the plot $\frac{I(\rho)}{\rho^3}$ against ρ. (Set-up: $\mathscr{K} = 7.82498$, $\rho_{IR} = 0.223527$, $\rho_{UV} = 20$ such that $I(\rho_{UV}) = 1$ and $I'(\rho_{UV}) = 0$). 103
8.2 Left: The regular solutions for the fluctuation of the instanton density f_1 against ρ. Right: $\frac{f_1}{\rho^3}$ against ρ. 104
8.3 Left: $\mathscr{C}/L$ against g_4 in Eq. (8.20); There is a minimum $\mathscr{C}/L = 0.143$ at $g_4 = \frac{2\pi}{\sqrt{3}} = 3.7$. Right: M_σ against g_4. 104
8.4 The mass spectrum of dual photons σ_1 and σ_2 for SU(3). The darker colours represent σ_1; The lighter colours represent σ_2. 106
8.5 SU(5) gauge theory with one Weyl adjoint field and $N_f^F = 16.9$ (as an approximation to $N_f = 17$): The running of Δm^2 for the adjoint rep. (blue), fundamental (red), and for the fundamentals with the higher dim rep. decoupled below the scale where it is on mass-shell leaving the fundamental running (green). The energy scales are given in units of the ρ-meson mass in the adjoint sector. BF bound violation occurs at 13.9 for the adjoint and -2.2 for the fundamental with the adjoint decoupled. 109
8.6 SU(5) gauge theory with $N_f^F = 17$ (approximates by $N_f^F = 16.9$): The $L_R(\rho)$ functions for the adjoint (blue) and 5 (green) representations with $m_{IR,A} \approx 0.29$ and $m_{IR,F} \approx 0.025$ respectively in units of the ρ-meson mass in the adjoint sector. 109
8.7 Mass spectra for the SU(5) theory, ρ-mesons in blue (adjoint) and dark yellow (fundamental), σ-mesons in green (adjoint) and orange (fundamental), axials in purple (adjoint) and brown (fundamental). The pions in both sectors are massless at zero fermion mass. 110
8.8 Decay constants for the SU(5) theory, ρ-mesons in blue (adjoint) and dark yellow (fundamental), σ-mesons in green (adjoint) and orange (fundamental), axials in purple (adjoint) and brown (fundamental) and pions in cyan (adjoint) and light yellow (fundamental). 110
8.9 The spectra and decay constants of the SU(N_c) gauge theory with one adjoint representation matter field and N_f^F fundamentals for $N_c = 2, 3, 4$. ρ-mesons in blue (adjoint) and dark yellow (fundamental), σ-mesons in green and orange (fundamental), axials in purple (adjoint) and brown (fundamental) and pions in cyan (adjoint) and light yellow (fundamental). 112

9.1 Left panel: The regions of parameter space denoted by their low energy spectrum. Right panel: the classification of the $N_c = 3$ theory, using the colours from the left in the N_F/N_F^c versus m_Q plane. The horizontal lines are for integer N_F where we compute. Regions 1-5 are present at these M_π (in units of M_ρ^0). Regions 6 and 9 lie to the right of the right panel where the gauge theories are transiting to weak coupling and holography is less reliable. 117
9.2 Mass spectrum (left) and decay constants (right) in units of M_ρ^0 for $N_f = 2$. The gray shaded areas correspond to the different regions of parameter space presented in Figure 9.1. 119
9.3 Mass spectrum (left) and decay constants (right) in units of M_ρ^0 for $N_f = 3$. The gray shaded areas correspond to the different regions of parameter space presented in Figure 9.1. 120
9.4 Mass spectrum (left) and decay constants (right) in units of M_ρ^0 for $N_f = 5$. The gray shaded areas correspond to the different regions of parameter space presented in Figure 9.1. 120

9.5 Mass spectrum (left) and decay constants (right) in units of M_ρ^0 for $N_f = 6$. The gray shaded areas correspond to the different regions of parameter space presented in Figure 9.1. 121
9.6 Mass spectrum (left) and decay constants (right) in units of M_ρ^0 for $N_f = 7$. The gray shaded areas correspond to the different regions of parameter space presented in Figure 9.1. 121
9.7 Mass spectrum (left) and decay constants (right) in units of M_ρ^0 for $N_f = 9$. The gray shaded areas correspond to the different regions of parameter space presented in Figure 9.1. 122
9.8 Mass spectrum (left) and decay constants (right) in units of M_ρ^0 for $N_f = 11$. The gray shaded areas correspond to the different regions of parameter space presented in Figure 9.1. 122
9.9 N_f dependence of the ρ and σ masses using the fits presented in table 9.1. . . . 123
9.10 Comparison of the theories with $N_f = 3$ (green), SU(4) with $N_f = 4$ (Purple) and SU(5) with $N_f = 5$ (Red) Left: data for the σ and ρ meson masses Right: the decay constants f_π, F_ρ, F_σ corrected by the rude N_f, N_c scaling discussed in the text. 124
9.11 Left: Comparison of the holographic predictions (blue) for QCD compared to the lattice results in Albouy, 2022 (red) for M_π/M_ρ vs $M_\pi^2/M_\rho^{0\,2}$ in units of the ρ mass at $m_Q = 0$. Right: a comparison of the holographic results (blue) for F_ρ/M_ρ vs M_π^2 in units of the ρ mass (note not at $m_Q = 0$) and the lattice results from DeGrand, 2019 (red). 125
9.12 The ratio M_π/f_π in the holographic model as a function of M_π for $N_c = 3$, and various N_f together with the lattice data (black line) from DeGrand, 2019. . . . 126
9.13 Matter content of the $N_f = 2 + N_X$ model as a moose diagram. 134

List of Tables

3.1 Massless spectra of type II superstrings. 40
3.2 D-brane content of Type IIB string theory 42
3.3 D-brane content of Type IIA string theory 42

4.1 Forms of AdS/CFT correspondence in different parameter limits 49
4.2 D3/D7 brane intersection for fundamental matter 52

5.1 Dictionary between the bulk AdS fields and the boundary field theory operators in a simple AdS/QCD model. The bulk field masses are obtained via the relation $M^2 = (\Delta - p)(\Delta + p - 4)$. 60

9.1 Fits for M_ρ, M_σ in units of M_ρ^0 as a function of N_f for $N_c = 3$ derived within our holographic model. N.b. $m \equiv M_\pi$ for brevity. 120
9.2 Fits for decay constants f_π, F_ρ, F_σ in units of M_ρ^0 as a function of N_f for $N_c = 3$ obtained using our holographic model. N.b. $m \equiv M_\pi$ for brevity. 121
9.3 Matter representation for a possible σ dark matter model. 133

Declaration of Authorship

I declare that this thesis and the work presented in it is my own and has been generated by me as the result of my own original research.

I confirm that:

1. This work was done wholly or mainly while in candidature for a research degree at this University;
2. Where any part of this thesis has previously been submitted for a degree or any other qualification at this University or any other institution, this has been clearly stated;
3. Where I have consulted the published work of others, this is always clearly attributed;
4. Where I have quoted from the work of others, the source is always given. With the exception of such quotations, this thesis is entirely my own work;
5. I have acknowledged all main sources of help;
6. Where the thesis is based on work done by myself jointly with others, I have made clear exactly what was done by others and what I have contributed myself;
7. Parts of this work have been published as: [1, 2, 3, 4]

Signed:..... Date:.....

Acknowledgements

First of all, I would like to thank Nick Evans, who not only supervised the projects that comprise this thesis, but also was patient enough to answer any questions I had, no matter how basic, and to reassure me on the occassions when I expressed doubt in my abilities.

I would also like to thank Jack Mitchell, with whom I 'cut my teeth', in holography as well as Wanxiang Fan, Suchita Kulkarni and Werner Porod, with whom I had the opportunity to collaborate during the course of my studies.

On a more personal note, I wish to thank my aunt, Mary, for keeping me company via phone on my lengthy commutes home from the university - sorry about that.

I owe so much to my family - my father Calogero, my brother Lorenzo, and my late mother, Eleanor Ann, without whose support, both material and emotional, I would never have had even the opportunity to study physics at all. I love you all.

Finally, I am forever thankful to my partner, Allie. Your love and support have been instrumental, your belief in me was relentless, even at my lowest ebb, and you never once wavered in your encouragement, even when the physics was far outside your wheelhouse. Ti vogghiu beni assai, me jattareḍḍa.

Part I

Foundations

Chapter 1

Introduction

Quantum Chromodynamics (QCD), the non-Abelian gauge theory of the strong nuclear force, is defined by a Lagrangian of remarkable simplicity. Yet, its low-energy behaviour presents some of the most enduring problems in theoretical physics. The theory is asymptotically free [5, 6], meaning that at high energies, quarks and gluons behave as nearly free particles, a regime where perturbative calculations are highly successful. However, at low energies, the coupling becomes strong, and the theory instead exhibits non-perturbative phenomena: confinement, which prevents the observation of free coloured particles [7], and dynamical chiral symmetry breaking, which is responsible for generating the bulk of the visible mass in the universe and the emergence of pions as pseudo-Nambu-Goldstone bosons.

Outside of numerical lattice gauge theory [7], which provides a first-principles computational framework, we possess few analytical tools to reliably calculate in this strong coupling regime. This gap in our understanding motivates the search for novel frameworks that can provide complementary physical insight and analytical traction.

The search for a quantum theory of gravity led to string theory, which posits that the fundamental constituents of reality are not zero-dimensional point particles, but rather one-dimensional strings. A notable feature of its modern development is the host of dualities relating different string theories, suggesting they are all limits of a single underlying theory.

A pivotal breakthrough in this area was the discovery of D-branes [8]. These are extended, non-perturbative objects within string theory on which strings can end. Crucially, the low-energy dynamics of a stack of N coincident D-branes is described by a $U(N)$ gauge theory [9]. This connection between gravitational objects and gauge theories laid the groundwork for a profound duality.

In a 1997, Juan Maldacena conjectured that type IIB string theory on an $AdS_5 \times S^5$ background is dual to $\mathcal{N} = 4$ Super Yang-Mills theory in four dimensions, a conformal field theory with

gauge group $SU(N)$ [10]. This AdS/CFT correspondence is a concrete realization of the holographic principle elaborated in [11, 12]. It establishes a complete equivalence where the non-gravitational, strongly coupled gauge theory is encoded in the geometry of the higher-dimensional gravitational theory.

The dictionary of this duality was swiftly elaborated upon by Witten and others [13, 14]. They established that the generating functional of the CFT is mapped to the partition function of the string theory in AdS, with the boundary conditions for bulk fields acting as sources for corresponding CFT operators. The radius of the AdS space is large when the 't Hooft coupling $\lambda = g^2_{\mathrm{YM}}N$ in the gauge theory is large, meaning the gravitational description simplifies to classical supergravity. This strong/weak coupling duality is the feature that makes AdS/CFT so powerful: it trades the intractable problem of strong coupling in a gauge theory for the computationally tractable problem of classical gravity in a curved background.

One limitation of the original AdS/CFT correspondence, is that it involves a highly symmetric, conformal gauge theory, which is far removed from the real-world dynamics of QCD. AdS/QCD (also known as holographic QCD) seeks to break these symmetries and engineer gravitational duals that capture the essential infrared physics of confinement and chiral symmetry breaking.

This programme proceeds along two complementary lines. Top-down approaches start from consistent string theory constructions (e.g. the Sakai-Sugimoto model [15]) and deform them to introduce features like mass scales and reduced supersymmetry. These models are theoretically rigorous but often phenomenologically restrictive.

Bottom-up approaches meanwhile, take a more pragmatic view. They construct effective $5D$ gravitational actions with fields chosen to match the symmetries of QCD, and then introduce an artificial "hard wall" [16] or a dilaton-driven "soft wall" [17] to generate a mass gap and discrete spectrum. These models sacrifice top-down derivability for flexibility and better phenomenological control.

We will employ bottom-up models, specifically dynamic AdS/QCD, whose key feature is that the gravitational background itself is solved for dynamically from the equations of motion, leading to a smoother, more physical infrared geometry than hard-wall cutoffs. This approach allows us to build versatile holographic tools to probe a wide array of strongly coupled gauge theories beyond just QCD itself.

This thesis is structured in two parts. In Part I, (Chapters 2-5) we cover essential pedagogical background on non-Abelian gauge theories, string theory, the AdS/CFT correspondence, and the development of holographic QCD models, culminating in the dynamic AdS/QCD framework that underpins the research work.

In Part II (chapters 6-9) we present novel research in the form of adapted versions of published work. In chapter 6 (based on [2]), we employ the holographic framework to study the approach to

the conformal window, identifying potential challenges for its identification using lattice methods; in particular, the possibility of a misidentification of a chiral symmetry breaking theory as being IR conformal.

We next consider mass generation in theories with multiple matter representations: in Chapter 7 (based on [1]) we investigate theories with matter in both the fundamental and two-index symmetric representations, predicting significant hierarchies in the meson spectra, while in Chapter 8 (based on [3]) we first develop a holographic description of confinement and chiral symmetry breaking for a theory with only adjoint fermions, examining whether these phenomena are joined or distinct. We then extend this analysis by adding fundamental flavours, showing how this can amplify the separation between symmetry breaking scales.

Finally, in Chapter 9 (based on [4]), we apply the AdS/QCD model to survey the space of strongly-coupled dark matter, systematically mapping the light mesonic spectrum of dark sectors to identify distinct phenomenological regions and their implications for relic density generation mechanisms.

Chapter 2

Non-Abelian Gauge Theories

This chapter will introduce the fundamental concepts of non-Abelian gauge theories (NAGTs), with quantum chromodynamics (QCD) as the primary example. Parts of this analysis will rely on [18]. We begin by establishing the mathematical framework of gauge theories based on non-commutative symmetry groups, contrasting their structure and consequences with Abelian counterparts like quantum electrodynamics (QED). The $\mathrm{SU}(3)$ gauge symmetry of QCD is discussed in detail, including its implications for quark and gluon dynamics.

The QCD Lagrangian is analysed to highlight its constituent terms: the gluon field strength tensor encoding self-interactions, and the quark sector governed by a gauge-covariant derivative. Key features such as colour charge, the role of Gell-Mann matrices in mediating interactions, and the non-linearities arising from the $\mathrm{SU}(3)$ group structure are systematically unpacked.

We then address renormalization procedures specific to non-Abelian theories, including the treatment of ultraviolet (UV) divergences through counterterms, the introduction of renormalization scales, and the derivation of renormalization group equations. Particular attention is given to the beta function governing the running of the strong coupling constant and the anomalous mass dimension encoded in the gamma function. The interplay between asymptotic freedom at high energies and infrared slavery at low energies is quantified through these renormalization group tools.

Subsequently, we explore chiral symmetry breaking (χSB) through the lens of spontaneous symmetry breaking (SSB) mechanisms, Goldstone's theorem, and the emergence of dynamical mass scales. Finally, confinement is examined via Wilson loop formulations, area law behaviour, and connections to string-theoretic descriptions of hadronic flux tubes. This discussion of confinement transitions naturally into the subsequent chapter on string theory, where these concepts will be expanded within a geometric framework.

The links with string theory will become more important later on, as NAGTs will resurface when we discuss holography, where their duality relations to gravitational theories in higher dimensions provide insights into strongly coupled systems.

2.1 QCD Lagrangian

QCD is formulated as a non-Abelian gauge theory with symmetry group SU(3), governing the interactions of quarks and gluons. We first consider the QCD Lagrangian density, which we can write in a compact form as [18]

$$\mathscr{L}_{QCD} = -\frac{1}{4} G_{\mu\nu,a} G^{\mu\nu}{}_a + \sum_f \bar{\psi}_f (i\not{D} - m_f)\psi_f, \tag{2.1}$$

where the first term describes the gluon fields, and the second governs the quarks. This Lagrangian's simple appearance belies a hidden complexity, rooted in the non-linearities of the SU(3) gauge symmetry.

The quark fields, comprising the 6 Dirac fermions ψ_f, labelled by flavour $f = u, d, s, c, b, t$ and grouped into broad 'light' (u, d, s) and 'heavy' (c, b, t) quarks, transform in the fundamental representation of SU(3), i.e. they carry a degree of freedom which we refer to as 'colour'.

For a massless Dirac fermion, the left- and right-handed components $\psi_{L,R} = \frac{1}{2}(1 \mp \gamma_5)\psi$ decouple in the Lagrangian. When the fermion mass $m_f = 0$, the QCD Lagrangian is invariant under independent $\mathrm{SU}(N_f)_L \times \mathrm{SU}(N_f)_R$ rotations of these components, i.e. they posses chiral symmetry. This symmetry is explicitly broken by non-zero quark masses in Eq. (2.1). For the heavy quarks, this breaking is substantial, but for the light quarks, whose masses are small compared to the QCD scale Λ_{QCD} (which will be discussed in more detail in section 2.3.1), chiral symmetry is approximately preserved in the Lagrangian. Regardless, the vacuum state spontaneously breaks chiral symmetry through the formation of a quark condensate $\langle \bar{q}q \rangle \neq 0$, which couples left- and right-handed quarks. As we will discuss in section 2.5, this SSB results in the generation of the near-massless Goldstone bosons - the pions.

Notably, quarks never appear independently (see section 2.6) but their degrees of freedom, along with the requirements of locality imply a vector field to mediate the colour force. These are the gluons, of which there are eight, forming an adjoint representation of SU(3), written as $(A_\mu)_{ij} = (T)^a_{ij} A^a_\mu$. The matrices $T_a = \lambda_a/2$ (with λ_a, the Gell-Mann matrices [19]) mediate interactions between quarks and gluons, with the coupling constant g setting the interaction strength. The dynamics of these fields are dictated by the gauge-covariant derivative

$$D_\mu = \partial_\mu - igA^a_\mu T^a, \tag{2.2}$$

which ensures invariance under local SU(3) transformations $\psi(x) \to \omega(x)\psi(x)$, with the covariant derivative similarly remaining invariant as $D_\mu \psi(x) \to \omega(x)(D_\mu \psi(x))$ with $\omega(x) \in \mathrm{SU}(3)$.

The gauge field strength tensor $G_{\mu\nu,a}$ (defined from the commutator of covariant derivatives [20]) is given by

$$G_{\mu\nu,a} = \frac{i}{g}\left[D_\mu, D_\nu\right]_a = \partial_\mu A_{\nu,a} - \partial_\nu A_{\mu,a} + g f_{abc} A_{\mu,b} A_{\nu,c}, \tag{2.3}$$

encapsulates the self-interacting nature of gluons.

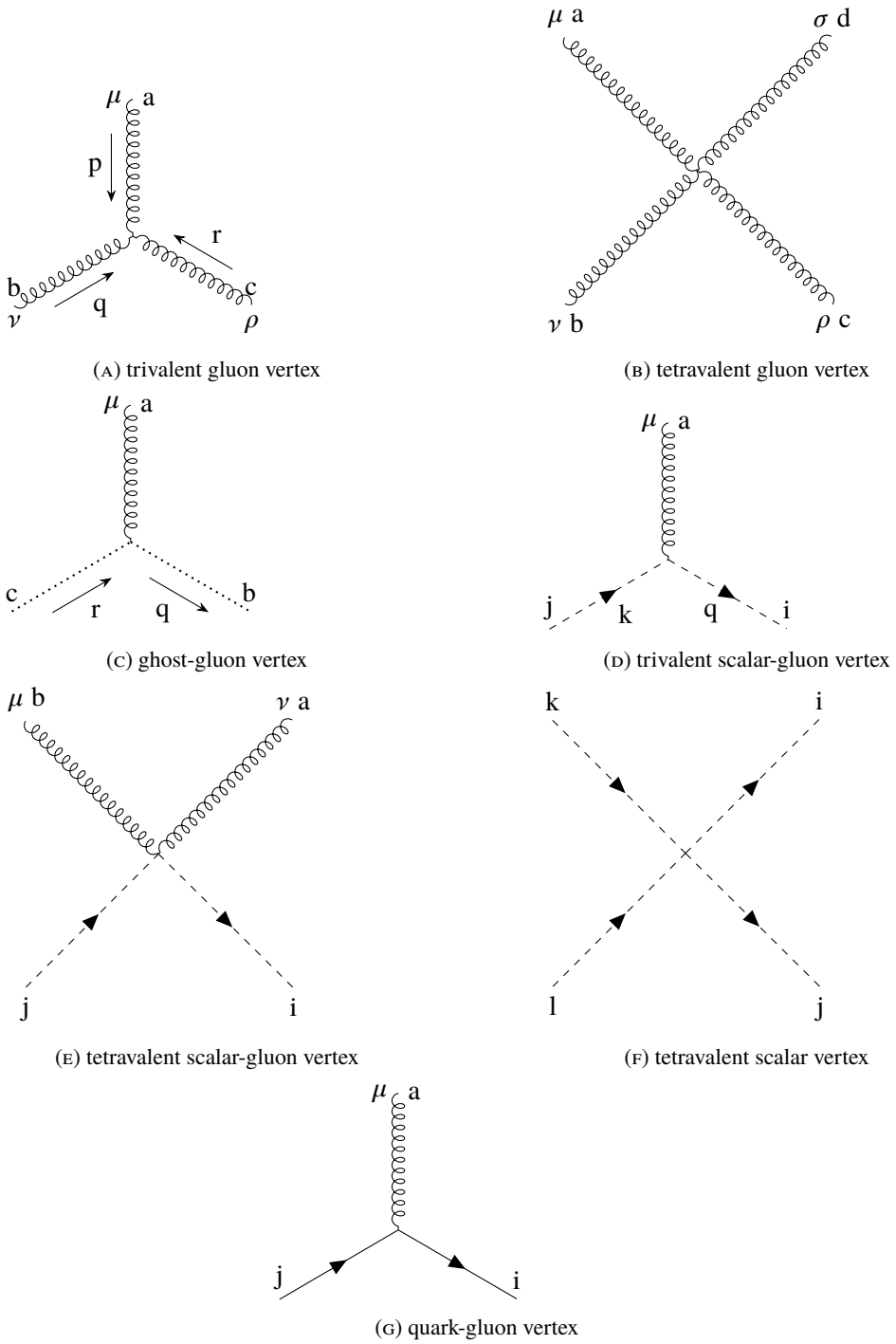

FIGURE 2.1: Interaction vertices for three- and four-gluon interactions

Unlike the photon in QED, the gluons carry colour charge *themselves*, leading to three- and four-gluon vertices (see Figure 2.1 (a) and (b)). The structure constants f_{abc} are derived from the

SU(3) Lie algebra, specifically the commutator of the generators T_a such that

$$[T_a, T_b] = if_{abc}T_c. \tag{2.4}$$

This quantifies the non-commutativity of the gluon field. The quadratic term $G_{\mu\nu,a}G^{\mu\nu}{}_a$ thus generates both kinetic terms and gluon self-interactions, absent in Abelian theories like QED. Note that in the non-abelian case, $A_{\mu,a}$ transforms as

$$A_{\mu,a}(x) \to A_{\mu,a}(x) - D_{\mu,ab}\omega_b(x) \tag{2.5}$$

for some gauge transformation ω. The presence of the covariant derivative D_μ rather than ∂_μ means that the path integral is ill-defined. We cannot avoid (infinite) over-counting of terms in the path integral related by a gauge transformation by excluding the components of A^a_μ parallel to k_μ. Instead we gauge fix via the Faddeev-Popov procedure [21], introducing the FP determinant - inserting '1' into the path integral in the following form:

$$1 = \int Du\delta(F^a({}^uA) - c^a)\Delta[{}^uA], \tag{2.6}$$

where

$$\Delta[A] = \det\left(\frac{\delta F^a(A(x))}{\delta A^c_\mu(y)}D^{cb}_\mu(A(y))\right), \tag{2.7}$$

and ${}^uA$ is the field A gauge transformed by $u = e^{i\omega^a T^a}$. This determinant encodes the over-counting and is essential for preserving unitarity. With this, we have a constrained path integral containing the original action, along with a additional terms for the gauge fixing and ghost field actions. The gauge fixing and ghost field Lagrangians respectively are of the form

$$\mathscr{L}_{\text{gf}} = -\frac{1}{2}\xi^{-1}(\partial^\mu A^a_\mu)^2 \tag{2.8}$$

$$\mathscr{L}_{\text{gh}} = -\partial^\mu\bar{c}^b D^{bc}_\mu c^c = -\partial^\mu\bar{c}^c\partial_\mu c^c + gf^{abc}A^a_\mu\partial^\mu\bar{c}^b c^c. \tag{2.9}$$

The resulting unphysical fields, so-called Faddeev-Popov ghosts $(c^a, \bar{c}^a)$, are anti-commuting scalars that effectively subtract off the unphysical gauge degrees of freedom. This yields an additional, trivalent ghost-gluon interaction vertex that appears at loop level.

2.2 Renormalization, Divergence and Scale Evolution

Before continuing, we must consider that the parameters of the theory - such as quark masses and the strong coupling constant - acquire radiative corrections from higher-order terms in the perturbative expansion [18]. These corrections arise from loop integrals with unbounded momenta, leading to UV divergences. To render the theory predictive, these divergences are systematically absorbed into a finite set of counterterms, a process constrained by the gauge symmetry of QCD which we will now briefly discuss.

The bare parameters in the QCD Lagrangian, which we denote as X_{bare}, are divergent and replaced by renormalized counterparts X_{renorm} via multiplicative renormalization constants Z_X:

$$X_{\text{bare}} = Z_X X_{\text{renorm}}, \tag{2.10}$$

where Z_X absorbs the divergences, order-by-order in perturbation theory. The Lagrangian is then split into a finite, "physical" part and a divergent counterterm contribution:

$$\mathscr{L}_{\text{bare}} = \mathscr{L}_{\text{phys}}(X_{\text{renorm}}) + \mathscr{L}_{\text{CT}}\left([Z_X - 1]X_{\text{renorm}}\right). \tag{2.11}$$

The counterterm Lagrangian $\mathscr{L}_{\text{CT}}$ cancels UV divergences, ensuring observables remain finite. A renormalization scale μ is introduced to define the renormalized parameters. While the bare parameters X_{bare} are μ-independent, the renormalized parameters $X_{\text{renorm}}(\mu)$ depend on μ. This leads to the Callan-Symanzik [22, 23] equation, governing the scale evolution of Green's functions $G^{(n)}(x_1, \ldots, x_n; \mu, g_s)$:

$$\left(\mu\frac{\partial}{\partial\mu} + \beta(g_s)\frac{\partial}{\partial g_s} - \sum_i \gamma_i(\mu)\right) G^{(n)}(x_1, \ldots, x_n; \mu, g_s) = 0, \tag{2.12}$$

where the beta function $\beta(g_s)$ and anomalous dimensions γ_i are defined as:

$$\beta(g_s) = \mu\frac{\partial g_s}{\partial\mu}, \tag{2.13}$$

$$\gamma_i = \mu\frac{\partial}{\partial\mu}\ln Z_i. \tag{2.14}$$

Here, g_s is the renormalized strong coupling, and Z_i are renormalization constants for fields or couplings. The beta function quantifies the running of g_s with μ, while γ_i encode the scale dependence of operators.

QCD's SU(3) gauge invariance imposes strict constraints on renormalization. The Slavnov-Taylor identities: generalized Ward-Takahashi identities for non-Abelian theories, enforce relationships between renormalization constants. For example, the gluon coupling renormalization Z_g is tied to the gluon field Z_A and quark field Z_ψ renormalizations:

$$Z_g = Z_A^{1/2} Z_\psi. \tag{2.15}$$

This ensures gauge invariance is preserved quantum mechanically. The quantized gauge symmetry manifests as Becchi-Rouet-Stora-Tyutin (BRST) invariance [24, 25], where ghost fields ensure divergences cancel consistently with BRST symmetry.

Divergences are regulated using schemes that preserve gauge invariance. Dimensional regularization (working in $d = 4 - \epsilon$ dimensions) is preferred in QCD because it avoids introducing explicit symmetry-breaking cutoffs and accommodates non-Abelian ghosts. In contrast, momentum cutoffs or lattice regularization complicate Slavnov-Taylor identities by breaking gauge invariance at intermediate steps.

While the perturbative beta function $\beta(g_s)$ predicts the weakening of the coupling g_s at high energies (asymptotic freedom), its reliability diminishes in the strong-coupling regime ($g_s \sim 1$). Non-perturbative methods, such as lattice QCD, are required to study confinement and hadronization. This framework sets the stage for analyzing the beta function's role in the running coupling and the anomalous mass dimension γ_m. Crucially, gauge invariance ensures renormalizability, restricting counterterms to those already present in the original Lagrangian: a cornerstone of QCD's predictive power.

2.3 β Function and the Running of the Coupling

The renormalization group evolution of the strong coupling in a generic SU(N_c) gauge theory with N_f massless fermions in a representation R is governed by the beta function. At two-loop order (beyond which point the function becomes renormalization scheme dependent) and at an arbitrary scale μ, this is expressed as [18]

$$\beta(\alpha_s) = \frac{\partial \alpha_s(\mu)}{\partial \ln \mu} = -\beta_0 \alpha_s^2 - \beta_1 \alpha_s^3 + \mathcal{O}(\alpha_s^4), \tag{2.16}$$

where we have exchanged the bare coupling $g_s(\mu)$ for $\alpha_s(\mu) \equiv \frac{g_s^2}{4\pi}$, a dimensionless parameter chosen to simplify the perturbative expansion, and the coefficients β_0 and β_1 depend on the gauge group and fermion content [26]:

$$\beta_0 = \frac{1}{2\pi}\left(\frac{11}{3}C_2(G) - \frac{4}{3}T(R)N_f(R)\right), \tag{2.17}$$

$$\beta_1 = \frac{1}{8\pi^2}\left(\frac{34}{3}[C_2(G)]^2 - \left[\frac{20}{3}C_2(G) + 4C_2(R)\right]N_f(R)T(R)\right). \tag{2.18}$$

Here, $C_2(G) \equiv N_c$ is the quadratic Casimir of the adjoint representation G, and $C_2(R)$ is the Casimir for the fermion representation R. The sign and magnitude of β_0 and β_1 determine the qualitative behaviour of $\alpha_s(\mu)$, as illustrated in Figure 2.2.

To see the emergence of the QCD scale and the infrared divergence explicitly, we may consider truncating at one-loop order: $\beta(\alpha_s) = -\beta_0\alpha_s^2$. Solving this equation we find

$$\alpha_s(\mu) = \frac{\alpha_s(\mu_0)}{1 + \beta_0\alpha_s(\mu_0)\ln(\mu/\mu_0)} = \frac{1}{\beta_0\ln\left(\mu/\Lambda_{\text{QCD}}\right)}, \tag{2.19}$$

where μ_0 is a reference scale. The integration constant defines the QCD scale:

$$\Lambda_{\text{QCD}} \equiv \mu_0 \exp\left[-\frac{1}{\beta_0\alpha_s(\mu_0)}\right]. \tag{2.20}$$

In QCD or similar theories we have $\beta_0 > 0$. In this case Eq. (2.19) clearly displays asymptotic freedom: $\alpha_s \to 0$ as $\mu \to \infty$. It also exhibits a Landau pole at $\mu = \Lambda_{\text{QCD}}$, where the coupling diverges. This infrared divergence at a finite scale indicates the breakdown of perturbation theory and signals the onset of non-perturbative phenomena like confinement. While the two-loop and higher-order terms modify the running quantitatively, the one-loop solution is sufficient to introduce Λ_{QCD} and demonstrate the basic UV/IR behaviour.

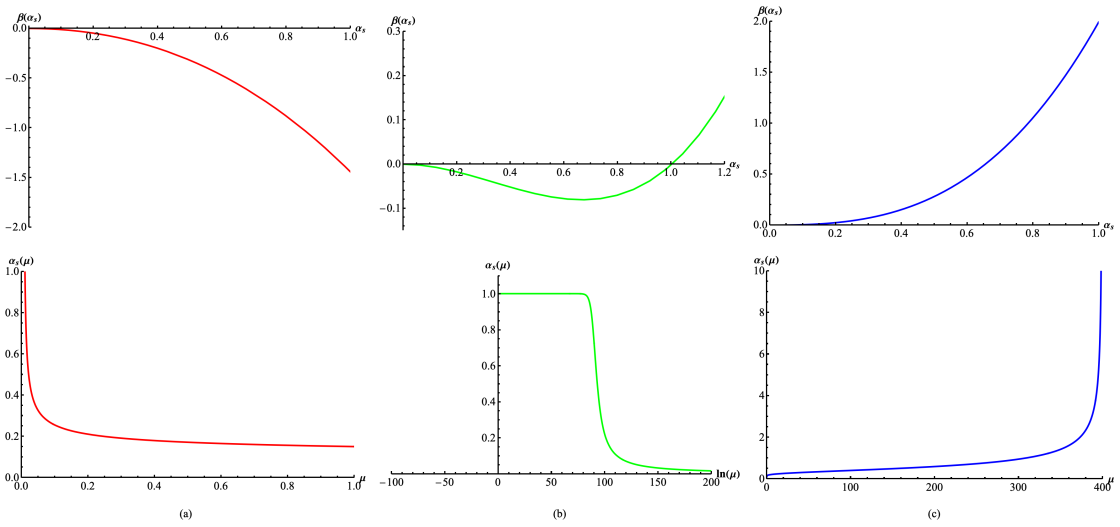

FIGURE 2.2: The beta function $\beta(\alpha_s)$ and its corresponding running $\alpha_s(\mu)$ for 3 distinct cases. (a) has $\beta_0 > 0$ and $\beta_1 > 0$ (asymptotic freedom). (b) has $\beta_0 > 0$ and $\beta 1 < 0$ (walking theory with NTIR fixed point). (c) has $\beta_0 < 0$ and $\beta_1 < 0$ (IR freedom). Note that (b) shows the running of the coupling as a function of $\ln \mu$.

In Figure 2.2(a), $\beta(\alpha_s) \leq 0$ for all α_s, driven by $\beta_0 > 0$ and $\beta_1 > 0$. This leads to a monotonically decreasing coupling that vanishes asymptotically at high scales ($\mu \to \infty$), a hallmark of asymptotic freedom [5, 6]. The sole fixed point at $\alpha_s = 0$ corresponds to a UV-trivial free theory.

For $\beta_0 > 0$ but $\beta_1 < 0$, the beta function develops a non-trivial infrared (NTIR) fixed point at $\alpha_s = \alpha_s^*$ (Figure 2.2(b)). Near α_s^*, the coupling evolves slowly—a regime called walking—as the theory approaches conformality. If α_s^* is small ($\alpha_s^* \ll 1$), the fixed point is perturbatively accessible, forming a (Caswell-)Banks-Zaks fixed point [26, 27]. As $\beta_0 \to 0^+$, α_s^* shifts toward zero, enlarging the walking regime. For $\beta_0 < 0$, asymptotic freedom is lost, and the beta function resembles that of QED, with a trivial IR fixed point (Figure 2.2(c)).

2.3.1 Walking Behaviour and the Conformal Window

One other important behaviour to note, for asymptotically free theories, is the increasing coupling as $\mu \to 0$; α_s grows until it diverges at a scale Λ_{QCD}, a phenomenon termed infrared slavery. This divergence signifies confinement [28], where coloured degrees of freedom bind into colour-neutral hadrons. The scale Λ_{QCD} sets the non-perturbative parameters of the theory, such as the chiral condensate $\langle \bar{q}q \rangle$.

We may also define another scale α_s^χ at which SSB of the chiral symmetry occurs. This χSB scale Λ_χ is typically defined by $\alpha_s(\Lambda_\chi) \equiv \alpha_s^\chi$, at which the anomalous dimension γ_m of the quark mass operator is thought to reach a critical value of $\gamma_m \sim 1$ (discussed in section 2.4). This heuristic criterion marks the transition into a strongly coupled regime where the formation of a chiral condensate is favoured. If $\alpha_s(\mu)$ crosses α_s^χ before reaching α_s^*, the massless fermions

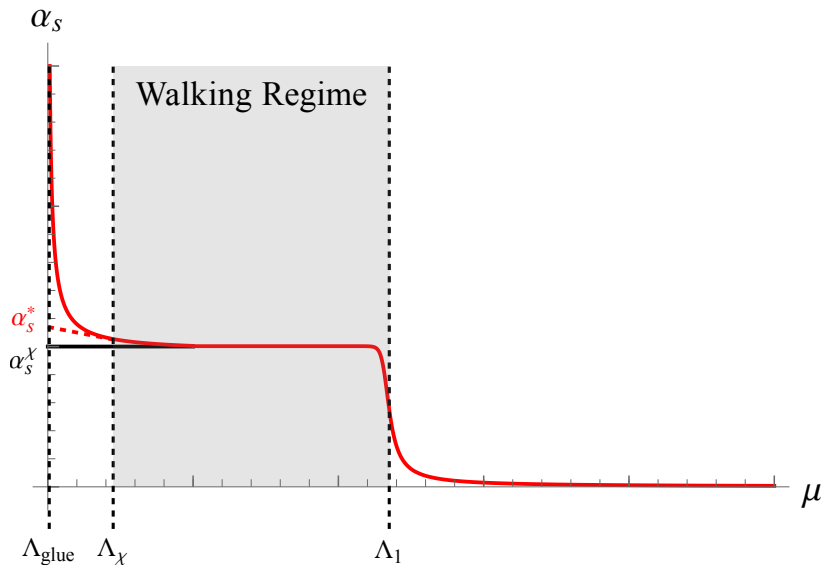

FIGURE 2.3: Plot of $\alpha_s(\mu)$ for the case $\alpha_s^* > \alpha_s^\chi$. The critical coupling is met at the scale, Λ_χ, triggering χSB and generating a dynamic mass for the quarks of order this scale. Below Λ_χ, the quarks decouple and the theory then runs into the IR as '$N_f = 0$'. The scale Λ_1 can be seen as the UV boundary of the walking regime and is dictated by the scale generated by the one-loop running.

acquire dynamical masses $m_q \sim \Lambda_\chi$ and decouple. Below Λ_χ, the theory transitions to a pure gauge (aka 'pure glue') sector that runs into the IR with its own confinement scale Λ_{glue}. This generates an intermediate walking regime (Figure 2.3), where $\alpha_s(\mu)$ lingers near α_s^* before triggering χSB. A third scale, Λ_1, marks the transition between UV-perturbative and IR-walking behaviours, roughly matching the one-loop running prediction.

Theories where $\alpha_s^* < \alpha_s^\chi$ reside in the conformal window [29, 30], so named as the running in this window is so shallow that it does not significantly change over a long period of the scale. Here, the coupling flows to α_s^* without triggering χSB, resulting in scale-invariant dynamics at low energies. The transition between confinement and conformality is conjectured to depend smoothly on N_c and N_f, as shown in the $N_f - N_c$ plane (Figure 2.4). For example, SU(3) with $N_f \sim 8$ fundamental fermions is hypothesized to denote the start of the walking regime, with $N_f \sim 12$ signalling the conformal window boundary and $N_f \sim 33/2$ marking the loss of asymptotic freedom.

These scenarios rely on extrapolating perturbative beta functions beyond their regime of validity. While lattice studies support walking and conformal window behaviours in specific theories, the existence of a Banks-Zaks fixed point or χSB scale Λ_χ in the full non-perturbative theory remains an open question. Crucially, the perturbative beta function cannot resolve whether the NTIR fixed point persists once non-perturbative effects (e.g., instantons, monopoles) are included.

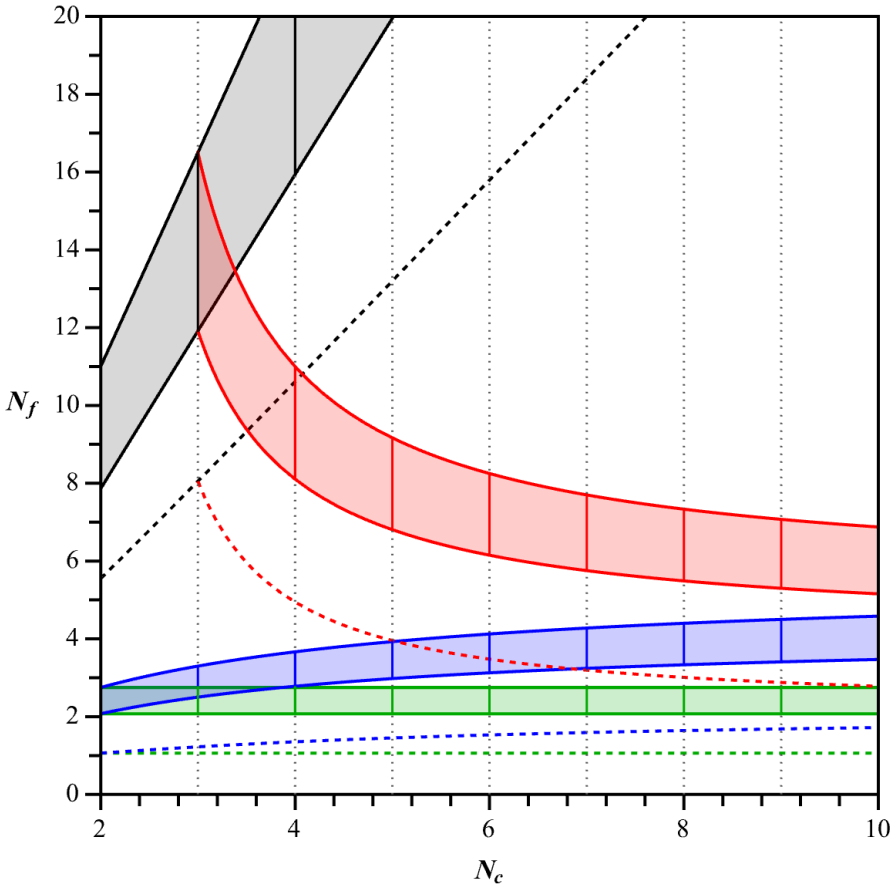

FIGURE 2.4: Phase diagram (adapted from [29]) for theories with fermions in the fundamental representation (grey), two-index antisymmetric (red), two-index symmetric (blue), and adjoint representation (green) as a function of the N_f and N_c. The shaded areas depict the corresponding conformal windows. For each colour, starting from the bottom, the dashed curve denotes the existence of a Banks-Zaks fixed point. Below this there is only a trivial UV fixed point, above it, there are walking regimes. Crossing the lower solid curve into the shaded region, χSB is lost. Crossing the upper solid curve, asymptotic freedom is lost.

The phase structure of SU(N_c) theories is further complicated by the interplay of Λ_{QCD}, Λ_χ, and Λ_1. For instance, in walking theories, Λ_1 separates the UV regime (where α_s runs perturbatively) from the IR regime (where it "walks" near α_s^*). If $\Lambda_\chi < \Lambda_1$, χSB occurs during the walking phase, dynamically altering the particle content of the theory. Conversely, if $\Lambda_\chi > 1$, the coupling diverges before walking can manifest, restoring QCD-like confinement.

In summary, the beta function's structure encodes a delicate balance between asymptotic freedom, infrared slavery, and potential conformality. While perturbative insights provide a scaffolding for these phenomena, non-perturbative effects ultimately dictate the theory's fate—a reminder that confinement, χSB, and the conformal window are emergent properties of the strongly coupled vacuum.

2.4 The Anomalous Mass Dimension

Looking once more at Eq. (2.12), we can see that the renormalization process introduced an additional running function, $\gamma_i(\mu)$, for each n-point operator. To understand this function, consider an operator $\mathcal{O}(x)$ with classical mass dimension Δ. Under a coordinate rescaling $x^\mu \to \lambda x^\mu$, $\lambda \in \mathbb{R}$. The operator transforms classically as

$$\mathcal{O}(x) \to \lambda^{-\Delta}\mathcal{O}(\lambda x), \tag{2.21}$$

preserving its dimensional structure. However, quantum corrections modify this scaling. The bare operator $\mathcal{O}_{\text{bare}}$ is related to its renormalized counterpart $\mathcal{O}_{\text{renorm}}$ by a scale-dependent renormalization constant:

$$\mathcal{O}_{\text{bare}} = Z_{\mathcal{O}}(\mu)\mathcal{O}_{\text{renorm}}, \tag{2.22}$$

where $Z_{\mathcal{O}}(\mu)$ absorbs divergences. To reconcile the classical scaling of $\mathcal{O}_{\text{renorm}}$ with the quantum theory, we define

$$Z_{\mathcal{O}}(\mu) = \mu^{-\gamma_{\mathcal{O}}}, \tag{2.23}$$

introducing the anomalous dimension. The bare operator now acquires a quantum scaling dimension, reflecting deviations from its classical behaviour. If $Z_{\mathcal{O}}(\mu) = 1$, the anomalous dimension vanishes, restoring naïve scaling. Taking the natural logarithm of both sides and differentiating with respect to $\ln \mu$, we obtain

$$\gamma_{\mathcal{O}} = -\frac{\partial}{\partial \ln \mu} \ln Z_{\mathcal{O}}(\mu). \tag{2.24}$$

which, of course, matches the definition of γ_i in the Callan-Symanzik equation in Eq. (2.12). For physical operators like the quark mass term, $m\bar{\psi}\psi$, the renormalized mass m_{renorm} evolves with μ as

$$m_{\text{bare}} = Z_m(\mu) m_{\text{renorm}}, \tag{2.25}$$

and

$$\gamma_m = \frac{\partial}{\partial \ln \mu} \ln Z_m(\mu), \tag{2.26}$$

where γ_m governs the energy scale-dependent running of the mass. Composite operators, such as $\mathcal{O} = (\bar{\psi}\psi)^2$, similarly develop anomalous dimensions through loop corrections, altering their scaling in correlation functions. The anomalous dimension is calculated perturbatively by isolating divergences in $Z_m(\mu)$. At one-loop order, for example, the quark mass operator in QCD yields

$$\gamma_m = \frac{3C_2(R)}{2\pi}\alpha_s + \mathcal{O}(\alpha_s^2). \tag{2.27}$$

This result underscores the interplay between gauge interactions - α_s - and the operator's group-theoretic structure - $C_2(R)$ - in determining quantum scaling.

2.5 Chiral Symmetry Breaking

Next we will briefly discuss the phenomenon of χSB as we first mentioned in section 2.3.1. The mechanism of SSB, famously applied in the Higgs mechanism for generating mass in the Standard Model [31, 32], also underlies χSB in QCD, albeit with key differences.

2.5.1 Spontaneous Symmetry Breaking

We first consider a simple case of SSB, using the example of a complex scalar field theory with a single field ϕ. The Lagrangian for this theory is

$$\mathcal{L} = \left|\partial_\mu \phi\right|^2 + m^2|\phi|^2 - \frac{\lambda}{4}|\phi|^4, \tag{2.28}$$

where $m, \lambda \in \mathbb{R}$ are coupling constants and $\lambda > 0$ to ensure the system is bounded from below. The Lagrangian is invariant under a global $U(1)$ symmetry: $\phi \to U\phi$, $\phi^* \to U^*\phi^*$ where U is a unitary operator, i.e. $U^*U = \mathbb{I}$ and $U = e^{i\alpha}$, $\alpha \in \mathbb{R}$. When $m < 0$, the system has a global minimum at $\phi = 0$, however for $m > 0$ the theory becomes unstable at the origin (having a local maximum) and assumes the so-called "Mexican Hat" potential (see Figure 2.5), with a minimum at $|\phi|^2 = \frac{2m^2}{\lambda}$, or rather, a ring of minima which we parametrise as $\langle \Omega_\theta | \phi | \Omega_\theta \rangle = m\sqrt{\frac{2}{\lambda}}e^{i\theta}$, $\theta \in \mathbb{R}$.

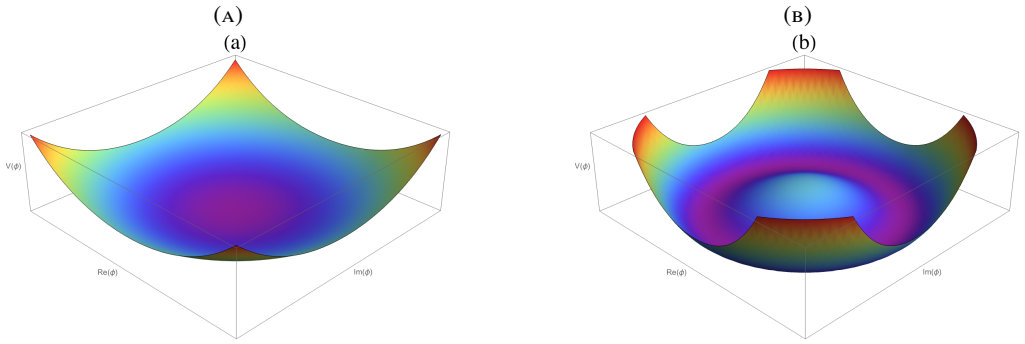

FIGURE 2.5: (a) The potential with global minimum occurring at $|\phi| = 0$ exhibiting a global $U(1)$ symmetry. (b) The old minimum becomes an unstable extremum of the potential. The new global minimum is a set of solutions at fixed $|\phi| \neq 0$ – there is a non-zero vacuum expectation value of the field ϕ.

Note that since there is a non-zero vacuum expectation value (VEV) of the field ϕ, i.e. $\langle \Omega_\theta | \phi | \Omega_\theta \rangle \neq 0$ and depends on the phase angle θ, the vacuum state $|\Omega_\theta\rangle$ is no longer invariant under the symmetry of the Lagrangian. Instead, it "chooses" a specific direction in the space of degenerate vacua, breaking the $U(1)$ symmetry. We can, without loss of generality, take $\theta = 0$ and thus arrive at the VEV

$$\langle \Omega_\theta | \phi | \Omega_\theta \rangle = m\sqrt{\frac{2}{\lambda}} \equiv v, \quad v \in \mathbb{R}^+. \tag{2.29}$$

We now wish to examine fluctuations around the vacuum. We rewrite the field ϕ in terms of its deviation from the VEV:

$$\phi(x) = \left(v + \frac{1}{\sqrt{2}}\sigma(x)\right) e^{\frac{i\pi(x)}{f_\pi}}, \tag{2.30}$$

where the fluctuations in ϕ are as follows: $\sigma(x)$ parametrizes the radial fluctuations about the VEV, v, while $\pi(x)$ parametrises the angular fluctuations around the chosen phase, $\theta = 0$, and $f_\pi \in \mathbb{R}$. Substituting for Eq. (2.30) into Eq. (2.28), after some simplification, we get

$$\mathscr{L} = \frac{1}{2}(\partial_\mu \sigma)^2 + \left(v + \frac{1}{\sqrt{2}}\sigma\right)^2 \frac{1}{f_\pi^2}(\partial_\mu \pi)^2 - m^2\sigma^2 - \frac{1}{2}\sqrt{\lambda} m\sigma^3 - \frac{1}{16}\lambda\sigma^4 + \frac{m^4}{\lambda}. \tag{2.31}$$

We can see from the potential terms that the σ field acquires a mass, while the π field remains massless. This Lagrangian can be made *canonically normalized* by taking $f_\pi = \sqrt{2}v$.

2.5.2 Goldstone's Theorem

The emergence of a massless mode in the angular fluctuation, $\pi(x)$, is not accidental; rather it reflects a universal consequence of SSB. From the parametrization of fluctuations around the VEV in Eq. (2.30), we observe that the angular mode, $\pi(x)$ has dynamics that are purely kinetic. Considering just the terms in $(\partial_\mu \pi)^2$ and taking $\sigma \to 0$ we see that

$$\mathscr{L}_{\partial_\mu \pi} = (v + \frac{1}{\sqrt{2}}\sigma)^2 \frac{1}{f_\pi^2}(\partial_\mu \pi)^2 \to \frac{v^2}{f_\pi^2}(\partial_\mu \pi)^2. \tag{2.32}$$

Using the canonical normalization ($f_\pi = \sqrt{2}v$) simplifies this to $\frac{1}{2}(\partial_\mu \pi)^2$, confirming $\pi(x)$ is massless. We know from Noether's theorem [33], that the $U(1)$ symmetry implies a conserved Noether current: $\partial_\mu j^\mu = 0$, with $j^\mu = i(\phi^* \partial^\mu \phi - \phi \partial^\mu \phi^*)$. Substituting $\phi = v e^{i\pi/f_\pi} \approx v\left(1 + \frac{i\pi}{f_\pi}\right)$, (to leading order in fluctuations, $\sigma \ll v$), the current becomes:

$$j^\mu \approx -\frac{2v^2}{f_\pi}\partial^\mu \pi. \tag{2.33}$$

The conserved charge is then

$$Q = \int d^3x j^0(x) = -\frac{2v^2}{f_\pi}\int d^3x\, \partial^0 \pi. \tag{2.34}$$

Crucially, the vacuum is not invariant under Q, i.e. $Q|\Omega\rangle \neq 0$, implies degenerate vacua $e^{i\theta Q}|\Omega\rangle$, $\theta \in \mathbb{R}$ indicating SSB. Acting with Q on the vacuum generates a state degenerate with $|\Omega\rangle$:

$$|\pi(p=0)\rangle \propto Q|\Omega\rangle. \tag{2.35}$$

The Fourier-transformed current creates π-states from the vacuum, i.e.

$$|\pi(p)\rangle \sim j^0(p)|\Omega\rangle = \int d^3x\, e^{ip\cdot x} j^0(x)|\Omega\rangle. \tag{2.36}$$

The energy of these states is $E_\pi(p) = E_\Omega + |\vec{p}|$, where E_Ω is the vacuum energy. In the limit as $\vec{p} \to 0$, then $|\pi(p)\rangle \to |\Omega\rangle$ and so of course, we see that $E_\pi \to E_\Omega$. This implies the dispersion relation of a massless particle, i.e. that $m_\pi = 0$. This is Goldstone's Theorem - a spontaneous breaking of a continuous global symmetry implies massless particles in the spectrum, these particles being the (Nambu-)Goldstone bosons [34, 35].

This generalizes to arbitrary symmetries, for example, given a theory with a global symmetry group G, spontaneously broken to $H \subset G$, the number of Goldstone bosons will be equal to $\dim(G/H)$, with each broken generator T_a of G having a corresponding current J_a^μ whose charge

generates a Goldstone $\pi^a(x)$. For example, if SU(2) breaks to $U(1)$, the two broken generators yield Goldstone bosons analogous to pions in χSB.

2.6 Confinement

Finally in this section, we will discuss the phenomenon of confinement. This is a property which is strongly evidenced from experiment. Experimental searches [36] have found no evidence of unbound quarks or gluons, rather only colour singlet states are found (e.g.: mesons, baryons) and lattice calculations provide numerical support for the notion that quarks must be confined at low energies. In [7], Wilson described confinement in terms of the *Wilson Loops* - non-local gauge invariant operators which act as order parameters for confinement.

We can explain this behaviour in terms of the formation of a flux tube. As a quark-antiquark pair are separated, the chromoelectric field lines connecting them do not spread out as they would in QED; rather they are constricted into a narrow tube of concentrated non-Abelian flux due to the self-interaction of the gluons. This results in a potential energy between the quarks that grows linearly with increasing separation: $V(r) \sim \sigma r$, where σ is a 'string tension' (as the potential is analogous to that of a vibrating string). The energy stored in this vibrating string eventually becomes sufficient to produce new quark-antiquark pairs from the vacuum, leading to jet formation and ensuring that observable final states are always colour singlets.

Wilson loops quantify the phase of a gauge theory. For a closed path γ in spacetime, the Wilson loop operator is defined as

$$W[\gamma] = \mathrm{Tr}\left(\mathcal{P} \exp\left[i \oint_\gamma A_\mu dx^\mu \right] \right), \tag{2.37}$$

where $\mathcal{P}$ enforces path ordering of the gauge field A_μ. The vacuum expectation value $\langle W[\gamma] \rangle$ distinguishes confined and deconfined phases. In the confined phase we have the *area law*

$$\langle W[\gamma] \rangle \propto e^{-A[\gamma]}, \tag{2.38}$$

where $A[\gamma]$ is the area enclosed by γ. In the deconfined phase we have the *perimeter law*

$$\langle W[\gamma] \rangle \propto e^{-L[\gamma]}, \tag{2.39}$$

where $L[\gamma]$ is the perimeter of γ. To derive the area law, we consider a rectangular Wilson loop in the (t, x)-plane with spatial extent $\mathcal{R}$ and temporal extent $\mathcal{T} \gg \mathcal{R}$. In axial gauge ($A_0 = 0$), the loop reduces to

$$\langle W[\gamma]\rangle = \left\langle \mathscr{P}\exp\left[i\int_0^R A_1(t=0)dx^1 - i\int_R^0 A_1(t=\mathscr{T})dx^1\right]\right\rangle. \tag{2.40}$$

Introducing the spatial Wilson line operator:

$$\Psi_{ij}(t) = \mathscr{P}\exp\left[i\int_0^R A_1(t)dx^1\right]_{ij}, \tag{2.41}$$

where i, j are colour indices, the expectation value becomes

$$\langle W[\gamma]\rangle = \left\langle \Psi ij(0)\middle|\Psi_{ij}^\dagger(\mathscr{T})\right\rangle. \tag{2.42}$$

Inserting a set of states, n gives

$$\langle W[\gamma]\rangle = \sum_n \langle \Psi ij(0)|n\rangle \left\langle n\middle|\Psi_{ij}^\dagger(\mathscr{T})\right\rangle = \sum_n \left|\left\langle \Psi_{ij}(0)\middle|n\right\rangle\right|^2 e^{-E_n\mathscr{T}}. \tag{2.43}$$

At large $\mathscr{T}$, the ground state dominates: $\langle W[\gamma]\rangle \propto e^{-E_0\mathscr{T}}$. In confinement, the potential $V(R)$ between a static quark-antiquark pair grows linearly with separation $\mathscr{R}$, i.e., $V(\mathscr{R}) = T\mathscr{R}$, where T is the QCD string tension. Thus

$$\langle W[\gamma]\rangle \sim e^{-T\mathscr{R}\mathscr{T}} = e^{-TA[\gamma]}, \tag{2.44}$$

confirming the area law. The tension $T \approx 1$ GeV/fm, derived from lattice QCD and meson spectroscopy, reflects the energy density of the confining colour flux tube.

2.7 Confinement as Motivation for String Theory

Prior to QCD, empirical observations revealed that the meson square masses (M^2) scale linearly with their spin J — a hallmark of Regge trajectories. Such behaviour is intrinsic to rotating relativistic strings. Consider a string of length $2L$ and tension T in its rest frame:

$$E_0 = \int_{-L}^{L} T dr = 2TL, \quad \vec{p_0} = 0. \tag{2.45}$$

When boosted to a frame rotating with angular velocity ω, the velocity profile becomes $v(r) = \frac{c}{L}r$, reaching light speed at the endpoints ($r = \pm L$). The relativistic energy and momentum densities are

$$dE = \gamma T dr, \quad d\vec{p} = \gamma \frac{v}{c} T dr, \tag{2.46}$$

where $\gamma = \sqrt{1 - \frac{v^2}{c^2}}$. The total mass M and angular momentum J are computed via

$$M = \int_{-L}^{L} \gamma T dr = TL \int_{-\pi/2}^{\pi/2} \cos\theta d\theta = TL\pi, \tag{2.47}$$

$$J = \int_{-L}^{L} r dp = \int_{-L}^{L} r\gamma \frac{v}{c} T dr = TL^2 \frac{\pi}{2}, \tag{2.48}$$

using the substitution $r = L\sin\theta$. Eliminating L yields the Regge relation:

$$M^2 = 2\pi TJ, \tag{2.49}$$

linking M^2 and J through the string tension T. This matches observed slopes in hadron spectra (e.g., ρ-mesons), with $T \approx 2\pi\alpha' - 1$ for a Regge slope $\alpha' \approx 0.9$ GeV^{-2} [36]. The flux tube's quantum fluctuations further produce universal corrections, such as the Lüscher term [37] $V(r) = Tr - \frac{\pi(D-2)}{24r} + ...$, observed in lattice simulations.

The string-like behavior of QCD flux tubes echoes string theory's origins as a model for strong interactions. While QCD replaced early string models (e.g., the Veneziano amplitude [38]), confinement's success in linking Wilson loops to string dynamics revitalized the connection. For example, the Nambu-Goto action—describing a fundamental string's worldsheet—parallels the effective action for QCD flux tubes:

$$S_{\text{NG}} = T \int d^2T \sqrt{-\det h_{ab}}, \quad h_{ab} = \partial_a X^\mu \partial_b X_\mu. \tag{2.50}$$

Though QCD strings are emergent (with finite thickness and breakable via quark pair production), their interplay with gauge theory dynamics laid groundwork for modern explorations of gauge/string duality.

Chapter 3

Strings

This chapter will provide an introduction to the core principles of string theory, serving as a foundation for holography in 4. We begin by establishing the classical dynamics of relativistic strings, where one-dimensional objects trace out two-dimensional worldsheets in spacetime. This framework naturally generalizes point particle mechanics and introduces key concepts: the Nambu-Goto and Polyakov actions, worldsheet symmetries, and the critical distinction between closed strings and open strings with Neumann or Dirichlet boundary conditions [39], the latter foreshadowing non-perturbative D-branes.

We then move on to quantizing the bosonic string, showing how vibrational modes generate quantum particle states. This quantization imposes consistency requirements, fixing spacetime to an uncomfortable 26 dimensions while exposing new limitations: a tachyonic instability and the absence of fermionic matter [40, 39]. These shortcomings motivate the introduction of superstring theory, which incorporates worldsheet supersymmetry. Here, fermionic partners to the string coordinates enable spacetime fermions and reduce the critical dimension to 10, but the tachyonic instability persists.

The instability is finally solved through the GSO projection, a Hilbert space truncation that enforces spacetime supersymmetry and distinguishes between Type IIA and Type IIB theories [41]. This projection reveals massless sectors containing gravity, gauge fields, and novel Ramond-Ramond forms. Finally, we explore D-branes: dynamical hypersurfaces where strings terminate. These non-perturbative objects emerge as essential carriers of Ramond-Ramond charge, provide a consistent framework for T-duality, and generate gravitational backgrounds that hint at holographic duality.

3.1 Classical String Dynamics in String Theory

The dynamics of relativistic strings are governed by their propagation through spacetime, where the one-dimensional string traces out a two-dimensional surface known as the worldsheet. This

generalizes the concept of a point particle's worldline, with the string's motion described by embedding functions $x^\mu(\tau, \sigma)$, where τ (a timelike parameter analogous to proper time) and $\sigma \in [0, \pi]$ (a spacelike parameter spanning the string's length) define coordinates on the worldsheet. These functions map points (τ, σ) on the worldsheet to positions in a d-dimensional spacetime (the target space), with the geometry of the worldsheet intrinsically tied to the string's physical behavior.

The simplest geometric action governing the string's motion is the Nambu-Goto action, which measures the area of the worldsheet:

$$S_{NG} = -T d\tau d\sigma \int \sqrt{-\det \mathcal{G}_{ab}} = -T \int d\tau d\sigma, \sqrt{-\det \left(g_{\mu\nu} \partial_a x^\mu \partial_b x^\nu \right)}, \tag{3.1}$$

where $T = \frac{1}{2\pi\alpha'}$ is the string tension, α' (the Regge slope parameter) sets the fundamental string length scale $l_s = \sqrt{\alpha'}$, and $g_{\mu\nu}$ is the spacetime metric. The induced metric on the worldsheet, $\mathcal{G}_{ab} = g_{\mu\nu} \partial_a x^\mu \partial_b x^\nu$, encodes how the worldsheet curves within spacetime. While this action elegantly generalizes the relativistic point particle's proper time action, its square-root structure introduces non-linearities that complicate quantization.

To circumvent this, the Polyakov action reformulates the dynamics by introducing an auxiliary worldsheet metric h_{ab} as an independent dynamical field:

$$S_P = -\frac{T}{2} \int d\tau d\sigma, \sqrt{-\det h_{ab}} h^{ab} g_{\mu\nu} \partial_a x^\mu \partial_b x^\nu. \tag{3.2}$$

Here, h_{ab} decouples the worldsheet's intrinsic geometry from its spacetime embedding, simplifying the equations of motion. The Polyakov action exhibits three fundamental symmetries:

- Target spacetime Poincaré invariance thanks to the metric ensures Lorentz (Λ^μ_ν) and translational (c^μ) symmetry in spacetime:

$$x^\mu \to x'^\mu = \Lambda^\mu_\nu x^\nu + c^\mu. \tag{3.3}$$

- Worldsheet diffeomorphism invariance, i.e. reparameterization of the worldsheet coordinates leaves the action invariant:

$$(\tau, \sigma) \to (\tilde{\tau}(\tau, \sigma), \tilde{\sigma}(\tau, \sigma)). \tag{3.4}$$

- Weyl invariance: the action is invariant under a local rescaling (a symmetry unique to two dimensions):

$$h_{ab} \to e^{\omega(\tau,\sigma)} h_{ab}. \tag{3.5}$$

The equations of motion for h_{ab} enforce the Virasoro constraints, i.e. the vanishing of the world-sheet stress-energy tensor:

$$T_{ab} = -\frac{2}{T}\frac{\delta S}{\delta h^{ab}} = \partial_a x \cdot \partial_b x - \frac{1}{2} h_{ab} h^{cd} \partial_c x \cdot \partial_d x = 0, \tag{3.6}$$

where $\partial_a x \cdot \partial_b x \equiv g_{\mu\nu} \partial_a x^\mu \partial_b x^\nu$.

The equivalence of the Nambu-Goto and Polyakov actions is demonstrated by solving for h_{ab} in the latter. Varying S_P with respect to h_{ab} yields:

$$\partial_a x \cdot \partial_b x = \frac{1}{2} h_{ab} h^{cd} \partial_c x \cdot \partial_d x, \tag{3.7}$$

and taking the negative determinant of both sides gives

$$-\det \mathcal{G}_{ab} = (-\det h_{ab})(\frac{1}{2} h^{cd} g_{\mu\nu} \partial_c x^\mu \partial_d x^\nu)^2, \tag{3.8}$$

where the root of both sides are the integrands of the Nambu-Goto and Polyakov action respectively.

The Virasoro constraints also affects the fields x^μ. For example, in conformal gauge ($h_{ab} = \eta_{ab}$), we have

$$T_{01} = T_{10} = \dot{x}^\mu x'_\mu = 0, \tag{3.9}$$

$$T_{00} = T_{11} = \frac{1}{2}\left(\dot{x}^\mu \dot{x}\mu + x'^\mu x'\mu\right) = 0, \tag{3.10}$$

eliminating unphysical degrees of freedom and ensuring the string's energy-momentum flow is purely longitudinal.

The symmetries of the Polyakov action allow gauge-fixing h_{ab} to a flat metric η_{ab}, simplifying the action to:

$$S_P = -\frac{T}{2}\int d\tau d\sigma \left(\dot{x}^\mu \dot{x}_\mu - x'^\mu x'_\mu\right), \tag{3.11}$$

where $\dot{x}_\mu = \partial_\tau x^\mu$ and $x'_\mu = \partial_\sigma x^\mu$. The equations of motion reduce to linear wave equations:

$$\Box x^\mu = \ddot{x}^\mu - x''^\mu = 0. \tag{3.12}$$

The string's finite spatial extent ($\sigma \in [0, \pi]$) necessitates careful treatment of boundary conditions. In general we require

$$x'^{\mu} \Delta x_{\mu} \Big|_{\sigma=0}^{\sigma=\pi} = 0, \tag{3.13}$$

For closed strings, periodicity ($x^{\mu}(\tau, 0) = x^{\mu}(\tau, \pi)$ and $x'^{\mu}(\tau, 0) = x'^{\mu}(\tau, \pi)$) eliminates endpoints, allowing independent left- and right-moving modes. For open strings, we have two possibilities:

- Neumann conditions: $\partial_{\sigma} x^{\mu} = 0$ at $\sigma = 0, \pi$, corresponding to free endpoints that conserve momentum.
- Dirichlet conditions: $\Delta x^{\mu} = 0$ (fixed endpoints), which fix the string's endpoints to hypersurfaces called Dirichlet- or D-branes. These break translational symmetry in the directions orthogonal to the brane, requiring momentum transfer to the brane itself.

Note that it is also possible for an open string to have mixed boundary conditions, i.e. a Neumann condition at one end and a Dirichlet at the other.

3.1.1 Mode Expansions

Solutions to the wave equation $\Box x^{\mu} = 0$ decompose into Fourier modes reflecting the string's vibrational degrees of freedom. For closed strings, using lightcone coordinates $\sigma^{\pm} = \tau \pm \sigma$, the general solution is

$$x^{\mu}(\tau, \sigma) = x_c^{\mu} + \alpha' p_c^{\mu} \tau + \frac{i}{2} \alpha'^{\frac{1}{2}} \sum_{n \neq 0} \frac{1}{n} \left(\alpha_n^{\mu} e^{-2in\sigma^-} + \tilde{\alpha}_n^{\mu} e^{-2ins^+} \right), \tag{3.14}$$

where x_c^{μ} is a centre of mass, reference position, $\alpha' p_c^{\mu} \tau$ is the displacement from the initial position of the centre of mass. Reality of x^{μ} imposes on the oscillator modes $(\alpha_n^{\mu})^* = \alpha_{-n}^{\mu}$ and $(\tilde{\alpha}_n^{\mu})^* = \tilde{\alpha}_{-n}^{\mu}$.

It is useful to split the general solution into left- and right-moving sectors:

$$x^{\mu}(\tau, \sigma) = x_L^{\mu}(\sigma^+) + x_R^{\mu}(\sigma^-), \tag{3.15}$$

with

$$x_L^\mu(\sigma^+) = \frac{1}{2}x_c^\mu + \frac{\alpha'}{2}p_c^\mu\sigma^+ + i\frac{\alpha'^{1/2}}{2}\sum_{n\neq 0}\frac{\tilde{\alpha}_n^\mu}{n}e^{-2in\sigma^+}, \tag{3.16}$$

$$x_R^\mu(\sigma^-) = \frac{1}{2}x_c^\mu + \frac{\alpha'}{2}p_c^\mu\sigma^- + i\frac{\alpha'^{1/2}}{2}\sum_{n\neq 0}\frac{\alpha_n^\mu}{n}e^{-2in\sigma^-}, \tag{3.17}$$

It is possible to relate the centre of mass momentum p_c^μ to the zero modes via

$$\alpha_0^\mu = \tilde{\alpha}_0^\mu = \frac{\alpha'^{\frac{1}{2}}}{2}p_c^\mu, \tag{3.18}$$

which allows us to rewrite the solutions as

$$\partial_+ x_R^\mu = 0, \quad \partial_- x_R^\mu = \alpha'^{\frac{1}{2}}\sum_{n=-\infty}^{\infty}\alpha_n^\mu e^{-2in\sigma^-}, \tag{3.19}$$

$$\partial_- x_L^\mu = 0, \quad \partial_+ x_L^\mu = \alpha'^{\frac{1}{2}}\sum_{n=-\infty}^{\infty}\tilde{\alpha}_n^\mu e^{-2in\sigma^+}. \tag{3.20}$$

For open strings with Neumann conditions, the solution projects out sine terms, yielding:

$$x_N^\mu(\tau,\sigma) = x_c^\mu + 2\alpha' p_c^\mu\tau + i\sqrt{2\alpha'}\sum_{n\neq 0}\frac{\alpha_n^\mu}{n}e^{-in\tau}\cos(n\sigma), \tag{3.21}$$

where endpoints at $\sigma = 0, \pi$ exhibit oscillatory motion with conserved momentum. Dirichlet conditions fix endpoints at $x^\mu(\tau,0) = a^\mu$ and $x^\mu(\tau,\pi) = b^\mu$, leading to:

$$x_D^\mu(\tau,\sigma) = a^\mu + \frac{(b^\mu - a^\mu)}{\pi}\sigma + i\sqrt{2\alpha'}\sum_{n\neq 0}\frac{\alpha_n^\mu}{n}e^{-in\tau}\sin(n\sigma), \tag{3.22}$$

where the linear term represents the stretched string between fixed endpoints, and sine terms encode vibrations. Momentum non-conservation in transverse directions hints at the dynamical role of D-branes, which absorb momentum and will be explored in later discussions.

Canonical quantization begins by defining the momentum conjugate to x^μ

$$p^\mu(\tau,\sigma) = \frac{\delta S}{\delta(\dot{x}_\mu)} = \frac{1}{2\pi\alpha'}\dot{x}^\mu, \tag{3.23}$$

and the Poisson brackets

$$\{p^\mu, p^\nu\}_{PB} = \{x^\mu, x^\nu\}_{PB} = 0, \tag{3.24}$$

$$\{p^\mu(\sigma,\tau), x^\nu(\sigma',\tau)\}_{PB} = \eta^{\mu\nu}\delta(\sigma-\sigma'). \tag{3.25}$$

Substituting our solutions for x^μ we get the oscillator mode Poisson brackets:

$$\{\alpha_m^\mu, \tilde{\alpha}_n^\nu\}_{PB} = 0, \tag{3.26}$$

$$\{\alpha_m^\mu, \alpha_n^\nu\}_{PB} = \{\tilde{\alpha}_m^\mu, \tilde{\alpha}_n^\nu\}_{PB} = -im\eta^{\mu\nu}\delta_{m,-n}, \tag{3.27}$$

with similar relations for open strings. Quantization promotes the oscillators to operators and the Poisson brackets become commutators. The Virasoro constraints $T_{ab} = 0$ become operator equations $L_n \left|\text{phys}\right\rangle = 0$, which eliminate negative-norm states [42] and fix the critical spacetime dimension $d = 26$ for bosonic strings.

The interplay of worldsheet geometry, symmetries, and boundary conditions bridges classical string motion to quantum mechanical structure, with vibrational modes encoding particle spectra and D-branes anchoring non-perturbative phenomena. This classical foundation underpins the quantum framework, tying spacetime dimensionality to consistency conditions and linking geometry to gravity and gauge theories.

3.2 Quantization of the Bosonic String

The classical string's vibrational modes, given by $x^\mu(\tau,\sigma)$, encode its degrees of freedom. To realize the string's proposed role as a unified theory of quantum gravity and matter, we now quantize these modes, promoting worldsheet fields (along with their conjugate moment and oscillator modes) to operators and Poisson brackets to commutators (via $-i\{A,B\}_{PB} \to [A,B]$). Thus, the canonical commutators become:

$$[x^\mu, p^\nu] = i\eta^{\mu\nu}, \tag{3.28}$$

$$[\alpha_m^\mu, \tilde{\alpha}_n^\nu] = 0, \tag{3.29}$$

$$[\alpha_m^\mu, \alpha_n^\nu] = [\tilde{\alpha}_m^\mu, \tilde{\alpha}_n^\nu] = m\delta_{m,-n}\eta^{\mu\nu}. \tag{3.30}$$

Rescaling the oscillators as

$$a_m^\mu = \frac{1}{\sqrt{m}}\alpha_m^\mu, \tag{3.31}$$

$$a_m^{\mu\dagger} = \frac{1}{\sqrt{m}}\alpha_{-m}^\mu, \tag{3.32}$$

with $m \in \mathbb{Z}^+$, reveals their role as harmonic ladder operators:

$$\left[a_m^\mu, a_n^{\nu\dagger}\right] = \eta^{\mu\nu}\delta_{m,n}. \tag{3.33}$$

The Fock space is constructed by acting $a_m^{\mu\dagger}$ on the momentum eigenstate $|0; p^\mu\rangle$, which satisfies $\alpha_m^\mu |0; p^\mu\rangle = 0$ for $m > 0$. However, the temporal ($\mu = 0$) modes generate negative-norm states:

$$\langle 0|\, \alpha_m^0 \alpha_m^{0\dagger} \,|0\rangle = -1, \tag{3.34}$$

threatening unitarity.

3.2.1 Physical State Constraints and Emergent Spectra

The classical Virasoro constraints emerge from the vanishing energy-momentum tensor $T_{ab} = 0$. Inserting the mode expansion, Eq. (3.14), into the expression for the vanishing of the stress-energy tensor (3.6) yields:

$$T_{--} = 4\alpha' \sum_{m=-\infty}^{\infty} L_m e^{-2im\sigma^-}, \tag{3.35}$$

$$T_{++} = 4\alpha' \sum_{m=-\infty}^{\infty} \tilde{L}_m e^{-2im\sigma^+}, \tag{3.36}$$

with Virasoro generators:

$$L_m = \frac{1}{2}\sum_{n=-\infty}^{\infty} \alpha_{m-n}\cdot\alpha_n, \tag{3.37}$$

$$\tilde{L}_m = \frac{1}{2}\sum_{n=-\infty}^{\infty} \tilde{\alpha}_{m-n}\cdot\tilde{\alpha}_n. \tag{3.38}$$

The constraints $L_m = \tilde{L}_m = 0$ ($\forall m \in \mathbb{Z}$) enforce worldsheet reparameterization invariance. Taking the $m = 0$ state, we have

$$L_0 = \sum_{n=1}^{\infty} \alpha_{-n} \cdot \alpha_n + \frac{1}{2}\alpha_0^2 = 0, \tag{3.39}$$

$$\tilde{L}_0 = \sum_{n=1}^{\infty} \tilde{\alpha}_{-n} \cdot \tilde{\alpha}_n + \frac{1}{2}\tilde{\alpha}_0^2 = 0. \tag{3.40}$$

Substituting $\alpha_0^\mu = \tilde{\alpha}_0^\mu = \sqrt{2\alpha'}p^\mu$ and $p^2 = -M^2$ yields the classical mass formulae for open

$$M^2 = \frac{1}{\alpha'} \sum_{n=1}^{\infty} \alpha_{-n} \cdot \alpha_n, \tag{3.41}$$

and closed strings

$$M^2 = \frac{2}{\alpha'} \sum_{n=1}^{\infty} \left(\alpha_{-n} \cdot \alpha_n + \tilde{\alpha}_{-n} \cdot \tilde{\alpha}_n \right). \tag{3.42}$$

Unfortunately, the quantum Virasoro generators: $L_m = \frac{1}{2} \sum_{n \in Z} \alpha_{m-n} \cdot \alpha_n$ (and $\tilde{L}_m$ also for closed strings) inherit normal-ordering ambiguities in L_0.

So, we define the regularized L_0:

$$L_0 = \frac{1}{2}\alpha_0^2 + \sum_{n=1}^{\infty} \alpha_{-n} \cdot \alpha_n - a, \tag{3.43}$$

where a is a "normal ordering" constant that resolves operator ordering, physical states satisfy $(L_n - a\delta_{n,0}) \left|\text{phys}\right\rangle = 0$ for $n \geq 0$. For closed strings, level matching enforces equality of left- and right-moving excitations:

$$(L_0 - \tilde{L}_0) \left|\text{phys}\right\rangle = \sum_{n=1}^{\infty} \left(\alpha_{-n} \cdot \alpha_n - \tilde{\alpha}_{-n} \cdot \tilde{\alpha}_n \right) \left|\text{phys}\right\rangle = 0, \tag{3.44}$$

where $N = \sum_{n=1}^{\infty} \alpha_{-n} \cdot \alpha_n$ is nothing other than the number operator. This implies that the number of left- and right-moving modes are equal for physical states, or

$$(N - \tilde{N}) \left|\text{phys}\right\rangle = 0. \tag{3.45}$$

The quantum mass formulae follow from the same logic, for open strings we have

$$\alpha' M^2 = \sum_{n=1}^{\infty} \alpha_{-n} \cdot \alpha_n - a = N - a, \tag{3.46}$$

and for closed strings

$$\alpha' M^2 = 2\left(\sum_{n=1}^{\infty}\left(\alpha_{-n}\cdot\alpha_n + \tilde{\alpha}{-n}\cdot\tilde{\alpha}n\right) - 2a\right) = 2N + 2\tilde{N} - 4a. \tag{3.47}$$

We now run into a problem, suppose we demand the open string have a massless spin-1 state, we would act on the vacuum:

$$\alpha^{\mu}_{-1}\left|0;p\right\rangle = \left|A^{\mu}\right\rangle. \tag{3.48}$$

For this state to be massles fixes $a = 1$ as we have $\alpha' M^2 = 1 - a$. This then exposes a tachyon: $M^2 = -1/\alpha'$ at $N = 0$. The closed string's $N = \tilde{N} = 1$ sector also contains a massless state of spin-2:

$$\alpha^{\mu}_{-1}\tilde{\alpha}^{\nu}_{-1}\left|0;p\right\rangle = \left|T^{\mu\nu}\right\rangle = G^{\mu\nu} + B^{\mu\nu} + \eta^{\mu\nu}\varphi, \tag{3.49}$$

which decomposes into a symmetric, traceless graviton $G_{\mu\nu}$ (which mediates spacetime curvature), an antisymmetric Kalb-Ramond two-form $B_{\mu\nu}$, and a dilaton φ. The Kalb-Ramond field (a generalization of electromagnetism to the string worldsheet) couples to the string via:

$$S_B = -\frac{T}{2}\int d\tau d\sigma, \epsilon^{ab}B_{\mu\nu}(x)\,\partial_a x^{\mu}\,\partial_b x^{\nu}, \tag{3.50}$$

analogous to a point particle's coupling $-q\int A_{\mu}dx^{\mu}$.

The quantum Virasoro algebra [43] acquires a central extension:

$$\left[L_m, L_n\right] = (m-n)L_{m+n} + \frac{c}{12}m(m^2-1)\,\delta_{m+n,0}, \tag{3.51}$$

with central charge $c = d$ (where d is the spacetime dimension). Ghost contributions from gauge-fixing yield $c_{\text{ghost}} = -26$. Cancelling the total central charge $c_{\text{total}} = d - 26 = 0$ mandates $d = 26$. Lorentz invariance provides an independent confirmation: computing $\left[J^{i-}, J^{j-}\right]$ in light-cone gauge ($x^+ = x_0^+ + \alpha' p^+\tau$) produces anomalies proportional to $(d-26)$, which vanish $\iff d = 26$.

The quantum-effective action coupling spacetime fields generalizes to:

$$S = -\frac{T}{2}\int d\tau d\sigma, \sqrt{-\det h_{ab}}\left[\left(h^{ab}G_{\mu\nu}(x) + \epsilon^{ab}B_{\mu\nu}(x)\right)\partial_a x^{\mu}\,\partial_b x^{\nu} - \alpha' R\varphi(x)\right], \tag{3.52}$$

where ϵ^{ab} is the 2D, totally antisymmetric tensor and R is the 2D Ricci scalar of the geometry. The dilaton term

$$\frac{1}{4\pi}\int d\tau d\sigma \sqrt{-\det h_{ab}} R\varphi(x), \tag{3.53}$$

contributes $\chi\varphi$. For constant $\varphi = \varphi_0$, the integral determines the Euler characteristic via the Gauss-Bonnet theorem: $\chi = 2-2g-b$ (with g the genus and b the number of boundaries). In the path integral, this weights scattering amplitudes by $g_s^{-\chi}$, with $g_s = e^{\varphi_0}$, determining interaction strength for different topologies (e.g., suppressing loop corrections as g_s^{2g}).

Despite unifying gravity and gauge interactions, the bosonic string's tachyon and lack of fermions necessitate superstrings. Introducing worldsheet supersymmetry adds fermionic partners ψ^μ, eliminates the tachyon via the GSO projection, and reduces the critical dimension to $d = 10$. The closed string's massless spin-2 graviton persists, while open strings host non-Abelian gauge fields on D-branes, non-perturbative objects revealed by T-duality.

3.3 Superstring Theory

The bosonic string theory, while geometrically elegant, suffers from two fundamental limitations that preclude its viability as a physical theory: the presence of a tachyonic ground state signaling vacuum instability, and the absence of fermionic degrees of freedom essential for describing matter. These deficiencies necessitate the introduction of supersymmetry - a symmetry relating bosons and fermions - directly on the string worldsheet pioneered by Ramond [44] for fermions and, at roughly the same time by Neveu and Schwarz [45] who combined their model with Ramond's into a "quark model of dual pions" [46]. Superstring theory thus emerged as the minimal extension that pairs each bosonic coordinate field $x^\mu(\tau,\sigma)$ with a fermionic counterpart $\psi^\mu(\tau,\sigma)$, transforming the worldsheet into a two-dimensional superconformal field theory [47]. This extension accomplishes three critical objectives: it enables the emergence of spacetime fermions, provides a natural mechanism for tachyon elimination, and reduces the critical spacetime dimension from 26 to 10, aligning with potential phenomenological relevance.

The complete Ramond-Neveu-Schwarz (RNS) action, which respects worldsheet supersymmetry, is

$$S_{\text{RNS}} = -\frac{T}{2}\int d\tau d\sigma \sqrt{-\det h_{ab}}\left(g_{\mu\nu}h^{ab}\partial_a x^\mu \partial_b x^\nu + 2i\alpha' g_{\mu\nu}\bar{\psi}^\mu \rho^a D_a \psi^\nu + g_{\mu\nu}F^\mu F^\nu\right), \tag{3.54}$$

The incorporation of fermionic degrees of freedom requires careful treatment of spinor representations on curved worldsheets. Unlike general coordinate transformations (which belong to

$\mathrm{GL}(d, \mathbb{R})$ and lack spinor representations), Lorentz transformations in locally inertial frames ($\mathrm{SO}(1, d-1)$) naturally accommodate spinors. This necessitates the *vielbein formalism*, where we introduce the spacetime vielbein:

$$g_{\mu\nu} = e^a_\mu e^b_\nu \eta_{ab}, \tag{3.55}$$

which allows us to swap the Einstein indices (μ, ν) of the manifold for the Lorentz indices (a, b) of the local Minkowski spacetime. Alongside this we define the worldsheet zweibein:

$$h_{ab} = e^\alpha_a e^\beta_b \eta_{\alpha\beta}, \tag{3.56}$$

from which we may define

$$\det h_{ab} = (\det e^\alpha_a)^2 \det \eta_{\alpha\beta}, \tag{3.57}$$

or alternately

$$\sqrt{-\det h_{ab}} = |\det e^\alpha_a| \tag{3.58}$$

The zweibein thus serves as the "square root of the metric", providing the scaffolding for spinor fields. The Ramond-Neveu-Schwarz (RNS) action, can be rewritten as

$$S_{\mathrm{RNS}} = -\frac{T}{2}\int d\tau d\sigma |\det e^\alpha_a| \left(\eta_{ab} h^{cd} \partial_c x^a \partial_d x^b + 2i\alpha' \eta_{ab} \bar{\psi}^a \rho^c D_c \psi^b + \eta_{ab} F^a F^b\right), \tag{3.59}$$

where $X^a = e^a_\mu X^\mu$ and $\rho^a = e^a_\alpha \rho^\alpha$ are worldsheet Dirac matrices satisfying the Clifford algebra $\{\rho^\alpha, \rho^\beta\} = \pm 2\eta^{\alpha\beta}\mathbb{I}_d$. The Majorana condition $\psi^* = \psi$ ensures reality of the fermionic fields and matches the bosonic and fermionic degrees of freedom on-shell. The action manifests three key symmetries: (1) worldsheet reparameterization invariance, (2) local Lorentz symmetry, and (3) $\mathcal{N} = (1, 1)$ supersymmetry mixing x^μ and ψ^μ.

In practice, we work primarily in *superconformal gauge* ($h_{ab} = \eta_{ab}$, $\chi_a = 0$), where the action simplifies to:

$$S = -\frac{T}{2}\int d\tau d\sigma \left(\partial_a x^\mu \partial_b x_\mu + i\eta_{\mu\nu} \bar{\psi}^\mu \rho^a \partial_a \psi_\mu\right). \tag{3.60}$$

Varying this action yields elegantly decoupled equations of motion:

$$\Box x^\mu = 0, \tag{3.61}$$

$$\rho^a \partial_a \psi^\mu = 0, \tag{3.62}$$

which in light-cone coordinates reveal chiral propagation:

$$\partial_+ \psi_-^\mu = \partial_- \psi_+^\mu = 0, \tag{3.63}$$

where ψ_+^μ and ψ_-^μ are the left and right Majorana components of the Dirac fermion. The boundary terms from variation impose critical endpoint constraints:

$$[\bar{\psi}\, \delta\psi]_{\sigma=0}^{\sigma=\pi} = 0, \tag{3.64}$$

whose resolution profoundly impacts the string's physical spectrum.

The freedom in satisfying these boundary conditions generates distinct sectors with dramatically different physical interpretations:

For **open strings**, the endpoints $\sigma = 0, \pi$ require correlated fermion fields:

- *Ramond (R) sector*: Periodic boundary conditions $\psi_\pm^\mu(\pi) = +\psi_\mp^\mu(\pi)$ imply integer-moded excitations:

$$\psi_\pm^\mu(\tau, \sigma) = \frac{1}{\sqrt{2}} \sum_{n \in \mathbb{Z}} d_n^\mu e^{-in\sigma^\pm}, \quad (d_n^\mu)^\dagger = d_{-n}^\mu \tag{3.65}$$

  Physically, periodicity allows fermionic strings to close smoothly, yielding *spacetime fermions* upon quantization. The zero modes d_0^μ will generate a Clifford algebra, foreshadowing spinorial states.

- *Neveu-Schwarz (NS) sector*: Antiperiodic conditions $\psi_\pm^\mu(\pi) = -\psi_\mp^\mu(\pi)$ enforce half-integer moding:

$$\psi_\pm^\mu(\tau, \sigma) = \frac{1}{\sqrt{2}} \sum_{r \in \mathbb{Z}+\frac{1}{2}} b_r^\mu e^{-ir\sigma^\pm}, \quad (b_r^\mu)^\dagger = b_{-r}^\mu \tag{3.66}$$

  Antiperiodicity introduces a topological twist, resulting in *spacetime bosons*. The absence of zero modes distinguishes this sector.

For **closed strings**, independent periodicity choices for left/right-movers generate four distinct sectors:

$$
\begin{aligned}
&\text{(R,R):} && \psi_+^\mu = \sum_n d_n^\mu e^{-in\sigma^+}, && \psi_-^\mu = \sum_n \tilde{d}_n^\mu e^{-in\sigma^-} \\
&\text{(NS,NS):} && \psi_+^\mu = \sum_r b_r^\mu e^{-ir\sigma^+}, && \psi_-^\mu = \sum_r \tilde{b}_r^\mu e^{-ir\sigma^-} \\
&\text{(R,NS):} && \psi_+^\mu = \sum_n d_n^\mu e^{-in\sigma^+}, && \psi_-^\mu = \sum_r \tilde{b}_r^\mu e^{-ir\sigma^-} \\
&\text{(NS,R):} && \psi_+^\mu = \sum_r b_r^\mu e^{-ir\sigma^+}, && \psi_-^\mu = \sum_n \tilde{d}_n^\mu e^{-in\sigma^-}
\end{aligned}
$$

The (R,R) and (NS,NS) sectors produce spacetime bosons (including the graviton), while the mixed (R,NS) and (NS,R) sectors yield spacetime fermions. This structure naturally accommodates matter and force carriers within a unified framework.

Canonical quantization promotes fields to operators with anticommutation relations:

$$\{d_m^\mu, d_n^\nu\} = m\eta^{\mu\nu}\delta_{m,-n}, \quad \{b_r^\mu, b_s^\nu\} = \eta^{\mu\nu}\delta_{r,-s} \tag{3.67}$$

The super-Virasoro constraints - quantum analogues of $T_{ab} = 0$ and $J_a = 0$ - eliminate negative-norm states and enforce critical consistency conditions:

- *Spacetime dimension*: The superconformal anomaly cancellation requires $d = 10$, reconciling quantum consistency with Lorentz invariance. This reduction from 26 dimensions occurs because fermionic degrees of freedom contribute negatively to the central charge.
- *Mass-shell conditions* for open strings reveal sector-dependent spectra:

$$\text{R:} \quad \alpha' M^2 = \sum_{n=1}^{\infty} \alpha_{-n}^i \cdot \alpha_n^i + \sum_{n=1}^{\infty} n d_{-n}^i \cdot d_n^i \tag{3.68}$$

$$\text{NS:} \quad \alpha' M^2 = \sum_{n=1}^{\infty} \alpha_{-n}^i \cdot \alpha_n^i + \sum_{r=\frac{1}{2}}^{\infty} r b_{-r}^i \cdot b_r^i - \frac{1}{2}, \quad i = 1, ..., 8 \tag{3.69}$$

- *R ground state*: The zero modes satisfy $\{d_0^\mu, d_0^\nu\} = \eta^{\mu\nu}$, forming a Dirac algebra. The degenerate ground state transforms as a $SO(9,1)$ spinor, providing the seed for spacetime supersymmetry.
- *NS ground state*: At an excitation level of zero, $\alpha' M^2 = -1/2$ signifies a persistent tachyon — a relic of bosonic string instability. This will be resolved in the next section via the GSO projection.

This quantization framework demonstrates a remarkable emergence of spacetime structure: vibrational modes of the string directly correspond to particle states, with R-sector excitations generating fermionic matter and NS-sector modes producing bosonic force carriers. The persistent

NS tachyon and mismatched boson/fermion degrees of freedom indicate that this is not the final physical theory. A consistent truncation of the Hilbert space - the GSO projection - is required to eliminate unphysical states and enable spacetime supersymmetry.

3.4 The GSO Projection

The RNS superstring quantization, while resolving the critical dimension issue, retains a fundamental pathology: the NS sector contains a tachyonic ground state with $\alpha' M^2 = -1/2$, signaling vacuum instability. Furthermore, the spectrum lacks the boson-fermion degeneracy required for spacetime supersymmetry. These issues are resolved by the Gliozzi-Scherk-Olive (GSO) projection [48], a consistent truncation of the Hilbert space that eliminates the tachyon, enforces spacetime supersymmetry, and distinguishes between type IIA and IIB theories.

The GSO projection is implemented via parity operators acting on the oscillator Fock spaces. For the NS sector, we define the G-parity operator:

$$G_{\text{NS}} = (-1)^{F+1}, \tag{3.70}$$

with

$$F = \sum_{r=\frac{1}{2}}^{\infty} b^i_{-r} b^i_r, \tag{3.71}$$

where F counts the number of b-oscillator excitations (summed over transverse spatial indices $i = 1, \ldots, 8$). Physical states must satisfy:

$$G_{\text{NS}} \left|\psi\right\rangle = + \left|\psi\right\rangle \tag{3.72}$$

The NS ground state $\left|0\right\rangle_{\text{NS}}$ has $F = 0$, yielding $G_{\text{NS}} \left|0\right\rangle_{\text{NS}} = (-1)^{0+1} \left|0\right\rangle_{\text{NS}} = - \left|0\right\rangle_{\text{NS}}$, and is therefore projected out. The first excited state $b^\mu_{-1/2} \left|0\right\rangle_{\text{NS}}$ has $F = 1$ (since $b_{-1/2} \cdot b_{1/2} = 1$), giving $G_{\text{NS}} b^\mu_{-1/2} \left|0\right\rangle_{\text{NS}} = (-1)^{1+1} b^\mu_{-1/2} \left|0\right\rangle_{\text{NS}} = + b^\mu_{-1/2} \left|0\right\rangle_{\text{NS}}$, and is retained. This state is massless ($\alpha' M^2 = 0$) and transforms as a vector under $SO(8)$, corresponding to the gauge boson.

For the R sector, the projection incorporates spacetime chirality:

$$G_{\text{R}} = \rho_{11} (-1)^F, \tag{3.73}$$

with

$$F = \sum_{n=1}^{\infty} d^i_{-n} d^i_n, \tag{3.74}$$

where we define F such that $(-1)^F = +1$ for even excitations and where $\rho_{11} = \prod_{\mu=0}^{9} \rho_\mu$ is the ten-dimensional chirality operator satisfying $(\rho_{11})^2 = 1$ and $\{\rho_{11}, \rho_\mu\} = 0$. The R ground state $|\mathbf{s}\rangle_{\mathrm{R}}$, being a $SO(9,1)$ Dirac spinor, decomposes into Weyl representations $|\mathbf{s}_+\rangle_{\mathrm{R}} \oplus |\mathbf{s}_-\rangle_{\mathrm{R}}$ so then

$$\rho_{11} |\mathbf{s}_\pm\rangle_{\mathrm{R}} = \pm |\mathbf{s}_\pm\rangle_{\mathrm{R}} . \tag{3.75}$$

The projection $G_{\mathrm{R}} |\psi\rangle = \pm |\psi\rangle$ (with consistent sign choice) selects definite chirality states. Since $F = 0$ for the ground state, $G_{\mathrm{R}} |\mathbf{s}\rangle_{\mathrm{R}} = \rho_{11} |\mathbf{s}\rangle_{\mathrm{R}}$, so the projection is equivalent to $\rho_{11} |\mathbf{s}\rangle_{\mathrm{R}} = \pm |\mathbf{s}\rangle_{\mathrm{R}}$.

For closed strings, independent GSO projections on left- and right-movers generate distinct theories. The chirality choice in the R-sector distinguishes the two consistent theories. In *Type IIA*, we apply left-moving R sector with negative chirality (R−) and right-moving R sector with positive chirality (R+):

$$G^{(L)}_{\mathrm{R}} |\psi\rangle = - |\psi\rangle \quad (\mathrm{R}-), \tag{3.76}$$
$$G^{(R)}_{\mathrm{R}} |\psi\rangle = + |\psi\rangle \quad (\mathrm{R}+) \tag{3.77}$$

yielding a non-chiral theory with $\mathcal{N} = (1,1)$ supersymmetry. For *Type IIB*, both left and right R sectors have negative chirality (R−):

$$G^{(L)}_{\mathrm{R}} |\psi\rangle = - |\psi\rangle , \tag{3.78}$$
$$G^{(R)}_{\mathrm{R}} |\psi\rangle = - |\psi\rangle \tag{3.79}$$

producing a chiral theory with $\mathcal{N} = (2,0)$ supersymmetry.

The GSO-projected massless spectra exhibit boson-fermion degeneracy and tachyon freedom. Crucially, the NS-NS sector contains an additional six-form field dual to the Kalb-Ramond field:

The six-form $B^{(6)}$ couples magnetically to the *NS5-brane*, a solitonic object that arises non-perturbatively. This is analogous to the Kalb-Ramond field coupling electrically to strings seen in Eq. (3.50). The R-R p-forms $C^{(p)}$ couple to D-branes.

The GSO projection corresponds to summing over spin structures on worldsheets with non-contractible loops [49], ensuring modular invariance at higher genera, cancellation of unphysical sectors, and emergence of spacetime supersymmetry. The term “G-parity” originates from

Sector	Type IIA	Type IIB
(NS,NS)	$G_{\mu\nu}$: graviton $B_{\mu\nu}$: Kalb-Ramond φ : dilaton $B^{(6)}$: 6-form dual to $B_{\mu\nu}$	Same as IIA
(R,R)	$C^{(1)}$: vector $C^{(3)}$: 3-form	$C^{(0)}$: axion $C^{(2)}$: 2-form $C^{(4)}$: 4-form
(NS,R) + (R,NS)	$\psi_\mu^\pm$: gravitini (opposite chirality)	ψ_μ^+ : gravitini (both positive chirality)

TABLE 3.1: Massless spectra of type II superstrings.

hadronic physics, and the GSO projection [48] was pivotal in establishing string theory as a supersymmetric framework.

The GSO projection thus achieves three critical objectives: eradicating tachyonic instability, enforcing spacetime supersymmetry, and distinguishing consistent closed string theories. The R-R sector p-forms $C^{(p)}$ emerging from GSO projection couple naturally to extended dynamical objects in spacetime, the D-branes, which we will explore next.

3.5 D-Branes

D-branes are dynamical $(p+1)$-dimensional hypersurfaces in spacetime where open strings with Dirichlet boundary conditions terminate. As introduced in 3.1, Dirichlet conditions $\delta x^\mu = 0$ fix string endpoints to these hypersurfaces, breaking translational symmetry in transverse directions. While initially appearing as rigid constraints, T-duality reveals D-branes are fundamental non-perturbative objects essential for string consistency.

T-duality, a target-space duality under circle compactification, relates distinct string theories. D-branes emerge as necessary for its consistency in open string sectors. Consider compactifying x^9 on S^1 with radius R. Closed strings gain Kaluza-Klein momenta $p^9 = K/R$ ($K \in \mathbb{Z}$) and winding numbers $W \in \mathbb{Z}$, with mass spectrum:

$$\tilde{M}^2 = M^2 + \frac{K^2}{R^2} + \frac{W^2 R^2}{\alpha'^2} + \text{oscillator terms.} \tag{3.80}$$

This is invariant under T-duality:

$$R \leftrightarrow \frac{\alpha'}{R}, \quad K \leftrightarrow W, \tag{3.81}$$

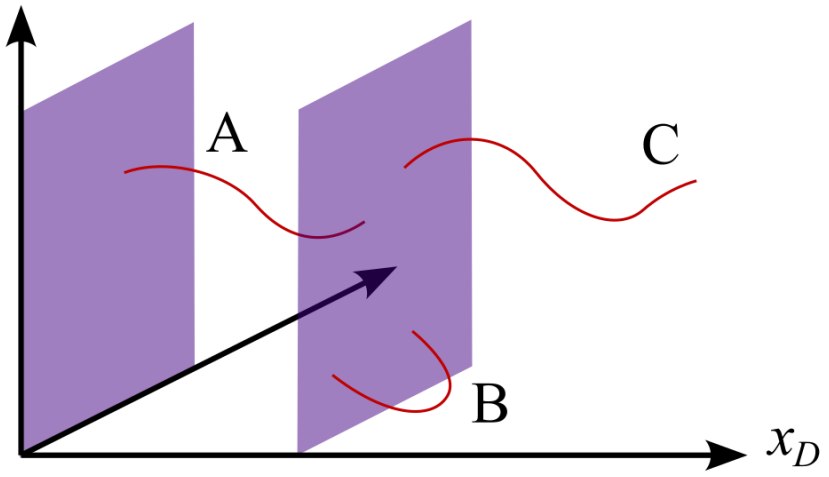

FIGURE 3.1: D-branes as hypersurfaces anchoring open strings: (A) stretched between distinct branes, (B) on a single brane, (C) with one Dirichlet endpoint.

which exchanges momentum and winding modes. For open strings with Neumann conditions, winding modes are absent. As $R \to 0$:

- Closed strings retain winding modes (light when $R \ll \sqrt{\alpha'}$)
- Neumann open strings lose access to x^9, seeing only 9D spacetime

This inconsistency violates T-duality, as open strings "detect" the compactification size. Resolution requires recognizing that T-duality along x^9 transforms Neumann $\leftrightarrow$ Dirichlet conditions:

- Neumann open string at large $R \xrightarrow{\text{T-duality}}$ Dirichlet open string at small $\tilde{R} = \alpha'/R$
- Endpoints become fixed to a $(p+1)$D hypersurface (Dp-brane)

Thus D-branes emerge [8] as necessary for T-duality invariance in open string sectors. These D-branes provide the foundation for holographic matter introduction via probe branes, as we will see in 4.3.

D-branes are electrically charged under type II Ramond-Ramond (R-R) p-form gauge fields $C^{(q)}$. The field strength $dC^{(4)} = F^{(5)}$ in IIB is self-dual ($*F^{(5)} = F^{(5)}$), making D3-branes special as they carry self-dual charge. Magnetic couplings follow from Hodge duality: Dp-branes magnetically couple to $C^{(7-p)}$ This is summarized in tables 3.2 and 3.3.

p-form	Electrically coupled brane	Magnetically coupled brane
$C^{(0)}$	D(-1)	D7
$C^{(2)}$	D1	D5
$C^{(4)}$	D3	D3
$C^{(6)}$	D5	D1
$C^{(8)}$	D7	D(-1)
$C^{(10)}$	D9	

Table 3.2: D-brane content of Type IIB string theory

p-form	Electrically coupled brane	Magnetically coupled brane
$C^{(1)}$	D0	D6
$C^{(3)}$	D2	D4
$C^{(5)}$	D4	D2
$C^{(7)}$	D6	D0
$C^{(9)}$	D8	

Table 3.3: D-brane content of Type IIA string theory

3.5.1 The Dirac-Born-Infeld Action

The bosonic Dp-brane [8] action combines Dirac-Born-Infeld (DBI) and Chern-Simons (CS) terms:

$$S_{\mathrm{D}p} = -\mu_p \int d^{p+1}\xi e^{-\varphi}\sqrt{-\det\left(\mathcal{G}_{ab} + \mathcal{B}_{ab} + 2\pi\alpha' F_{ab}\right)} + \mu_p \int \sum_q \mathcal{C}_{(q+1)} \wedge e^{\mathcal{B}+2\pi\alpha' F} \tag{3.82}$$

where, examining the DBI term first we have

$$\mathcal{G}_{ab} = G_{\mu\nu}\partial_a x^\mu \partial_b x^\nu, \tag{3.83}$$

$$\mathcal{B}_{ab} = B_{\mu\nu}\partial_a x^\mu \partial_b x^\nu, \tag{3.84}$$

are the pullbacks of the metric and Kalb-Ramond antisymmetric tensor, ξ^a are the $p+1$ coordinates of the worldvolume, $\mu_p = \frac{1}{(2\pi\sqrt{\alpha'})^p\sqrt{\alpha'}} g_s^{-1}$ is the tension/charge of the D-brane, and F_{ab} is the field strength tensor associated to the additional U(1) gauge field induced by open string fluctuations on the brane. The DBI action is the generalization of the NG action from strings to higher dimensional surfaces. (Unfortunately, there is no equivalent analogue to the Polyakov action for D-branes).

The second, CS term, encodes the coupling of RR-forms to the D-brane, where the $C_{(q+1)}$ are the RR-forms sourced by other, Dq-branes in the system. For this reason, the CS term is of interest in systems with multiple D-branes. When $q < p$ and $\frac{1}{2}(p-q) \in \mathbb{Z}$, a D$p$-brane may couple to a $q+1$ form. Type II theories automatically satisfy the second condition, having only odd (IIA) or even (IIB) p and q. So then, if $q < p$, the brane will couple to the $q+1$ form via repeated wedge products of $\mathcal{B} + F$.

For N coincident D-branes, indices known as Chan-Paton factors [50] identify which brane in the stack each string endpoint attaches to. The low-energy worldvolume theory of a stack of N Dp-branes is a maximally supersymmetric $U(N)$ Yang-Mills theory in $p+1$ dimensions, possessing 16 supercharges. The specific amount of supersymmetry is denoted differently depending on the dimension; e.g. in 4D on a D3-brane we get $\mathcal{N} = 4$ SYM, while for 10D on a D9-brane the same field content gives $\mathcal{N} = 1$ SYM.

From the perspective of closed strings and supergravity, D-branes are massive, extended objects that curve spacetime. They are described by specific black p-brane (geometric generalizations of black holes to p spatial dimensions) solutions to type II supergravity [51]. The extremal limit of these solutions - stable states whose mass is exactly equal to their Ramond-Ramond charge, saturating the Bogomol'nyi-Prasad-Sommerfield (BPS) bound - was identified with the D-branes of string theory in [8]. In this picture, a stack of N Dp-branes sources the following supergravity solution (in the string frame):

$$ds^2 = H(r)^{-\frac{1}{2}} dx_{\parallel}^2 + H(r)^{\frac{1}{2}} (dr^2 + r^2 d\Omega_{8-p}^2) \tag{3.85}$$

$$F_{01\ldots pr} = \partial_m (H(r)^{-1}), \tag{3.86}$$

$$H(r) = 1 + \frac{\alpha}{r^{7-p}}, \quad p < 7, \tag{3.87}$$

$$e^{\varphi} = H(r)^{\frac{3-p}{4}}, \tag{3.88}$$

$$\alpha = (4\pi)^{\frac{5-p}{2}} \Gamma\left(\frac{7-p}{2}\right) (\alpha')^{\frac{7-p}{2}} g_s N \tag{3.89}$$

The interplay between these two descriptions - the gauge theory on the branes and the gravitational geometry they source - is the foundation of the gauge/gravity duality. This is importantant for our purposes in D3-branes, where the geometry near the horizon ($r \to 0$ in $H(r)$) becomes $AdS_5 \times S^5$, leading to the AdS/CFT correspondence [10] which we will explore in the next chapter.

Chapter 4

Gauge/Gravity Duality

4.1 The AdS/CFT Conjecture

The AdS/CFT correspondence, first proposed by Maldacena in [10], establishes a remarkable equivalence between gravitational theories in anti-de Sitter (AdS) spacetime and conformal field theories (CFTs) living on its boundary [52, 53, 54, 55]. This profound duality emerges naturally from considering the physics of D-branes in string theory from two complementary perspectives, analogous to describing an electron-proton system: one can either study the detailed interactions through Feynman diagrams (open string perspective) or examine motion in a background field (closed string perspective).

4.1.1 Motivating the Conjecture

Consider N_c coincident D3-branes in type IIB string theory, extending along the (x^0, x^1, x^2, x^3) directions. Their low-energy dynamics admit two distinct interpretations governed by the value of the 't Hooft coupling $\lambda = g_s N_c$, given both interpretations must describe the same physics, we insist that the two limit cases are equivalent. This equivalence motivates AdS/CFT.

Open String Perspective ($\lambda \ll 1$): When λ is small, the gravitational backreaction of the branes is negligible. The stress-energy tensor scales as $T_{\text{brane}} \sim \lambda/\kappa_{10}$, where $\kappa_{10} \sim g_s \alpha'^2$ is the 10D gravitational constant. In the low-energy limit ($\alpha' \to 0$), the full action can be expressed in terms of three sectors:

$$S = S_{\text{brane}} + S_{\text{bulk}} + \cancel{S_{\text{int}}}^{\,0}. \tag{4.1}$$

The D3-brane action S_{brane} reduces (via the decoupling of the U(1) centre-of-mass) to $\mathcal{N} = 4$ SU(N_c) super Yang-Mills theory in 4D, with bosonic sector:

$$S_{\rm SYM} = \frac{2}{g_{\rm YM}^2}\int d^4x\,{\rm Tr}\left(-\frac{1}{4}F_{\mu\nu}F^{\mu\nu} - \frac{1}{2}D_\mu\Phi^i D^\mu\Phi^i + \cdots\right), \quad g_{\rm YM}^2 = 4\pi g_s. \tag{4.2}$$

This theory is conformally invariant ($\beta = 0$ to all orders) and possesses an $SO(6)_R$ symmetry rotating its six scalar fields Φ^i, which parameterize transverse brane fluctuations. $S_{\rm bulk}$ contains the closed string states in type IIB supergravity. The interaction term $S_{\rm int}$ vanishes because its coupling scales as $g_s\alpha'^2 \to 0$, this decouples the brane and bulk actions as

$$({\rm SU}(N_c)\mathcal{N} = 4{\rm SYM\ Gauge\ Theory}) \oplus ({\rm IIB\ supergravity\ in\ 10D}). \tag{4.3}$$

Closed String Perspective ($\lambda \gg 1$): For large λ, the branes' gravitational backreaction significantly warps spacetime. The solution to Einstein's equations

$$R_{MN} - \frac{1}{2}g_{MN}R = 8\pi\kappa_{10}T_{MN}^{\rm brane} \tag{4.4}$$

yields the metric:

$$ds^2 = \left(1+\frac{R^4}{r^4}\right)^{-1/2}\eta_{ij}dx^i dx^j + \left(1+\frac{R^4}{r^4}\right)^{1/2}(dr^2 + r^2 d\Omega_5^2), \tag{4.5}$$

where $i,j = 0,1,2,3$ are the directions parallel to the D3-branes and r, Ω_5 are the radial and angular coordinates that describe the transverse plane with $r = \sqrt{\sum_{i=4}^{9} x_i^2}$. We have

$$R^4 = 4\pi\lambda\alpha'^2, \tag{4.6}$$

which sets the radius of the curvature of the space[56], i.e. the supergravity limit is only valid when the curvature is low.

The decoupling of the near-horizon physics is somewhat subtle. Naïvely taking $\alpha' \to 0$ in Eq. (4.6) would simply return us to 10D Minkowski space, as $H(r) \to 1$. However, the physically relevant low-energy limit, often called the *Maldacena* or *decoupling limit*, requires simultaneously taking $\alpha' \to 0$ while keeping the energy scale $U \equiv r/\alpha'$ fixed. This fixed scale U corresponds to the mass of W-bosons, i.e. $m_W \sim U$, arising from strings stretched between the stack of N_c D3-branes and a probe brane a distance r away.

In this combined limit, the constant 1 in the harmonic function $H(r) = 1+\frac{R^4}{r^4}$ becomes negligible compared to $\frac{R^4}{r^4} \sim \frac{\lambda}{U^4}$. The region described by $r \ll R$ is therefore 'zoomed into'. The geometry in this limit becomes

$$ds^2 = \alpha'\left[\frac{U^2}{L^2}(-dt^2 + d\vec{x}^2) + \frac{L^2}{U^2}dU^2 + L^2 d\Omega_5^2\right], \tag{4.7}$$

which, up to the overall factor of α' is that of $AdS_5 \times S^5$. Henceforth, we will indulge in some abuse of notation, and relabel this AdS radius L as R, with $R^4 = 4\pi\lambda\alpha'^2$, and also use r to denote the radial coordinate proportional to U. The resulting near-horizon geometry is then given by

$$ds^2 = \frac{r^2}{R^2}(-dt^2 + d\vec{x}^2) + \frac{R^2}{r^2}dr^2 + R^2 d\Omega_5^2. \tag{4.8}$$

An observer at infinity ($r \to \infty$) measures redshifted energies for strings near $r = r_0$:

$$E_\infty = \sqrt{-G_{tt}}\,\tilde{E} = \left(1 + \frac{R^4}{r_0^4}\right)^{-1/4} \tilde{E}, \tag{4.9}$$

where G_{tt} is the time-time metric component. As $r_0 \to 0$, $E_\infty \to 0$ regardless of $\tilde{E}$, implying all near-horizon modes appear low-energy to the asymptotic observer. In the $\alpha' \to 0$ limit, near-horizon and asymptotic regions decouple as

$$\text{(IIB superstring theory on } AdS_5 \times S^5) \oplus \text{(IIB supergravity in 10D)}. \tag{4.10}$$

4.1.2 Maldacena's Conjecture

Comparing both perspectives in the low-energy limit ($\alpha' \to 0$), Maldacena [10] conjectured their equivalence:

$$\boxed{\mathcal{N} = 4 \text{ SU}(N_c) \text{ SYM Gauge Theory} \quad \longleftrightarrow \quad \text{Type IIB Superstring Theory on } AdS_5 \times S^5} \tag{4.11}$$

This correspondence is governed by precise parameter mappings that establish the quantitative relationship between gauge theory and gravity descriptions. The 't Hooft coupling $\lambda = g_{\text{YM}}^2 N_c$ in the SYM theory corresponds to $4\pi g_s N_c$ in the string theory, where g_s is the string coupling. This identification is crucial as it determines the validity regimes: when $\lambda \gg 1$, the large curvature radius $R^4 = 4\pi\lambda\alpha'^2$ ensures small spacetime curvatures ($R^2/\alpha' \gg 1$), permitting classical supergravity approximations in the bulk. Conversely, when $\lambda \ll 1$, perturbative SYM calculations become reliable while stringy corrections dominate the gravitational side. Furthermore, the large-N_c limit ($N_c \to \infty$ with λ fixed) corresponds to weakly coupled (classical) string theory, where $1/N_c$ serves as the string loop-counting parameter and with $g_s = \lambda/(4\pi N_c) \to 0$ suppressing quantum loops. These mappings collectively provide a non-perturbative definition of both theories, with the dimensionless parameters λ and N_c controlling the approximation schemes on either side of the duality.

4.1.3 Symmetry Matching

The consistency of the duality is anchored in the exact matching of global symmetries between both descriptions, which constrains their dynamics and operator spectra.

The **conformal symmetry** manifests identically through the $SO(2,4)$ group. In $\mathcal{N} = 4$ SYM, this includes Poincaré transformations $x^\mu \to \Lambda^\mu_\nu x^\nu + a^\mu$, scaling $x^\mu \to \lambda x^\mu$, and special conformal transformations, with exact conformal invariance confirmed by the vanishing β-function to all orders. Remarkably, these transformations are realized geometrically in AdS_5 as its isometries, where scaling acts as $r \to r/\lambda$:

$$ds^2 \to \frac{(r/\lambda)^2}{R^2}\eta_{\mu\nu}(\lambda dx^\mu)(\lambda dx^\nu) + \frac{R^2}{(r/\lambda)^2}d(r/\lambda)^2 = \frac{r^2}{R^2}\eta_{\mu\nu}dx^\mu dx^\nu + \frac{R^2}{r^2}dr^2 = ds^2. \quad (4.12)$$

This identification establishes the radial coordinate r as encoding renormalization group (RG) flow, with $r \to \infty$ (boundary) corresponding to the UV and $r \to 0$ (interior) to the IR.

The **R-symmetry** $\mathrm{SO}(6)_R \simeq \mathrm{SU}(4)_R$ in SYM rotates the six scalar fields Φ^i and acts on supercharges, with charged operators transforming in its representations. This is precisely mirrored by the isometries of the S^5 factor, whose rotational symmetry provides an identical SO(6) group action. The Kaluza-Klein modes of supergravity fields on S^5 decompose under this symmetry, matching the R-charge quantum numbers of SYM operators. For instance, the spherical harmonics Y^k on S^5 transform in symmetric traceless representations of SO(6), corresponding to chiral primary operators $\mathrm{Tr}(\Phi^{(i_1}\cdots\Phi^{i_k)})$ in the gauge theory.

The **supersymmetry** structure is preserved through the superconformal algebra $\mathrm{PSU}(2,2|4)$, which combines 16 ordinary supersymmetries and 16 conformal supersymmetries into 32 fermionic generators—the maximal possible in any 4D theory. On the gravitational side, the $AdS_5 \times S^5$ background preserves exactly 32 Killing spinors (16 from AdS_5 and 16 from S^5), matching the fermionic generators. This maximal supersymmetry ensures identical protected spectra: BPS operators in SYM correspond to shortened supergravity multiplets, with their scaling dimensions protected from quantum corrections.

Collectively, this symmetry matching provides compelling evidence for the duality. The scaling symmetry $x^\mu \to \lambda x^\mu$, $r \to r/\lambda$ establishes the holographic renormalization group interpretation where motion along r encodes energy scale evolution in the QFT. This geometric realization of RG flow will be central to applications beyond conformal theories.

4.2 Formalizing the Correspondence

4.2.1 Parameter Matching and Correspondence Forms

The AdS/CFT correspondence establishes precise relationships between gauge theory parameters and their gravitational duals. The 't Hooft coupling $\lambda = g_{\mathrm{YM}}^2 N$ maps to string theory parameters through $\lambda = 2\pi g_s N$ and $R^4 = 4\pi\lambda\alpha'^2$, where R is the AdS curvature radius. This reveals λ as the fundamental control parameter determining duality regimes.

In the 't Hooft limit ($g_s \to 0$, $N \to \infty$ with λ fixed), string perturbation theory reduces to genus-zero worldsheets, corresponding to the planar limit of SYM where $1/N$ corrections are suppressed. Here, the string genus expansion directly maps to the $1/N$ expansion in gauge theory, with zero-genus surfaces corresponding to planar diagrams.

When $\lambda \gg 1$, the large curvature radius ($R^2/\alpha' \gg 1$) enables reliable classical supergravity approximations while SYM becomes strongly coupled. This weak/strong duality permits non-perturbative QFT calculations via classical gravity. The correspondence manifests in three primary forms: the *strongest form* (valid for any parameters), the *'t Hooft form* ($g_s \to 0$, fixed R, α'), and the *weak form* ($g_s \to 0$, $R^2/\alpha' \to \infty$) where supergravity dominates. These are summarized in Table 4.1.

Form	String Theory	SYM
Strongest	Any g_σ, R, α'	Any N, λ
't Hooft	$g_\sigma \to 0$, fixed R, α'	$N \to \infty$, λ fixed
Weak	$g_\sigma \to 0$, $R^2/\alpha' \to \infty$	$N \to \infty$, $\lambda \to \infty$

TABLE 4.1: Forms of AdS/CFT correspondence in different parameter limits

4.2.2 Conformal Boundary and Holographic Principle

Taking $r = \frac{1}{\zeta}$, we get the AdS_5 metric in Poincaré coordinates,

$$ds^2 = \frac{R^2}{\zeta^2}(d\zeta^2 + \eta_{\mu\nu}dx^\mu dx^\nu) + R^2 d\Omega_5^2, \tag{4.13}$$

which exhibits its conformal boundary in the limit as $\zeta \to 0$. Under conformal rescaling $g_{\mu\nu} \to (\zeta^2/R^2)g_{\mu\nu}$, this boundary becomes equivalent to 4D Minkowski space. This foliation reveals the holographic nature: bulk physics at radial slice ζ corresponds to QFT at energy scale $E \sim 1/\zeta$, with $\zeta \to 0$ (UV) and $\zeta \to \infty$ (IR).

The holographic principle, inspired by black hole thermodynamics where entropy scales with horizon area $S_{\mathrm{BH}} = A/(4G_N)$ rather than volume, finds explicit realization here. All bulk information is encoded on the boundary, with bulk degrees of freedom scaling exponentially with

area in Planck units, and radial evolution mapping to renormalization group flow. The matching isometry group SO(2,4) of AdS_5 to the conformal group of SYM confirms the boundary encodes bulk symmetries.

4.2.3 Field-Operator Dictionary

The Gubser-Klebanov-Polyakov-Witten (GKPW) formula establishes the core dictionary:

$$Z_{\text{CFT}}[\phi_0] = \left\langle \exp\left(\int d^4x \phi_0(\vec{x}) \mathcal{O}(\vec{x}) \right) \right\rangle = Z_{\text{grav}}[\phi \to \phi_0], \tag{4.14}$$

where bulk fields $\phi(\zeta, \vec{x})$ approach boundary values $\phi_0(\vec{x})$ as $\zeta \to 0$, sourcing CFT operators $\mathcal{O}$.

For a bulk scalar field with action

$$S = \frac{1}{2} \int d^4x dr \sqrt{-g} \left(g^{\mu\nu} \partial_\mu \phi \partial_\nu \phi + M^2 \phi^2 \right), \tag{4.15}$$

the equations of motion yield asymptotic behaviour $\phi(\zeta, \vec{x}) \sim \zeta^{4-\Delta} \phi_0(\vec{x}) + \zeta^{\Delta} \langle \mathcal{O}(\vec{x}) \rangle$. The scaling dimension Δ relates to mass via $M^2R^2 = \Delta(\Delta - 4)$, solved by $\Delta = 2 \pm \sqrt{4 + M^2R^2}$. As $\zeta \to 0$, the non-normalizable mode $\zeta^{4-\Delta}\phi_0$ sources $\mathcal{O}$ while the normalizable mode $\zeta^{\Delta} \langle \mathcal{O} \rangle$ gives the operator VEV.

Witten [14] verified this dictionary by matching Kaluza-Klein modes in $AdS_5 \times S^5$ to chiral primary operators in $\mathcal{N} = 4$ SYM. Spherical harmonics Y^k on S^5 (transforming as $\mathbf{Sym}_k(\mathbf{6})$) correspond to SYM operators $\mathcal{O}^k = \text{Tr}(\Phi^{(i_1} \cdots \Phi^{i_k)})$ – traces with $\Delta = k$, satisfying $M_k^2 R^2 = k(k+4) - k(k-4) = 8k$. This extends to gravitons mapping to the stress-tensor $T_{\mu\nu}$, vector fields to R-currents J_μ^a, and p-forms to conserved higher-spin currents.

4.2.4 Bulk Dynamics and Stability

The scalar field equation in AdS_5,

$$\zeta^5 \partial_\zeta \left(\zeta^{-3} \partial_\zeta \phi \right) - M^2 R^2 \zeta^{-2} \phi - \Box_x \phi = 0, \tag{4.16}$$

has solutions $\phi(\zeta) \sim \zeta^{\Delta}$ requiring $\Delta = 2 \pm \sqrt{4 + M^2R^2}$ to be real. This imposes the Breitenlohner-Freedman (BF) bound [57]:

$$M^2R^2 \geq -4. \tag{4.17}$$

Unlike flat space where $M^2 < 0$ implies instability, AdS stabilizes modes with $-4 \leq M^2R^2 < 0$ due to its gravitational potential.

This stability mechanism has an interesting holographic interpretation. The BF bound, is the gravitational dual of the condition for stability of the symmetric vacuum in the boundary field theory. Violating this bound, i.e. taking $M^2R^2 < -4$, triggers a dynamical instability in the bulk: the scalar field becomes tachyonic and condenses, forming a non-trivial background configuration. This is the holographic realization of SSB on the boundary.

In this way, the BF bound is analogous to the critical condition for chiral symmetry breaking in QCD. Just as in QCD, where if the quark mass or coupling pushes the theory beyond a critical point, the symmetric vacuum becomes unstable and a chiral condensate $\langle \bar{q}q \rangle$ forms, here, if the bulk scalar mass violates the BF bound then the AdS vacuum becomes unstable and a scalar condensate forms. This condensate is the dual of a symmetry-breaking operator acquiring a VEV in the boundary CFT.

In a top-down holographic QCD model, the bulk field whose condensation triggers symmetry breaking would be specifically chosen to be dual to the $\bar{q}q$ operator. Its condensation would then be the direct holographic description of $\langle \bar{q}q \rangle \neq 0$. In the general case discussed here, the scalar field is a stand-in for any operator that can condense.

Such BF bound violations can model various phenomena: bulk tachyonic condensation analogous to Higgs mechanisms, boundary spontaneous symmetry breaking in QFT, and energy-dependent phase transitions through holographic RG flow ($\zeta \sim 1/E$). As previewed earlier, such BF bound violations model chiral symmetry breaking when fundamental matter is introduced via probe branes, which we will discuss in the next section.

4.3 D3/D7 Probe Brane Setup

4.3.1 Fundamental Matter via Probe Branes

To introduce quarks in the fundamental representation of $SU(N_c)$, we embed N_f *probe* D7-branes (flavour branes) within the $AdS_5 \times S^5$ geometry generated by N_c D3-branes (colour branes). When $N_c \gg N_f$, flavour branes act as non-backreacting probes—corresponding to the quenched approximation in QCD. This holds because the D7-brane tension $T_7 \sim N_f g_s^{-1}$ is subleading to the D3-brane tension $T_3 \sim N_c g_s^{-1}$ when $N_f \ll N_c$, making gravitational backreaction negligible. The brane intersection (Table 4.2) preserves $\mathcal{N} = 2$ supersymmetry since the number of ND directions is four, satisfying the stability condition [58]. Open strings between D3 and D7 branes yield N_f quark supermultiplets with masses proportional to the D3-D7 separation L (this relates to the confinement scale Λ_{QCD} seen in 2.6).

	x_0	x_1	x_2	x_3	x_4	x_5	x_6	x_7	x_8	x_9
D3	•	•	•	•	–	–	–	–	–	–
D7	•	•	•	•	•	•	•	•	–	–

TABLE 4.2: D3/D7 brane intersection for fundamental matter

4.3.2 Embedding Geometry and Chiral Symmetry

The D7-brane extends along (x^μ, ρ, Ω_3) where $\rho = \sqrt{x_4^2 + \cdots + x_7^2}$, embedding non-trivially in the transverse (x_8, x_9) plane. The induced metric is:

$$ds^2_{\mathrm{D7}} = \frac{\rho^2 + L^2}{R^2} dx_\mu dx^\mu + \frac{R^2}{\rho^2 + L^2}\left(d\rho^2 + \rho^2 d\Omega_3^2\right) \tag{4.18}$$

with $L(\rho)$ describing the brane's shape. Rotations in the (x_8, x_9) plane correspond to $U(1)_A$ axial subgroup of the $U(N_f)_L \times U(N_f)_R$ chiral symmetry, explicitly broken when $L \neq 0$. From the DBI action:

$$S_{\mathrm{D7}} = -T_7 \int d^8x \sqrt{-\det \mathcal{G}_{ab}} = -T_7 \int d^8x \rho^3 \sqrt{1 + (\partial_\rho L)^2} \tag{4.19}$$

$$S_{\mathrm{D7}} = -T_7 \int d^8x \frac{r^4}{R^4} \rho^3 \sqrt{1 + (\partial_\rho L)^2} \tag{4.20}$$

the embedding equation $\partial_\rho \left(\rho^3 \partial_\rho L / \sqrt{1 + (\partial_\rho L)^2} \right) = 0$ has asymptotic solution:

$$L(\rho) \sim m_q + \frac{c}{\rho^2} \quad \text{as} \quad \rho \to \infty \tag{4.21}$$

Here, $m_q \propto L(\infty)$ defines the quark mass, while $c \propto \langle \bar{q}q \rangle$ represents the chiral condensate. Supersymmetry requires $c = 0$ for $m_q = 0$; spontaneous chiral symmetry breaking ($c \neq 0$) necessitates additional SUSY-breaking deformations.

4.3.3 Meson Spectroscopy From Brane Fluctuations

Mesons emerge as fluctuations of the D7-brane. The two primary types of fluctuations are:

1. **Scalar Mesons (e.g. sigma mesons):** Fluctuations in the radial embedding, $L(\rho, x^\mu) = m + \delta L(\rho, x^\mu)$.
2. **Pseudoscalar Mesons (e.g. pions):** Fluctuations in the angular direction, $X^8 = L(\rho) + (2\pi\alpha')\phi(\xi^a)$, $X^9 = (2\pi\alpha')\psi(\xi^a)$.

For the scalar sigma meson, expanding the DBI action to second order in δL yields the linearized equation of motion. For a mode $\delta L = e^{ik\cdot x} f(\rho)$ with $M^2 = -k^2$, the radial equation becomes:

$$\frac{d}{d\rho}\left(\rho^3 \frac{df}{d\rho}\right) + \frac{M^2 R^4 \rho^3}{(\rho^2 + m^2)^2} f(\rho) = 0. \tag{4.22}$$

This equation admits a discrete spectrum of normalizable solutions:

$$M_n = \frac{2m}{R^2}\sqrt{(n+1)(n+2)}, \quad n \in \mathbb{Z}^+. \tag{4.23}$$

The lightest state ($n = 0$) is the sigma meson, with mass $M_\sigma = \frac{2\sqrt{2}m}{R^2}$.

For the pseudoscalar mesons, the linearized equation of motion is:

$$\partial_a\left(\frac{\rho^3 g^{ab}\partial_b \phi}{\rho^2 + L^2}\right) = 0. \tag{4.24}$$

Assuming a Kaluza-Klein ansatz $\phi(x^\mu, \rho, \Omega_3) = e^{ik\cdot x} f(\rho) \mathscr{Y}^l(\Omega_3)$ with $M^2 = -k^2$, we obtain the radial equation:

$$\frac{d}{d\rho}\left(\rho^3 \frac{df}{d\rho}\right) + \frac{M^2 R^4 \rho^3}{(\rho^2 + L^2)^2} f(\rho) = 0 \tag{4.25}$$

For constant embeddings ($L = m_q \alpha'$), normalizable solutions require:

$$M_{n,l} = \frac{2m_q \alpha'}{R^2}\sqrt{(n+1)(n+2)}, \quad n \in \mathbb{Z}^+. \tag{4.26}$$

This spectrum exhibits key features: a mass gap proportional to the quark mass m_q, linear radial trajectories ($M_n^2 \propto n$), and degeneracy for $m_q = 0$ where the pseudoscalars become massless Goldstone bosons. This provides a holographic description of mesons as fluctuations of the probe brane. A more detailed phenomenological analysis, including vector mesons and decay constants, will be presented in Section 5.3.3 within the Dynamic AdS/QCD model.

Chapter 5

Holographic QCD

While the $\mathcal{N} = 4$ SYM duality provides a foundational example of gauge/gravity correspondence, it differs from realistic QCD in three crucial aspects: it lacks asymptotic freedom, contains only adjoint matter, and preserves exact supersymmetry. The D3/D7 system introduced in 4.3 resolves the absence of fundamental matter, but it still exhibits 3 important limitations. First, it has the same UV conformality as in $\mathcal{N} = 4$ SYM, requiring external deformations (e.g. temperature, magnetic fields). Secondly, Wilson loops (at zero temperature) obey a perimeter law rather than the area law signaling confinement. Third, $\mathcal{N} = 2$ SUSY constrains the chiral symmetry breaking pattern, requiring additional SUSY-breaking deformations (e.g., temperature, magnetic fields) for spontaneous breaking. The goal of holographic QCD is to construct dualities for confining SU(N_c) gauge theories with fundamental matter by adapting the AdS/CFT framework. This presents significant challenges: QCD's perturbative regime would dualize to a strongly coupled string theory on a non-trivial background whose analysis exceeds current capabilities; asymptotic freedom requires logarithmic running couplings absent in conformal theories; and both confinement and chiral symmetry breaking must emerge dynamically from the dual description.

Current approaches navigate these challenges through two complementary philosophies. Top-down models start from consistent string theory constructions (e.g., D-brane intersections) and modify them to approach QCD-like behaviour. These preserve mathematical rigour but face complexity from the smörgåsbord of gravity fields inherent to string theory. Bottom-up models implement QCD phenomenology directly in asymptotically AdS geometries, sacrificing formal rigour for tractability. These often emerge as truncations of top-down constructions where undesired fields have been omitted. We now systematically examine both approaches, using top-down insights to motivate bottom-up constructions.

5.1 Top-Down Approaches

Top-down approaches adapt string-theoretic constructions to incorporate fundamental matter while preserving holographic control. The D3/D7 system serves as the foundational framework for this work, providing a mathematically consistent embedding of quarks in the AdS/CFT correspondence. We now examine its refined implementation for QCD-like phenomenology, focusing on aspects most relevant to chiral symmetry breaking.

5.1.1 D3/D7 System: Fundamental Matter From Strings

The $\mathcal{N} = 4$ SYM contains only adjoint matter, corresponding to 3-3 strings in the D3-brane stack (Fig. 5.1). To introduce fundamental quarks, we add N_f probe D7-branes, generating new string sectors: 3-3 strings form the adjoint $\mathcal{N} = 4$ multiplet (gauge bosons, scalars, fermions); 3-7 strings yield bifundamental hypermultiplets transforming as $(\mathbf{N_c}, \mathbf{N_f})$ under $SU(N_c) \times SU(N_f)$; and 7-7 strings represent mesonic operators in the adjoint of $SU(N_f)$.

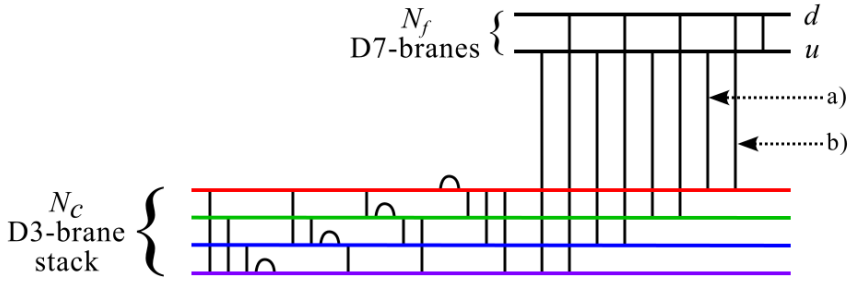

FIGURE 5.1: String configurations in D3/D7 system: (a) 3-3 strings (adjoint gluons), (b) 3-7 strings (fundamental quarks), (c) 7-7 strings (mesonic operators)

The probe limit $N_f \ll N_c$ suppresses backreaction, corresponding to the quenched approximation. We set the $AdS_5 \times S^5$ to

$$ds^2 = r^2 \eta_{\mu\nu} dx^\mu dx^\nu + \frac{1}{r^2}\left[\partial\rho^2 + \rho^2 d\Omega_3^2 + dL^2 + L^2 d\phi^2\right], \tag{5.1}$$

where $r^2 = \rho^2 + L^2$ implements holographic RG flow (cf. 4.2.2), and ρ parametrizes an $S^3 \subset S^5$. The induced metric on D7-branes at separation L in $AdS_5 \times S^5$ is then

$$ds^2_{\mathrm{D7}} = r^2 \eta_{\mu\nu} dx^\mu dx^\nu + \frac{1}{r^2}\left(\partial\rho^2 + \rho^2 d\Omega_3^2\right). \tag{5.2}$$

5.1.2 Embedding Dynamics and Chiral Symmetry

The D7-brane embedding $L(\rho)$ is determined by the DBI action

$$S_{\mathrm{D7}} = -T_7 \int d^8\xi \sqrt{-\det(\mathcal{G}_{ab} + 2\pi\alpha' F_{ab})}, \tag{5.3}$$

where, as before, $\mathcal{G}_{ab}$ is the pullback of the metric on Eq. (5.3). We can explicitly express this matrix as

$$\det(\mathcal{G}_{ab}) = \left| \begin{pmatrix} -r^2 & 0 & 0 & 0 & 0 & 0 & 0 & 0 \\ 0 & r^2 & 0 & 0 & 0 & 0 & 0 & 0 \\ 0 & 0 & r^2 & 0 & 0 & 0 & 0 & 0 \\ 0 & 0 & 0 & r^2 & 0 & 0 & 0 & 0 \\ 0 & 0 & 0 & 0 & \frac{1}{r^2}\left(1 + (\partial_\rho L)^2\right) & 0 & 0 & 0 \\ 0 & 0 & 0 & 0 & 0 & \frac{\rho^2}{r^2} & 0 & 0 \\ 0 & 0 & 0 & 0 & 0 & 0 & \frac{\rho^2}{r^2} & 0 \\ 0 & 0 & 0 & 0 & 0 & 0 & 0 & \frac{\rho^2}{r^2} \end{pmatrix} \right|. \tag{5.4}$$

Setting $F_{ab} = 0$ (actually the integration over the angular coordinates gives a constant which we ignore), the action becomes

$$S_{\mathrm{D7}} \sim \int d^4x d\rho\, \rho^3 \sqrt{1 + (\partial_\rho L)^2}. \tag{5.5}$$

The resulting equation of motion

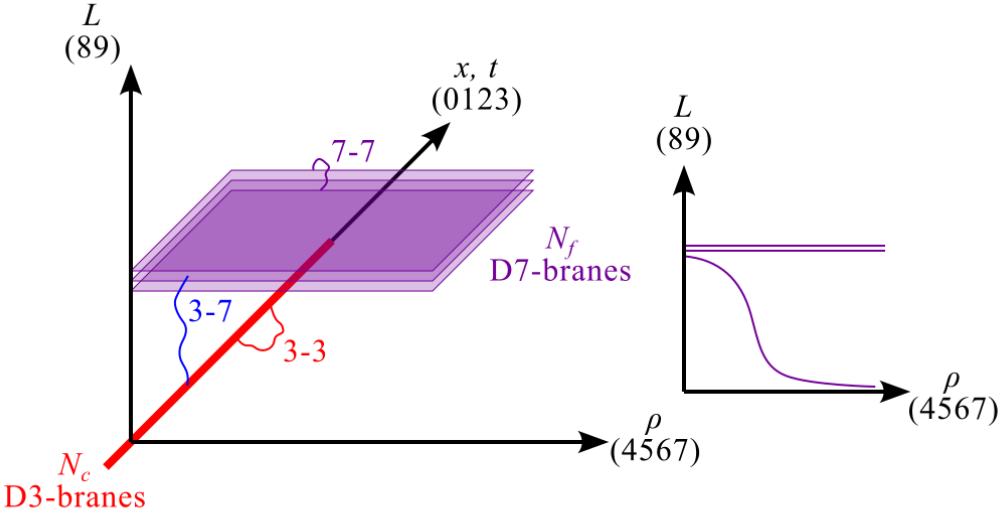

FIGURE 5.2: 10D spacetime diagram of the D3/D7 probe brane setup. As seen in the right hand diagram, The D7 brane may have either $L = const$ or $L = L(\rho)$.

$$\partial_\rho \left(\frac{\rho^3 \partial_\rho L}{\sqrt{1 + (\partial_\rho L)^2}} \right) = 0, \tag{5.6}$$

admits constant solutions $L(\rho) = m$. Rotations in the (x_8, x_9)-plane correspond to $U(1)_A$ subgroup of the $\mathrm{U}(N_f)_L \times \mathrm{U}(N_f)_R$ chiral symmetry, explicitly broken when $m \neq 0$.

5.1.3 Holographic Renormalization and Condensate

Asymptotic analysis ($\rho \to \infty$) reveals the quark mass and condensate through the expansion

$$L(\rho) = m + \frac{c}{\rho^2} + \mathcal{O}(\rho^{-4}) \tag{5.7}$$

where $m \propto$ quark mass and $c \propto \langle \bar{q}q \rangle$. This follows from interpreting the linearized action as a Klein-Gordon action for $\phi = L(\rho)/\rho$ with $M^2R^2 = -3$. Taking the limit $\partial_\rho L \to 0$, we can linearize the D7 action as

$$S \sim \int d\rho \rho^3 (\partial_\rho L)^2 = \int d\rho \rho^3 \left(\rho^2 (\partial_\rho \phi)^2 + \phi^2 + 2\rho\phi\partial_\rho\phi \right), \tag{5.8}$$

Integrating the last term by parts (to give $-4\int d\rho \rho^3 \phi^2$) we get the form

$$S \sim \int d\rho \rho^3 \left(\rho^2 (\partial_\rho \phi)^2 - 3\phi^2 \right), \tag{5.9}$$

satisfying the BF bound. The mass dimensions are $\Delta = 3$ for $\langle \bar{q}q \rangle$ and $4 - \Delta = 1$ for the quark mass (corresponding to ρ^{-2} and ρ^0 terms in L respectively) and so we can say

$$\phi(\rho) = \frac{m}{\rho} + \frac{\langle \bar{q}q \rangle}{\rho^3}, \tag{5.10}$$

$$\implies L(\rho) = m + \frac{\langle \bar{q}q \rangle}{\rho^2}, \tag{5.11}$$

where we see that $\langle \bar{q}q \rangle = c$.

5.1.4 Constable-Myers and Dilaton Flow

To incorporate running couplings absent in conformal theories, we introduce radially dependent dilaton profiles. The Constable-Myers solution [59] deforms $\mathrm{AdS}_5 \times S^5$ while preserving SO(4) $\times$ SO(2) symmetry:

$$ds^2 = \frac{1}{\sqrt{H(r)}}\left(\frac{r^4+b^4}{r^4-b^4}\right)^{\frac{\delta}{4}}\eta_{\mu\nu}dx^\mu dx^\nu + \sqrt{H(r)}\left(\frac{r^4+b^4}{r^4-b^4}\right)^{\frac{2-\delta}{4}}\frac{r^4-b^4}{r^4}(d\rho^2+\rho^2 d\Omega_3^2+dL^2+L^2d\phi^2)+\cdots, \tag{5.12}$$

with

$$e^{\phi} = e^{\phi_0}\left(\frac{r^4+b^4}{r^4-b^4}\right)^{\frac{\Delta}{2}}, \tag{5.13}$$

and

$$H(r) = \left(\frac{r^4+b^4}{r^4-b^4}\right)^{\delta} - 1, \tag{5.14}$$

where $r^2 = \rho^2 + L^2$, b sets the deformation scale, and $\Delta^2 + \delta^2 = 10$. This geometry approaches $AdS_5 \times S^5$ as $r \to \infty$, recovering UV $\mathcal{N} = 4$ SYM behaviour, while diverging at $r = b$ to establish an IR scale $\Lambda_{QCD} \sim b$ that mimics QCD's confinement scale. Crucially, the radial dilaton profile e^{ϕ} generates a running coupling through the identification $g_{YM} \sim e^{\phi/2}$, directly linking bulk geometry to boundary RG flow.

Embedding probe D7-branes yields the action:

$$S_{D7} \sim e^{\phi_0}\int d\rho\,\lambda(r)\rho^3\sqrt{1+(\partial_\rho L)^2}, \tag{5.15}$$

where

$$\lambda(r) = \frac{r^8-b^8}{r^8}\left(\frac{r^4+b^4}{r^4-b^4}\right)^{\frac{\Delta}{2}}. \tag{5.16}$$

Expanding near chiral limit ($L, \partial_\rho L \to 0$) reveals how dilaton flow induces running anomalous dimensions:

$$S \sim \int d\rho\,\rho^3\left[\frac{1}{2}\lambda(r)|_{L=0}(\partial_\rho L)^2 + \underbrace{\frac{\partial\lambda}{\partial(L^2)}\Big|_{L=0}}_{\text{running mass}}L^2\right] \tag{5.17}$$

The L-dependent mass term $\partial_{L^2}\lambda \sim r^{-1}\partial_r\lambda$ demonstrates how bulk field masses acquire radial dependence, mapping to energy-dependent operator dimensions $\gamma(\mu)$ in the dual theory. This

mechanism—where geometric deformations generate running couplings—provides the foundation for the Dynamic AdS/QCD model in §5.3.

5.2 Bottom-Up Approaches

While top-down models provide string-theoretic consistency, their complexity motivates phenomenological bottom-up approaches. The latter sacrifice formal rigour for computational tractability while preserving key QCD features identified in 4.3: confinement → IR cutoffs/dilaton profiles, χ_{SB} → BF-bound violation and the running coupling → $\Delta m^2(\rho)$.

Bottom-up models start from a simplified AdS_5 spacetime

$$ds^2 = r^2 \eta_{\mu\nu} dx^\mu dx^\nu + r^{-2} dr^2, \tag{5.18}$$

with bulk fields mapped to QCD operators via the holographic dictionary shown in Table 5.1.

Bulk Field	**Mass**	**QFT Operator**	Δ **= dim**	p**-form**
$X(x,\rho)$	$M^2 = -3$	$\bar{q}q$	3	$p = 0$
$L^{M,a}(x,\rho)$	$M^2 = 0$	$L^{\mu,a} = \bar{q}_L \gamma^\mu t^a q_L$	3	$p = 1$
$R^{M,a}(x,\rho)$	$M^2 = 0$	$R^{\mu,a} = \bar{q}_R \gamma^\mu t^a q_R$	3	$p = 1$

Table 5.1: Dictionary between the bulk AdS fields and the boundary field theory operators in a simple AdS/QCD model. The bulk field masses are obtained via the relation $M^2 = (\Delta - p)(\Delta + p - 4)$.

The minimal action incorporates chiral symmetry through

$$S = \int d^4x dr \sqrt{-g}\, \mathrm{Tr}\left[(D_\mu X)^\dagger (D^\mu X) + 3X^\dagger X - \frac{1}{4g_5^2}\left(F_{L,\mu\nu} F_L^{\mu\nu} + F_{R,\mu\nu} F_R^{\mu\nu} \right) \right], \tag{5.19}$$

where $D_\mu X = \partial_\mu X - iL_\mu X + iXR_\mu$, and $X = L(r) e^{2i\pi^a t^a}$ encodes the chiral condensate.

5.2.1 Confinement Mechanisms

To break conformal symmetry, two primary approaches exist. The hard-wall model imposes an IR cutoff at $r = r_0$ [16], generating a mass gap $\Lambda_{\mathrm{QCD}} \sim r_0$, area-law Wilson loops $V_{q\bar{q}} \sim \sigma r$, but unnatural Regge trajectories $M_n^2 \propto n^2$. Alternatively, the soft-wall model introduces a dilaton $\phi(r) \sim \kappa^2 r^2$ [17] that modifies the action as

$$S \to \int d^4x dr \sqrt{-g} e^{\phi(r)} \mathscr{L}, \tag{5.20}$$

producing linear Regge trajectories $M_n^2 \propto n$ while suppressing IR fluctuations.

5.3 Dynamic AdS/QCD Model

This research-oriented model for chiral symmetry breaking dynamics [60] incorporates key insights from D3/D7 embeddings [61, 52]. It is similar in spirit to the soft-wall AdS/QCD models of [16, 62] but incorporates the explicit running of the gauge theory and the chiral symmetry breaking is dynamically determined rather than input and fitted. A comparison of the model to SM QCD can be found in [63] - it is good at describing the broad features of the light mesonic spectrum but quantitatively can differ at the 20% level.

The gravity action includes the bulk fields: the scalar X, which is dual to the operator $\bar{q}q$; its phase, which is dual to $\bar{q}\gamma_5 q$; the flavour gauge field V^M (appearing in F^{MN}), which is dual to the vector current $\bar{q}\gamma^\mu q$; and the axial field A^M, which is dual to the axial vector current $\bar{q}\gamma^\mu\gamma_5 q$. For our purposes, it will be useful to consider the theory generalized to representations, R. The action then takes the form

$$S_{boson} = \sum_R \int d^4x d\rho\, \rho^3 \left[\frac{1}{r^2}(D^M X_R)^\dagger (D_M X_R) + \frac{\Delta m_R^2}{\rho^2}|X_R|^2 + \frac{1}{2g_{R5}^2}\left(F^V_{R,MN}F_R^{V,MN} + F^A_{R,MN}F_R^{A,MN}\right]\right], \quad (5.21)$$

where $\sqrt{-g} = \rho^3$ ensures soft-IR wall behaviour ($r \geq L$), and $\Delta m_R^2(\rho)$ introduces the running anomalous dimension $\gamma_R(\mu)$. Note the only interplay between the two representations is through their contributions to Δm_R^2. The UV fixed point occurs when $\Delta m_R^2 = 0$ and $M^2R^2 = -3$.

The vector coupling g_{R5} only enters into quantities that explicitly compare different terms in the action and is fixed by matching the vector-vector correlator to perturbative QCD [16]. The fit to QCD in [63] suggested $g_{R5}^2 = 76$[1].

The metric for each representation is a five-dimensional asymptotically AdS spacetime

$$ds_R^2 = r^2 dx_{(1,3)}^2 + \frac{d\rho^2}{r^2}, \quad (5.22)$$

with $r^2 = \rho^2 + |X_R|^2$ the holographic radial direction corresponding to the energy scale, and with the AdS radius set to one. The setup shares many aspects of the top-down D3/probe D7 system [58, 55, 52].

[1] We take g_5 to be scale, N_f, and N_c independent by ansatz here.

5.3.1 The Running Mass and the Anomalous Dimension

The energy-dependent correction $\Delta m_R^2(\rho)$ encodes the running gauge coupling's effect on the dual scalar field's mass. Its form follows from the holographic dictionary relating the bulk scalar mass to the scaling dimension Δ of the dual operator $\bar{q}q$. For an operator with classical dimension 3 and anomalous dimension $\gamma(\mu)$, $\Delta = 3 - \gamma(\mu)$. The AdS/CFT mass-dimension relation $M^2R^2 = \Delta(\Delta - 4)$ then gives

$$\Delta m^2(\rho) \equiv M^2(\rho)R^2 - (M^2R^2)_{\rm UV} = (3-\gamma)(-1-\gamma) - (-3) = \gamma(\gamma - 2). \tag{5.23}$$

We now need to make a choice of Δm^2 (and hence γ) that matches the perturbative UV of the gauge theory and provides a sensible IR ansatz. A simple choice would be to take the perturbative running of the anomalous dimension γ_p - including extrapolating it into the IR - and substitute it into the holographic formula, Eq. (5.23). However, if one does this naïvely with the full formula Δm^2 will fall to -1 and then rise again. There will be no BF bound violation and no chiral symmetry breaking. To see chiral symmetry breaking, the ansatz for Δm^2 must pass through -1 so that γ becomes imaginary and there is an instability to chiral symmetry breaking. The simplest solution is to match in the perturbative UV where γ is small using the linearized version of Eq. (5.23) so we have

$$\Delta m^2 = -2\gamma_p \tag{5.24}$$

this matches the UV gauge theory result which we call γ_p. If we now extrapolate this formula to the IR then Δm^2 will pass through -1 as γ_p rises. N.b.: $\Delta m^2 = -1$ corresponds to $\gamma_p = 1/2$. Below we will use γ_p for the perturbative running anomalous dimension but γ to mean the full theory's anomalous dimension, either computed for example on the lattice or in our models the γ that is linked to Δm^2 via the full Eq. (5.23).

The two-loop result for the running coupling, $\alpha(\mu)$, in a gauge theory with multi-representational matter is

$$\mu\frac{d\alpha}{d\mu} = -\beta_0\alpha^2 - \beta_1\alpha^3\,, \tag{5.25}$$

with

$$\begin{aligned}\beta_0 &= \tfrac{1}{6\pi}\left(11C_2(G) - 4\textstyle\sum_R T(R)N_f(R)\right), \\ \beta_1 &= \tfrac{1}{24\pi^2}\Big(34C_2^2(G) \\ &\quad - \textstyle\sum_R \left(20C_2(G) + 12C_2(R)\right) T(R)N_f(R)\Big).\end{aligned} \tag{5.26}$$

where $T(R)$ is half the Dynkin index, $C_2(R)$ the quadratic Casimir of the representation R and $N_f(R)$ its number of Dirac flavours (for Weyl fermions we would include a factor of 1/2 in the flavour count). Although our running coupling is computed at two loop, we use the one-loop anomalous mass dimension (γ_p),

$$\gamma_p = \frac{3C_2(R)}{2\pi}\alpha. \tag{5.27}$$

We use the one loop definition of γ_p since it is already a guess non-perturbatively and no additional qualitative features are added beyond.

Finally we note that for calculation purposes, we must numerically set α at some scale. Throughout the research portion of this thesis we set $\alpha = 0.65$ at $\mu = 1$. We are careful though to rewrite all our results in units of the ρ mass in the theory with $m_Q = 0$ to remove this arbitrary choice.

5.3.2 Vacuum Structure and Chiral Symmetry Breaking

The vacuum solution $|X_R| = L_{R0}(\rho)$ is found by solving the equation of motion:

$$\partial_\rho(\rho^3\partial_\rho L_R) - \rho\Delta m_R^2 L_R = 0. \tag{5.28}$$

This incorporates the running mass $\Delta m^2(\rho) = -2\gamma_p$ (for $\Delta = 3$). Solutions take the asymptotic form $L_R(\rho) \sim m_R\rho^{\gamma_R - 3} + \langle\bar{q}_R q_R\rangle\,\rho^{-\gamma_R}$ (following the GKPW dictionary in Eq. (4.14)) near fixed points.

Chiral symmetry breaking occurs when the BF bound $M^2R^2 \geq -4$ (see Eq. (4.17)) is violated ($\Delta m_R^2 < -1$).

The relation between Δm^2 and the anomalous dimension γ derives from the conformal dimension formula:

$$\Delta m^2 = \gamma(\gamma - 2) \tag{5.29}$$

This exact relation reduces to the perturbative approximation $\Delta m^2 = -2\gamma_p$ when expanded at small γ. Consequently, the BF bound is violated when $-2\gamma_p < -1$, or equivalently, when $\gamma_p > 0.5$. In the UV where $\gamma \to 0$, the solution $L_R(\rho) \sim m_R \rho^{\gamma-3} + \langle \bar{q}_R q_R \rangle \rho^{-\gamma}$ recovers the expected source (dimension 1) and condensate (dimension 3) scaling.

The metric modification $r^2 = \rho^2 + L^2$ stabilises the system by preventing access to $r < L$. Boundary conditions generalize the IR regularity condition in 4.3.2:

$$L_R(\rho_R^{\text{IR}}) = \rho_R^{\text{IR}}, \quad \partial_\rho L_R|_{\rho=\rho_R^{\text{IR}}} = 0, \tag{5.30}$$

These boundary conditions enforce constituent mass generation at Λ_χ and are motivated by the D3/D7 probe system [58, 55, 52], where the D7 brane embedding solutions for the massless theory can be interpreted as the source vanishing in the UV and the operator vanishing in the IR. The DBI action for the D7 brane embedding field L, takes the form $\mathscr{L} = \rho^3(\partial_\rho L)^2$, and the solution is of the form $L = m + c/\rho^2$, where m is the quark mass and c the quark condensate operator. For massless theories, one seeks solutions where m vanishes in the UV, and in the IR, a regular brane embedding requires $L'_{IR} = 0$, i.e. vanishing condensate, conditions generalized to Eq. (5.30) for dynamic AdS/QCD. In multi-scale theories, higher-dimensional representations decouple at their condensation scale ρ_R^{IR}.

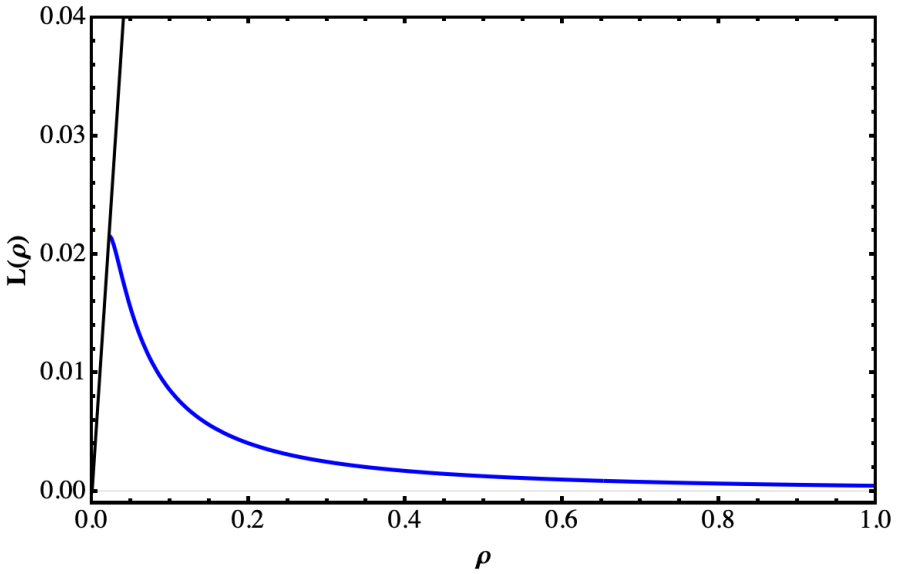

FIGURE 5.3: Dynamic AdS/QCD embeddings: $L(\rho) \to 0$ in UV with IR mass generation

5.3.3 Meson Spectroscopy and Decay Constants

The mesons are fluctuations in the various fields of the model in Eq. (5.21). A fluctuation is written as $F(\rho)e^{-ik\cdot x}$, $M^2 = -k^2$ and IR boundary conditions $F(L_R^{IR}) = 1, F'(L_R^{IR}) = 0$

are used. One seeks the values of M^2 where the UV solution falls to zero, so there is only a fluctuation in the operator and not the source.

The fluctuations of $L_R(\rho)$ give rise to scalar σ mesons [64]. They are obtained by writing $L_R = L_{R0} + S_R$ and where $r^2 = \rho^2 + L_{R0}^2$. The equation of motion for the fluctuation reads

$$\begin{aligned} &\partial_\rho(\rho^3\partial_\rho S_R(\rho)) - \rho(\Delta m_R^2)S_R(\rho) \\ &-\rho L_{R0}(\rho)S_R(\rho)\tfrac{\partial\Delta m_R^2}{\partial L}|_{L_{R0}} + M^2\tfrac{\rho^3}{r^4}S_R(\rho) \quad = 0. \end{aligned} \tag{5.31}$$

The vector-mesons are obtained from fluctuations of the vector gauge field and satisfy the equation of motion

$$\partial_\rho(\rho^3\partial_\rho V_R(\rho)) + M_V^2\frac{\rho^3}{r^4}V_R(\rho) = 0. \tag{5.32}$$

A canonically normalized kinetic term for the vector meson requires

$$\int d\rho\ \frac{\rho^3}{g_5^2 r^4}V_R^2 = 1. \tag{5.33}$$

The dynamics of the axial-mesons is described by

$$\partial_\rho(\rho^3\partial_\rho A_R(\rho)) - g_{R5}^2\frac{\rho^3 L_{R0}^2}{r^4}A_R(\rho) + \frac{\rho^3 M_A^2}{r^4}A_R(\rho) = 0\,. \tag{5.34}$$

To compute decay constants, we couple the meson to an external source. Those sources are described as fluctuations with a non-normalizable UV asymptotic form. We fix the coefficient of these solutions by matching to the gauge theory in the UV. In the UV we expect $L_{R0}(\rho) \sim 0$ and we can solve the equations of motion for the scalar, $L = K_S(\rho)e^{-iq\cdot x}$, vector $V^\mu = \epsilon^\mu K_V(\rho)e^{-iq\cdot x}$, and axial $A^\mu = \epsilon^\mu K_A(\rho)e^{-iq\cdot x}$ fields. Each satisfies the UV asymptotic equation

$$\partial_\rho[\rho^3\partial_\rho K] - \frac{q^2}{\rho}K = 0\,. \tag{5.35}$$

with solution

$$K_i = N_i\left(1 + \frac{q^2}{4\rho^2}\ln\left(\frac{q^2}{\rho^2}\right)\right), \quad (i = S, V, A), \tag{5.36}$$

where N_i are normalization constants that are not fixed by the linearized equation of motion. Substituting these solutions back into the action gives the scalar, vector, and axial vector correlators. Performing the usual AdS/QCD matching to the UV gauge theory requires us to set [16, 60]

$$N_S^2 = \frac{d(R)\, N_f(R)}{24\pi^2}, \qquad N_V^2 = N_A^2 = \frac{g_{R5}^2\, d(R)\, N_f(R)}{24\pi^2}. \tag{5.37}$$

Scaling of Physical Observables These UV matching conditions determine how physical quantities in the model scale with the number of colours N_c and flavours N_f for a given representation R. The key factor is the dimension of the representation, $d(R)$. The decay constants scale as:

$$\begin{aligned} F_{RV}^2 &\sim \sqrt{g_{R5}^2\, d(R)\, N_f(R)}, \\ F_{R\sigma}^2 &\sim \sqrt{d(R)\, N_f(R)}, \\ f_{R\pi}^2 &\sim d(R)\, N_f(R), \end{aligned}$$

where $F_{R\sigma}$ is the decay constant for the scalar meson to couple to an external scalar source. Note that for our ansatz $g_{R5}^2 = 76$ (or any constant value of the coupling), the explicit g_{R5}-dependence cancels in the decay constants. For specific representations:

- **Fundamental:** $d(F) = N_c, \implies f_\pi^2 \sim N_c N_f, F_V^2 = F_\sigma^2 \sim \sqrt{N_c N_f}$.
- **Adjoint:** $d(G) = N_c^2 - 1 \approx N_c^2, \implies f_\pi^2 \sim N_c^2 N_f, F_V^2 = F_\sigma^2 \sim N_c\sqrt{N_f}$.
- **Symmetric:** $d(S_n) = N_c(N_c+1)/2 \approx N_c^2/2, \implies f_\pi^2 \sim N_c^2 N_f, F_V^2 = F_\sigma^2 \sim N_c\sqrt{N_f}$.

These scaling laws are a direct result of the holographic construction and the large-N counting of degrees of freedom. All dimensionful quantities are calculated in units of the ρ-meson mass in the chiral limit M_ρ^0 to remove the dependence on the arbitrary initial condition for the gauge coupling $\alpha(\mu)$.

The vector meson decay constant is then given by the overlap term between the meson and the external source

$$F_{RV}^2 = \int d\rho \frac{1}{g_{R5}^2} \partial_\rho \left[-\rho^3 \partial_\rho V_R\right] K_{RV}(q^2 = 0)\,. \tag{5.38}$$

The axial meson normalization and decay constant are given by Eqs. (5.33) and (5.38) with replacement $V \to A$, and thus scale similarly to F_{RV}^2. Note the normalizations of the normalizable and non-normalizable fields combine to remove any g_5^2 dependence.

The scalar meson decay constant $F_{R\sigma}$, defining the coupling of the scalar meson to an external scalar source, is given by an overlap integral analogous to Eq. (5.38):

$$F_{R\sigma}^2 = \int d\rho\ \partial_\rho \left[-\rho^3 \partial_\rho S_R\right] K_{RS}(q^2 = 0). \tag{5.39}$$

Note this is not the coupling to an external spin two source considered as the dilaton decay constant [65].

The pion decay constant can be extracted from the expectation that $\Pi_{AA} = f_\pi^2$ here in the QCD conventions i.e. $f_\pi = 93$MeV.

$$f_{R\pi}^2 = \int d\rho \frac{1}{g_5^2} \partial_\rho \left[\rho^3 \partial_\rho K_{RA}(q^2 = 0)\right] K_{RA}(q^2 = 0)\,. \tag{5.40}$$

Explicit g_5^2 dependence again cancels against the normalization but g_5^2 enters through the solution for K_A.

To compute the pion mass we work in the $A_\rho = 0$ gauge and write $A_\mu = A_{\mu\perp} + \partial_\mu \phi$. The ϕ and π fields (the phase of X) mix to describe the pion

$$\begin{aligned} \partial_\rho(\rho^3 \partial_\rho \phi_R(\rho)) - g_{R5}^2 \frac{\rho^3 L_{R0}^2}{r^4}(\pi_R(\rho) - \phi_R(\rho)) = 0\,, \\ q^2 \partial_\rho \phi_R(\rho) - g_5^2 L_{R0}^2 \partial_\rho \pi_R(\rho) = 0\,. \end{aligned} \tag{5.41}$$

Substituting the lower equation of Eq. (5.41) into the upper gives

$$\partial_\rho \left(\rho^3\ L_{R0}^2\ \partial_\rho \pi_R\right) + M_\pi^2 \frac{\rho^3\ L_{R0}^2}{r^4}\ (\pi_R - \phi_R) = 0\,. \tag{5.42}$$

We may simplify the numerics, however, by neglecting the mixing between the heavy axial sector and the light π_R field, setting $\phi_R = 0$. The results continue to be consistent with expectations such as the Gell-Mann-Oakes-Renner relation.

Part II

Research

Chapter 6

Scale Separation, Strong Coupling UV Phases, and the Identification of the Edge of the Conformal Window

At large numbers of colours, N_c, and quark flavours, N_f, SU(N_c) gauge theories are known to possess weakly coupled Banks-Zaks IR fixed points [27]. These fixed points lie at N_f values just below where the theory gains asymptotic freedom at $N_f = 11N_c/2$ and result from a cancellation between the one- and two-loop β function terms. A sensible story has been proposed for how these fixed points evolve into the strongly coupled regime and away from large N_c [66, 29]. That account says that the IR fixed point remains as N_f lowers until the fixed point is sufficiently strongly coupled that the anomalous dimension of the quark anti-quark bilinear operator has risen to one ($\gamma = 1$). This criterion is natural since it is when the mass and condensate are of equal dimension and emerges in both gap equation [67] and holographic analyses [68, 69, 61].

A recent lattice study of SU(3) gauge theory with $N_f = 10$ [70] appears to support this account, placing the theory in the conformal window. In Figure 6.1 we reproduce their result for the β function of the theory as a function of g^2. It shows a clear fixed point around $g^2 = 15$. They compute that the theory has $\gamma = 0.6$. It is argued that this theory lies in the strongly coupled conformal window.

Here, though, we want to play the role of devil's advocate and use that example to discuss whether such an identification could go wrong? The lattice analysis was done on a lattice that had at most $28^3 \times 56$ sites and so the analysis might in principle miss large scale separations of thirty or more. We will show such a case by enacting the running that the lattice study finds in a simple holographic model of the chiral symmetry breaking. To allow ourselves a "parameter space" we relax the condition $\gamma = 1$ which is sensibly argued for but not proven.

In holography in AdS_5 space (with radius one) a quark condensate of dimension three, $\Delta = 3$, is described by a scalar in the bulk of mass squared -3 (as for example, in the D3/probe D7 system

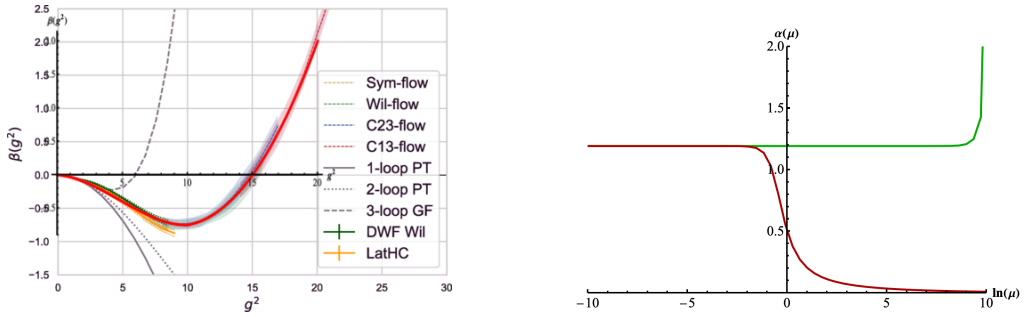

FIGURE 6.1: The beta function plot taken from [70]; our fit is overlaid in red. The resulting $\alpha(\mu)$, on integrating up the beta function, is plotted below, showing an IR fixed point at $\alpha = 15/4\pi$. We show UV boundary conditions that approach the fixed point from above and below.

[58, 55, 52]). This follows from the relation $M^2 = \Delta(\Delta - 4)$ [14]. In top down chiral symmetry breaking models (where supersymmetry is broken [71] or with a magnetic field [72]) this mass squared becomes dependent on the radial (renormalization group flow) direction, decreasing into the IR [61]. When it passes through $M^2 = -4, \Delta = 2, \gamma = 1$ the BF bound [57] is violated and the scalar becomes unstable to acquiring a vev, and chiral symmetry breaking is triggered.

This discussion though is only strictly valid in AdS_5, yet, generically, the space will be deformed by the relevant perturbation causing the chiral symmetry breaking. It is therefore not proven that when the BF bound is violated in a deformed space, that $\gamma = 1$. Thus below, although we will use a fixed AdS_5 geometry, we will only assume that the deviation of the scalar mass from -3 (Δm^2) is proportional to the running α. We will study the behaviour of the theory as a function of the proportionality constant k. We will study the separation in scale between where the BF bound is violated and the chiral condensate forms. If a theory is sufficiently walking and just barely above the BF bound violation point in the IR then a big gap between these scales is possible. This is simply an energetic argument - if the energy cost of "living with" the instability is small it can take a spread of scales for the benefit of allowing condensation to be felt. We find a separation of scales greater than 35 if Δm^2 lies between 1-1.3 of its critical value.

So, do we trust the lattice assignment [70] of the $N_f = 10$ theory to the conformal window? If the reader believes a strict $\gamma = 1$ criteria, then yes. If one instead believes that the critical value might lie between $\gamma = 0.4$-1.4 then the measured value of 0.65 would be a concern if the true critical value were between 0.5-0.65, i.e. 15% of the range. The lattice work [70] seeks to resolve this by studying the theory with a choice of bare coupling at the UV cut off (lattice scale) that lies above the fixed point value. These theories have a UV Landau pole in the continuum, but the lattice UV cut off can protect the IR from knowledge of its existence. They observed no chiral symmetry breaking even with the UV coupling 30% or so above the fixed point value, and this indeed suggests that the fixed point preserves chiral symmetry. This analysis is a crucial and convincing aspect of their work.

The second part of our work is to ask: can this method of studying the theory at couplings above the critical coupling always be easily used? As the coupling is raised in the UV in the holographic model, it will at some point violate the BF bound at the UV scale. If it does, then there is no

stable vacuum in the holographic model. We associate this phase to the "lattice artefact phase" often seen in lattice simulations if the bare coupling is taken too large [73]. It is associated with chiral symmetry breaking at the lattice scale (and is also not rotationally invariant). In particular we point out that as the fixed point coupling value moves towards the BF bound violating value, this artefact phase moves very close to the physical phase. A lattice simulation would need to fine tune the coupling to the fixed point value, from above, to be fully certain that the theory is in the conformal window.

Our conclusion is that, were a theory to lie within 10% (for example in N_f) of the edge of the conformal window, it would be very difficult to identify the phase. On a finite lattice, chiral symmetry breaking theories may look conformal on the lattice when the UV coupling is picked below the fixed point value. On the other hand, picking UV couplings above the fixed point will likely leave a theory in the artefact phase. The resolution of the behaviour becomes arbitrarily harder the closer one approaches the edge of the conformal window. Thus studies of the $N_c = 3, N_f = 8, 9$ theories, such as in [74, 75] may encounter these problems, and indeed [76] suggests that the artefact phase may lie close to the physical theory at $N_f = 8$. We hope our simple model helps elucidate the behaviours that are likely to be found in future first principle lattice studies.

6.1 The Holographic Model

We implement the framework from 5.3, restricting to a single representation. Here we allow for a general potential $V(\phi)$ (in Eq. (5.21) this would be $V(X)$) instead of the simple X^2 term seen there. We set by hand

$$\frac{dV}{d\phi} = \frac{1}{r^2}\Delta m^2[r^2 + \phi^2]\ \phi. \tag{6.1}$$

This corresponds to the lowest order term in ϕ (essentially a mass squared) which dictates the dimension of the dual operator along the RG flow. In the IR this term usually triggers any instability to chiral symmetry breaking in top down models [61] when it violates the BF bound. The term therefore contains the minimum information to construct a sensible model.

As noted in 5.3.2, if $\Delta m^2 = 0$, then the scalar describes a dimension 1 source and a dimension 3 operator (its solution is $\phi = m + c/r^2$). If Δm^2 is a constant, then it corrects the dimensions as in Eq. (5.29).

We allow Δm^2 to depend on r to represent the holographic running of the theory. In addition we correct r to $\sqrt{r^2 + \phi^2}$ which is dimensionally allowed but crucially plays the role that when ϕ grows from zero it can relieve a BF bound violation in the deep IR, allowing for a stable solution for ϕ.

As we have discussed above we will simply assume that

$$\Delta m^2 = -k\alpha, \tag{6.2}$$

where k is a constant and α is the running coupling of the gauge theory which we extract from the lattice results for the SU(3) gauge theory with $N_f = 10$ (Figure 6.1).

Note that in the perturbative regime at one-loop in the gauge theory $\gamma_{\text{pert}} = 3C_2(R)\alpha/2\pi$. For the fundamental representation $C_2(F) = (N_c^2 - 1)/2N_c$. For $N_c = 3$ this gives $\gamma = 0.64\alpha$. In this regime, where γ is small, we can expand (5.29) and find $\Delta m^2 = -2\gamma$, so $k = 3C_2(R)/\pi$, which for $N_c = 3$ gives $k = 1.27$. This approximation would say that the $N_c = 3, N_f = 10$ theory would break chiral symmetry when $g^2 = 9.9$, before $g^2 = 15$.

On the other hand, if one wishes $\gamma = 1$ to equate to the BF bound point when $\Delta m^2 = -1$ then one would pick k to be half this value, $k = 0.64$. This would predict the $N_c = 3, N_f = 10$ theory would break chiral symmetry at $g^2 = 19$, above the $g^2 = 15$ fixed point identified on the lattice.

If one takes the lattice value of the fixed point for $\alpha = 15/4\pi$ and wanted $\Delta m^2 = -1$ in the IR to enforce that it is the edge of the conformal window, then one would pick $k = 0.84$.

The lattice data itself has $\gamma = 0.6$ when $\alpha = 15/4\pi$, and so suggests $\gamma = 0.5\alpha$, which is smaller than the one-loop result. The lattice analysis places the theory in the conformal window and would hence propose that $k < 0.84$. Our analysis is now to question whether the lattice might have misidentified the value of k linking α and the BF bound violation, so that these values of γ or α actually place the theory in the chirally broken phase.

Below, in theories that break chiral symmetry, we will call the scale at which the BF bound is violated Λ_{BF}. For very walking theories, this will essentially be the scale where the theory hits its IR fixed point.

N.b.: we can view changing k for a fixed running profile as studying a range of theories near the conformal window edge - one is basically just assuming the coupling as a function of RG scale varies by an overall constant as one changes between theories. In the IR this is probably a reasonable ansatz for the $\alpha(\mu)$ function.

We first choose our running coupling function. We fit the lattice results [70] for the beta function in the $N_c = 3, N_f = 10$ theory, constructing an interpolating function that we show in red in Figure 6.1. We then integrate to obtain the running α shown also in Figure 6.1.

Now to find our vacuum solutions we solve the equation of motion with the on shell boundary conditions as established in Eq. (5.30):

$$\phi(r_{\text{min}}) = r_{\text{min}}, \qquad \partial_r \phi(r_{\text{min}}) = 0. \tag{6.3}$$

This boundary condition is motivated by that of similar D3/probe D7 system equations [60]. We interpret $\phi(r_{\text{min}})$ as the IR constituent quark mass. We will consider cases where the choice of k places this theory either in the conformal window or in the chiral symmetry breaking phase above the conformal window edge.

We will now consider approaching the edge of the conformal window from above (the set of theories that break chiral symmetry) and from below (theories that are conformal).

6.2 Approaching the edge of the Conformal Window from above

First, let us consider the cases with $k > 0.84$ - these theories will break chiral symmetry, approaching the edge of the conformal window as $k \to 0.84$.

In Figure 6.2 we plot the solutions of ϕ against r for several k values. For this plot, we have rescaled the energy scale of the theories so that the IR quark mass is equal in each case. We have coloured the segments of the solutions (the range of r) where the BF bound is violated (at $\phi = 0$) in red. This shows that at lower k where the BF bound is violated less strongly, the theory takes a longer period in RG running to respond to the instability. In the limit where $k \to 0.84$ the gap between the BF bound violation scale and the IR mass scale diverges.

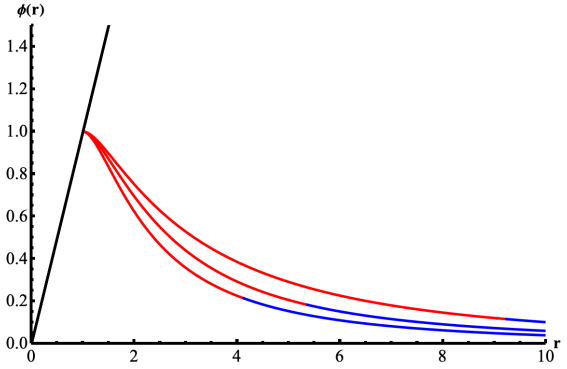

FIGURE 6.2: The vacuum solutions ϕ for $k = 3, 1.8, 1.4$ with the scale of r_{min} scaled to one in each case. The red part of each solution shows the r range where the BF bound is broken at $\phi = 0$.

Note that if one increases k too much, then chiral symmetry breaking is triggered in the far UV, where the running of the coupling is also slow. Here too, one sees a separation in scale between the BF bound violation point and the mass gap scale. Since these theories are breaking chiral symmetry in the very weakly coupled regime, we consider this unphysical. Thus, k values above 3-4 are not sensible.

To quantify the scale separation, we can define a scale where Δm^2 lies at $\Lambda_x = x\Lambda_{BF}$. In other words, if $x = 0.95$ then it is the scale where the theory reaches a ΔM^2 of 95% of its value to cause a BF bound violation. In Figure 6.3 we plot the ratio of the IR quark mass scale to this

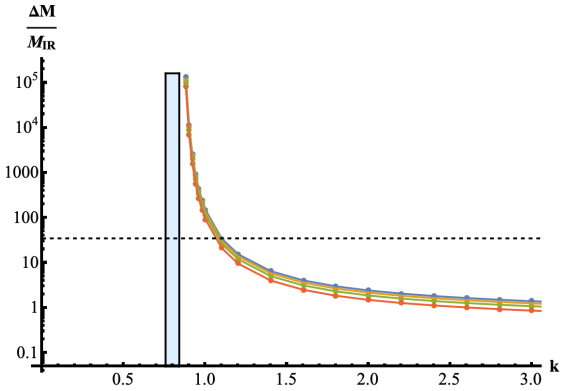

FIGURE 6.3: Mass ratio as a function of k for the four values of x along with a 10% area (blue box) under the minimum BF-bound violating value of $k = 0.84$. Curves pass through a mass ratio of 35 at: $k = 1.099$ for $x = 0.8$, $k = 1.088$ for $x = 0.85$, $k = 1.076$ for $x = 0.9$ and $k = 1.058$ for $x = 0.95$. The blue shaded region below the critical k value shows where the critical coupling lies within 10% above the fixed point value.

scale for a variety of values of x. Note that the scale separation between this UV scale and the IR mass scale is greater than 35 if $0.84 < k1.1$.

Let's put this in context for the lattice simulations: one might believe that one has a theory that lies in the conformal window and see fixed point behaviour. One could set the UV lattice coupling at 95% of the fixed point value and use a $(35)^4$ point lattice and not see chiral symmetry breaking for these theories near the edge of the conformal window. However, we see that if k lies in the range discussed, then it could be that just before the fixed point, an instability to chiral symmetry breaking sets in, yet the IR mass scale is below the IR resolution scale of the lattice.

Could this be the case for the SU(3) $N_f = 10$ theory? If one reasonably thought the critical k lies in the range 0.4-1.4 then 15% of that range could actually be unseen chiral symmetry breaking if one didn't pick the UV coupling very carefully! In the next section, we will see that the work done with UV values of the coupling above the fixed point value strongly suggest this is not the case for that particular simulation. We will highlight additional concerns though, for theories nearer the conformal window edge.

6.3 Approaching the edge of the Conformal Window from below

If a lattice simulation of a theory suggests that a theory lies in the conformal window, then there is a simple proof of consistency. One studies the theory with UV lattice coupling value lying above the fixed point value. Such a theory in the continuum flows to the IR fixed point in the IR but will have a UV Landau pole. The UV cut off though, of the lattice provides protection from this pole and one can happily simulate. If such a case, with UV coupling above the fixed point, remains IR conformal then the evidence is overwhelming that the theory is indeed in the conformal window. This is the case for the SU(3) $N_f = 10$ simulation [70] and so its conclusions seem very robust.

Is this methodology always available though? It is well known that if on a lattice you raise the bare coupling too far, then a first order transition occurs to a new phase that is gapped on the scale of the lattice (and doesn't display rotational symmetry) [73]. This phase is often called a "lattice artefact phase". Here we want to connect that high coupling phase to the chiral symmetry breaking phase in the holographic model. We will argue that as one approaches the edge of the conformal window that phase lies very close to the true phase of the theory.

In the holographic model one can also naïvely study the theories with a Landau pole that flow to the IR fixed point from above. To exclude the pole one can include an explicit maximum value of r and impose that ϕ should vanish there. Solutions of the form in Figure 6.2 exist - and continue to exist even as the UV cut off is moved close to the Landau pole. At some point as the UV cut of is raised, the UV value of Δm^2 violates the BF bound. In fact, even here there are solutions of the form in Figure 6.2 with the action choosing to minimize the r derivatives in the IR as compensation for the UV BF bound violating potential term. These solutions should not be viewed as physical though. If there is a BF bound violation in the UV, there is an instability at that scale to the unlimited growth of $\bar{q}q$. The theory will gap at the UV scale and never reach the IR values of r. If one tracks back the picture in Figure 6.2 to the D3/probe D7 model, then the statement is that there is a D7 embedding situated at the UV cut off and perpendicular to the r axis which is energetically preferred (in fact, since the UV cut off there is for the radial distance $\sqrt{r^2+\phi^2}$, the embedding is just a point and the theory is rather nonsensical). This transition, the instant the BF bound for ϕ is violated by the UV coupling, which is first order since the condensate jumps from zero to very large, seems analogous to the lattice artefact phase. Likely both the holographic and lattice model share this instability at the UV cut off scale. In the lattice case, since the regulator does not obey rotational symmetry, the instability may also be localized at some points on the lattice, but the spirit of the transition is shared.

There is a natural concern that arises from this discussion. At the edge of the conformal window, we expect the fixed point value of the coupling to just violate the BF bound. Were one to place the UV coupling to the fixed point value though, one would trigger a transition to the artefact phase. In other words, the artefact phase lies arbitrarily close to the physical phase as one approaches the conformal window.

To quantify this issue, we plot in Figure 6.3, as a band, the range of k below $k = 0.84$ in our theory where setting the UV coupling to 10% above the fixed point value violates the BF bound. In this region a lattice simulation is going to have to tune the UV coupling above the fixed point to confirm the conformal nature of the fixed point. We can see from Figure 6.3 that theories with $0.76 < k < 0.84$ are very hard to study in this way - this is 12% of the range $k = 0.4 - 1.4$.

Let's assume the artefact phase is caused by a chiral instability as discussed: then we can use the fixed point values at $N_c = 3, N_f = 10$ ($g^2 = 15$ and $\gamma = 0.6$) to estimate the coupling where $\gamma = 1$, assuming they are proportional, to be $g^2 = 25$. This indeed broadly matches the value for the onset of the artefact phase seen in [73]. An added complication on the lattice, that we will not study here, is that the rotational symmetry breaking nature of the lattice cut off will distort

the nature of the transition to the artefact phase. The variation of the critical coupling to enter the artefact phase with different regulators is studied in [73]. Hence there is an additional uncertainty in the precise value of the critical coupling in any lattice simulation.

6.4 Discussion

We have used a holographic model of chiral symmetry breaking in SU(N_c) gauge theories with quarks in the fundamental representation to study the transition from the conformal window to the chiral symmetry breaking phase. We have used the running determined by the lattice simulations in [70] at $N_f = 10$ but included an additional parameter, k, that determines the relation between the anomalous dimension of $\bar{q}q$ γ and the coupling α. Here, varying k effectively moves us through the edge of the conformal window, playing the role of N_f.

There have been some recent lattice studies [77, 78] that suggest that for particular N_f values (e.g.: $N_f = 8$ for $N_c = 3$) an additional phase is possible where a four fermion operator condenses and the theory gaps without breaking chiral symmetry. This crucially depends on the absence of anomalies in these theories. Our model does not include this operator so we do not include this possibility. It would be interesting to provide a holographic model of this phase in future work.

For the transition from the conformal window to a chiral symmetry breaking phase, we have highlighted two issues. The first is that when one places the UV coupling below the fixed point value in chiral symmetry breaking theories, there are two scale separations near the edge of the conformal window. Firstly, there is a separation between the scale where the theory enters strong coupling and the scale where the instability to chiral symmetry breaking occurs. But in addition there can be a scale separation between the scale where the instability sets in and the actual scale of condensation. As one reaches the conformal window edge, both of these scale separations diverge.

The second issue is in theories that lie in the conformal window and where one simulates with the UV cut off coupling above the fixed point value. Here, the chosen UV coupling can lie above the critical coupling and this triggers an instability in the holographic model which we believe is equivalent to the lattice "artefact phase" where chiral symmetry is broken at the lattice scale. As one approaches the conformal window edge, this artefact phase lies arbitrarily close to the fixed point value.

We estimate that for theories within 10% (above and below) of the conformal window edge, considerable tuning will be needed. Placing the UV coupling of the theory below the fixed point value is likely to not show chiral symmetry breaking even if it is present because of the scale separation. Moving the UV fixed point above the critical coupling will place the simulation in the artefact phase. One will be left tuning the UV coupling above the fixed point value seeking a lower edge to the artefact phase that may be very close to the fixed point value.

To finish on a more positive note though, our analysis does support the recent $N_f = 10$ lattice analysis [70]. There, a chiral symmetry preserving phase has been found for UV couplings above the fixed point value and that provides strong confirmation that the theory lies in the conformal window.

Chapter 7

Mass Hierarchies in Gauge Theory With Two Index Symmetric Representation Matter

In QCD the logarithmic running of the asymptotically free gauge coupling leads to an infra-red strong coupling regime in which chiral symmetry is dynamically broken, generating the scale of the baryon masses. QCD also exhibits confinement at the same or very similar scale (although there is no formal order parameter for confinement in the light quark theory). These same behaviours are expected in many asymptotically free non-supersymmetric gauge theories with fermionic matter and, for example, lattice studies have confirmed this for theories: with N_f^F fundamentals other than $N_f^F = 3$ [74, 75]; fermions in the adjoint [79]; two index symmetric representation [80]; and two index anti-symmetric representation (with fundamentals) [81].

It is an interesting question as to whether such theories can generate multiple scales [82, 83]. A natural way to do this is to include fermions in two (or more) representations which might interact with the strongly coupled glue differently. Were higher dimension representations to condense at a lower coupling value a gap to the confinement scale might also be possible.

A criterion for the formation of a chiral symmetry breaking bi-fermionic operator (with perturbative dimension $\Delta = 3$) has been deduced from both gap equation analysis [67] and holographic models [68, 69, 61]. It is: when the anomalous dimension of the bi-fermion operator, γ, rises to one, so that the mass and operator are of equal dimension $\Delta = 2$, there is an instability to condensation. This is most simply seen in holography where a bulk scalar in AdS_5 (with unit radius), dual to an operator has mass squared $M^2 = \Delta(\Delta-4)$ [14] and the Breitenlohner-Freedman stability bound in AdS_5 is $M^2 = -4$ which is precisely saturated at $\Delta = 2$ [57].

In [83] we performed a simple analysis of using perturbative results, extrapolated into the non-perturbative regime. We estimated the scales where the $\gamma = 1$ criteria occurred for different multi-representation theories. Of course the results depend on the extrapolation - there, and

here, we follow the ansatz of [66] which for example places the edge of the conformal window with fundamentals at approximately $4N_c$. Lattice results suggest it may be as low as $N_f^F = 10$ in the SU(3) gauge theory [70] but the ansatz we take provides some sensible estimate for the running with the associated physical flavour numbers adjustable by the readers expectations for where the conformal windows begin. We will also use a different ansatz where the anomalous mass of the AdS scalar, Δm^2, is double the perturbative estimate to provide a most pessimistic scenario.

In a theory with a single Dirac fermion in the two-index symmetric representation and N_f^F Dirac fermions in the fundamental representation it was possible to find theories where the separation of scales was possibly of order ten. These theories are therefore of potential interest and also look open to lattice analysis. The most extreme cases are quite walking theories and this might present problems on the lattice.

In this chapter, therefore, we perform a further analysis where we study the meson spectrum of these theories ($SU(N_c)$ gauge theory with one two index symmetric representation fermion and N_f^F fundamentals) as a function of N_c and N_f^F. Our goal is to go beyond the naïve perturbative analysis by including the dynamics of chiral symmetry breaking, not just estimating the scale where the instability sets in. We are also interested in how finely tuned N_f^F needs to be for the gap to be explorable. For example, the lattice can study fermions in multiples of four more easily than arbitrary choices. Reaching the massless limit can also be challenging on the lattice as we will discuss.

Our tool is a holographic model of the dynamics [60]. We have previously used this model to study walking dynamics [84, 85] and composite higgs models [86, 87, 88]. The model is based on the D3/probe D7 system [58, 55, 52] in holography. It is a simple system in which one uses the weakly coupled Dirac-Born-Infeld (DBI) action to study the position and fluctuations of the D7 branes in AdS_5. Remarkably this is believed to be an exact study of quarks in the $N = 2$ supersymmetric gauge theory with $\mathcal{N} = 4$ glue. Further one can perturb this system, breaking supersymmetry and seeing chiral symmetry breaking (for example by adding a magnetic field [72] or by deforming the background geometry [71]). From the perspective of the DBI action these changes manifest in the mass squared for the scalar dual to the quark bilinear (the position of the D7 brane). That mass squared becomes dependent on the radial coordinate in AdS, dual to the renormalization group scale [61]. The duality translates this to a running dimension of the operator and condensation is triggered when $\gamma = 1$. Our AdS/Yang-Mills model [60] simply takes this precise system and imposes the running of a gauge theory to determine the dynamics. Here we use the perturbative two loop results for the running of α extended into the non-perturbative regime as our ansatz for this running. Whilst this may be insecure we can at least see the response of the theory to different runnings and critical couplings.

The main conclusions, as we will see, are that the holographic model does support the presence of the gaps seen in the perturbative analysis (in part, of course, because it incorporates those runnings). These gaps can be larger than an order of magnitude: for example in SU(4) theory

with $N_f^F = 11$, SU(5) with $N_f^F = 15$, and SU(7) with $N_f^F = 22$. We caveat this with a more pessimistic translation of the running coupling to the AdS scalar mass correction, Δm^2, but even there the gaps can be a factor of 2 which is still a clear scale separation. We show the theories with large gaps are quite slowly running and live close to the fixed points which only just trigger chiral symmetry breaking. We also identify theories with smaller gaps and more QCD-like running. We hope to inspire lattice simulations of these theories, which can show from first principles a separation between chiral symmetry breaking scales and even the confinement scale.

7.1 The Holographic Model

We make use of the holographic AdS/Yang-Mills model first developed in [60] and which we detailed in 5.3. Before continuing we will make note of a few things.

The dynamics of a particular gauge theory, including quark contributions to any running coupling, are included through the choices of Δm_R^2 in Eq. (5.21). Our starting point is the perturbative result for the running of γ_p. Expanding $M^2 = \Delta(\Delta - 4)$ at small γ gives $\Delta m^2 = -2\gamma$. As discussed in sec. 5.3 we therefore take the ansatz

$$\Delta m^2 = -2\gamma_p. \tag{7.1}$$

Since the true running of γ is not known non-perturbatively, we extend the perturbative results as a function of renormalization group (RG) scale μ to the non-perturbative regime. We will directly set the field theory RG scale μ equal to the holographic RG scale $r = \sqrt{\rho^2 + |X_R|^2}$.

Further, we use the one-loop anomalous dimension result (going beyond one loop does not introduce any new structures into what is already a guess as to the form of the running).

To find the vacuum of the theory, with chiral condensates, we set all fields to zero except for $|X_R| = L_R(\rho)$. For Δm_R^2 a constant, the equation of motion from Eq. (5.21) is

$$\partial_\rho(\rho^3 \partial_\rho L_R) - \rho\ \Delta m_R^2 L_R = 0\,. \tag{7.2}$$

At large ρ - the UV - the solution is given by $L_R(\rho) = m_R + c_R/\rho^2$, with c_R the fermion condensates of dimension three and m_R, the mass, of dimension one. We numerically solve Eq. (7.2) with our input Δm_R^2 for the function $L_R(\rho)$. We use IR boundary conditions at the point where the fermions move on mass shell

$$L_R(\rho)|_{\rho=\rho_R^{IR}} = \rho_R^{IR}\,, \qquad \partial_\rho L_R(\rho)|_{\rho=\rho_R^{IR}} = 0\,. \tag{7.3}$$

We numerically vary ρ_{IR} until the value of L_R at the boundary is the desired fermion mass. We call the vacuum solutions $L_{R0}(\rho)$ with IR value L_R^{IR}.

In the models we study the two index symmetric representation always condenses at a higher ρ_R^{IR} than the fundamental representation. At that scale we integrate out the symmetric representation fermions and remove their contribution to the beta function at lower scales. We show an example running of Δm_R^2 for the two representations in Figure 7.1.

Finally we note that, regarding the running of γ, a more pessimistic ansatz which we will also use below is to remove the factor of 2 in (7.1) which then requires α to be larger in the IR to trigger chiral symmetry breaking for the symmetric representation. This reduces the number of flavours of fundamentals one can include in the theory before one enters the conformal window. Further the speed of running in the fundamental theory below the symmetric representation dynamical mass will be faster since it itself is controlled by the value of α and this will tend to close the gap between the scales where the two representations condense. We will use this to show how big the errors in the analysis could potentially be.

7.2 N_c and N_f^F Dependence In the Massless Theory

We can now move to discussion of the predictions of the holographic model.

7.2.1 $N_c = 5$ Theory

We will begin by looking at an extreme theory that encapsulates the gains and losses in these models. So first we pick the SU(5) gauge theory with one two index symmetric, dimension 15 representation and N_f^F fundamental flavours. This model was identified as having the largest gap between the condensation scales of the two representations in [83] for $N_f^F = 15$. In that discussion the 15 were eliminated from the running at the scale where $\gamma_{15} = 1$ and the $\gamma_F = 1$ RG scale computed from the running, giving a separation of a factor of 15.

We can now enact this theory in the holographic model which includes the chiral symmetry breaking dynamics. We show the running of Δm_{15}^2 against the log of the RG scale in Figure 7.1 in blue. Here we work in units of the eventual ρ-meson mass made of the 15 dimensional representation matter.

Note the theory looks to have an IR fixed point but this will not be realized because chiral symmetry breaking will be triggered before it is fully reached. The 15 hits $\gamma = 1$ first at a scale

$\ln \mu = 14.2$. This seems like a very high scale relative to the emergent ρ-meson mass and it is! The reason is that the IR fixed point value of the γ_{15} is very close to 1 (that is Δm^2_{15} at the fixed point is just -1.05). Although there is an instability at a high scale we must include the full

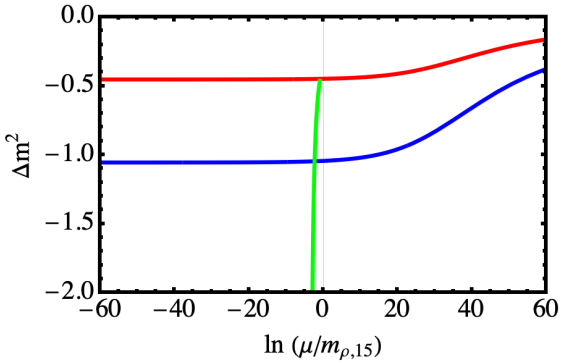

FIGURE 7.1: SU(5) gauge theory with $N_f^F = 15$: The running of Δm^2 for the two index symmeric 15 dimensional rep. (blue), fundamental (red) and for the fundamentals with the higher dim rep. decoupled below the scale where it is on mass shell (green). The energy scales are given in units of the ρ-meson mass in the 15 sector. BF bound violation occurs at 14.2 for the 15 and -2.3 for the fundamental with the 15 decoupled.

chiral symmetry breaking dynamics to see how speedily the condensate formation responds to the instability.

In Figure 7.2 we show the resulting field $L_{15}(\rho)$ in the holographic model (also in blue) - it can be thought of as the effective fermion mass as a function of RG scale. It shows chiral symmetry breaking, bending away from $L = 0$ in the infra-red. As hinted at above the IR value of $L_{15}(\rho)$ is much smaller than the scale where the $\gamma = 1$/BF bound is violated.

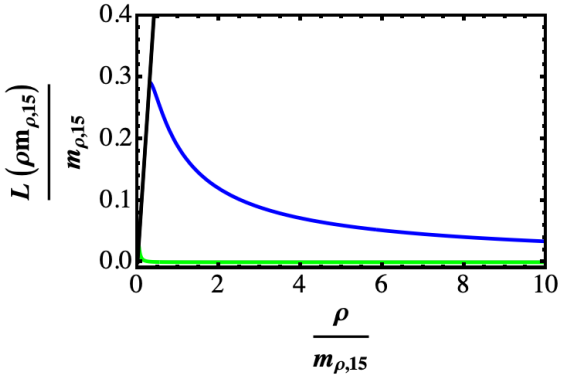

FIGURE 7.2: SU(5) gauge theory with $N_f^F = 15$: The $L_R(\rho)$ functions for the 15 (blue) and 5 (green) representations with $m_{IR,S} \approx 0.29$ and $m_{IR,F} \approx 0.027$ respectively in units of the ρ-meson mass in the 15 sector.

The reason for this is that the BF bound violation comes with a potential energy cost, but equally, derivatives of the $L(\rho)$ function also cost energy. The resultant solution is a balance between these costs. In this theory at the scale of the BF bound for the 15 the running is so slow and centred essentially on the violation value that the solution prefers to "live with it" rather than bending off axis immediately. Only at a much lower scale does the chiral symmetry breaking set

in because the cost of the BF bound violation has built up over several orders of magnitude in RG scale. This is an example of why incorporating the chiral symmetry breaking dynamics in the model is important to understand the true mass scales. The extreme walking behaviour in the UV of this theory would make its study on the lattice quite problematic.

We now move to the fundamental sector. The running Δm_5^2 is shown in Figure 7.1 - above the scale where the 15 goes on mass-shell the running is given by the red curve. We integrate out the 15 at the IR value of $L_{15}(\rho)$ where $L_{15}(\rho) = \rho$. The running is then that of the green curve in Figure 7.1. It is straightforward to set up an interpolating function that incorporates the UV red running and the IR green running. $\gamma = 1$ for the fundamentals is reached at $\ln \mu = -2.3$.

We can now solve for the $L(\rho)$ function for the 5 representation. We display this in green in Figure 7.2. We can see there is a gap of a factor of 10.7 between the IR mass values for the two representations. This is of order, but not quite as large as the factor of 15 we naïvely expected. Here there is not a large gap between the BF bound violation scale and the emergent IR mass because the running is much faster once the 15 have decoupled (although we have chosen N_f^F to slow this running to generate the gap). The gap size is therefore in line with the expectations of the running analysis of [83] although both scales are significantly lower than expected from the $\gamma_{15} = 1$ criteria.

It is now possible to use the holographic model to compute the spectrum of the gauge theory. We do this not just for $N_f^F = 15$ but at all N_f^F values (recomputing the vacuum equivalent to Figure 7.2 at each value). We show the results in Figure 7.3. In each theory we normalize the spectrum by the ρ-meson mass of the 15 representation matter so the symmetric representation ρ line (blue) is flat at one by construction. We display the decay constants of the theory also in Figure 7.4. We see that the symmetric representation ρ decay constant is also essentially independent of the number of fundamental fermions (it would grow with the number of 15 representation flavours but we keep that fixed at one here).

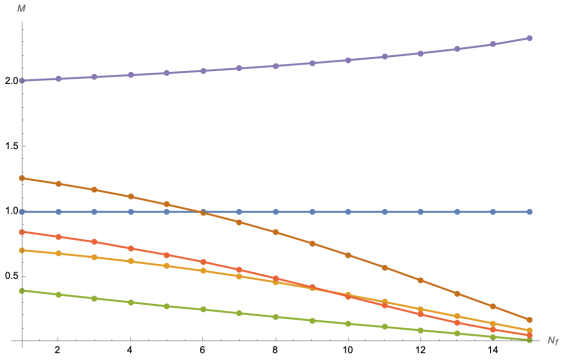

FIGURE 7.3: Mass spectra for the SU(5) theory, ρ-mesons in blue (symmetric) and dark yellow (fundamental), σ-mesons in green (symmetric) and orange (fundamental), axials in purple (symmetric) and brown (fundamental). The pions in both sectors are massless at zero fermion mass.

The axial meson mass (purple) in the symmetric representation sector is larger than those of the ρ, its decay constant is also marginally larger, but they are essentially unresponsive to the number of light fundamental fermions also.

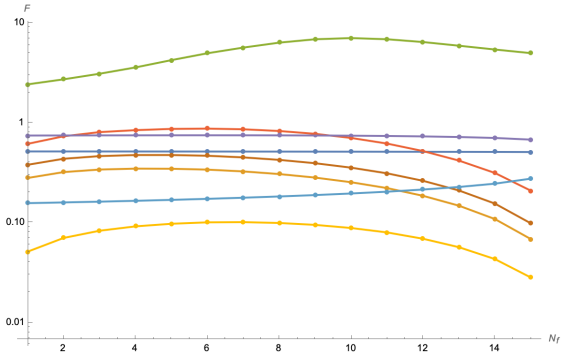

FIGURE 7.4: Decay constants for the SU(5) theory, ρ-mesons in blue (symmetric) and dark yellow (fundamental), σ-mesons in green (symmetric) and orange (fundamental), axials in purple (symmetric) and brown (fundamental) and pions in cyan (symmetric) and light yellow (fundamental).

The ρ-meson mass in the fundamental sector (dark yellow) is a good measure of the gap. We see from Figure 7.3 that this ρ mass falls relative to the ρ mass in the 15 sector. The extreme value is a gap of ~11.3 between these masses for $N_f^F = 15$ (at higher N_f^F the UV theory is in the conformal window). The fundamental sector ρ decay constant initially rises with N_f^F but then falls as the scale of the gap falls at larger N_f^F.

The σ-meson in the symmetric representation sector (green) is the lightest state reflecting the walking in the high energy theory. Its decay constant initially grows, before falling off at high N_f^F in the more walking theory. The symmetric sector pion decay constant (cyan) is $\sim 2/3$ that of the symmetric sector ρ-meson and rises slowly with N_f^F.

The σ-meson mass in the fundamental sector (orange) falls as N_f^F rises as the theory below the 15's mass gap becomes also more walking. The theory is never as walking as the far UV theory though. The fundamental sector axial meson (brown) displays similar mass spectra and both it and the fundamental pion (light yellow) show similar decay constant behaviour.

Although the gap between the ρ-mesons in the two sectors is slightly smaller than the naïve factor of 15 that one obtains from taking the ratio of the scales at which the BF bounds are broken, it is still significant. Below the mass scale of the 15 the perturbative computation of how long the coupling takes to run to the BF bound remains the core mechanism. In principle one could study the theory at finite temperature and expect to find an intermediate phase where the 15 representation experiences chiral symmetry breaking but the fundamentals do not and presumably this phase also has no confinement.

7.2.2 Other N_c

Given the gap in the SU(5) theory has not been quite as large as we expected it is interesting to look at the N_c dependence of the spectrum. We have studied the $N_c = 3, 4, 6, 7$ cases as well. In each case again there is one two index symmetric representation fermion and N_f^F fundamental fermions. We compute for all N_f^F up to the limit in each case where our ansatz for the running of γ places the theory in the conformal window, The results are shown in Figure 7.5 and are similar to the SU(5) case. The largest gaps between the ρ-meson masses of the two sectors are:

- SU(3), $N_f^F = 8$: 7.34;
- SU(4), $N_f^F = 11$: 11.34;
- SU(6), $N_f^F = 18$: 9.70;
- SU(7), $N_f^F = 22$: 13.54.

At this point it is important to quantify at least in some way how reliable these results are. In particular they depend on the running ansatz at a given N_f^F and N_c and also the translation of the running γ to Δm^2. In particular the key point is at what scale the BF bound is violated and the derivative in the running at that point. One way to test this is as discussed below (5.24) - we by hand remove the factor of 2 in (7.1) effectively doubling the critical coupling value required. This lowers the value of N_f^F where the edge of the conformal window lies (to $N_f^F = 6$ for example in the theory with $N_c = 3$). It also narrows the gap between the two representation sectors since the coupling is running quicker in the interval below the constituent mass of the symmetric representation matter.

As an example we show the mass spectrum for the SU(3) gauge theory in this approximation in Figure 7.6. The gap at $N_f^F = 6$ is a factor of 2 which is not hugely different from that we saw at the same N_f^F value above. However since it is the closest we can tune to the conformal window edge this result is considerably smaller than the value for the gap we had for $N_f^F = 8$ previously of 7.34. As a pessimistic example it still displays a gap of a factor of 2 which is discernible and could be split by a theory with temperature between these two scales.

Returning now to the original version of (7.1), we consider if one were to seek this behaviour on the lattice. Then it is usually simplest to study fermions in multiples of four N_f^F. One needs to be careful though, because our ansatz for where the edge of the conformal window lies need not be accurate, so one does not want to lie too close to that boundary. The majority of the mass gap is gained only at the last few N_f^F increments. Given lattice computations are easier with $N_f^F = 4n$, the gaps in the following theories may be of interest:

- SU(3), $N_f^F = 8$: $\frac{m_{\rho 15}}{m_{\rho F}} = 7.34$
- SU(4), $N_f^F = 8$: $\frac{m_{\rho 15}}{m_{\rho F}} = 2.93$

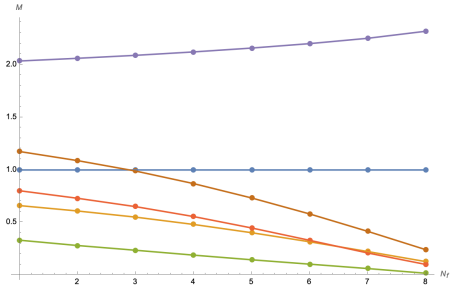

(A) Mass spectra for the SU(3) theory.

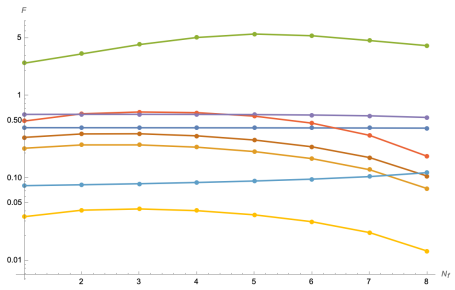

(B) Decay constants for the SU(3) theory.

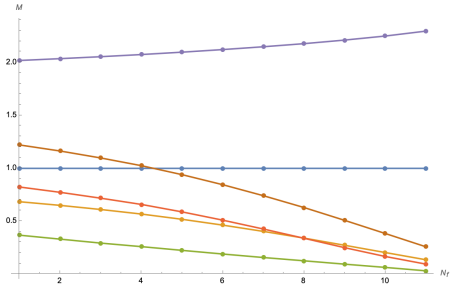

(C) Mass spectra for the SU(4) theory.

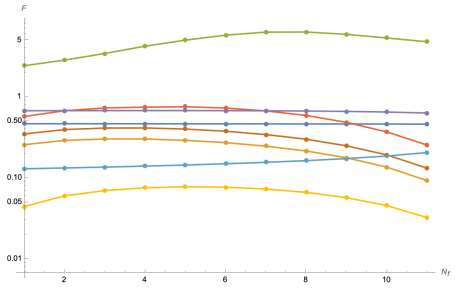

(D) Decay constants for the SU(4) theory.

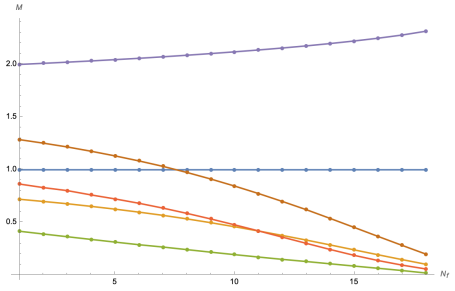

(E) Mass spectra for the SU(6) theory.

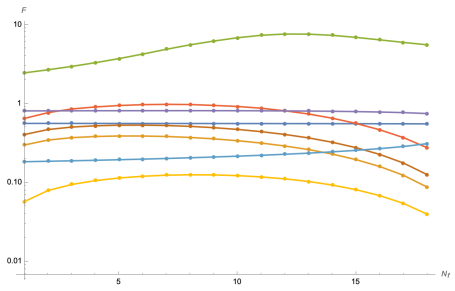

(F) Decay constants for the SU(6) theory.

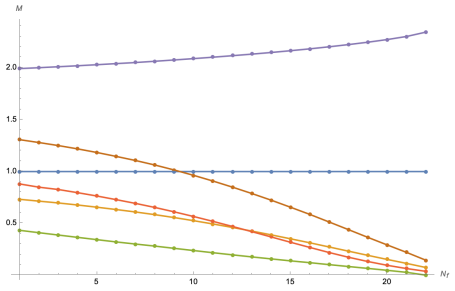

(G) Mass spectra for the SU(7) theory.

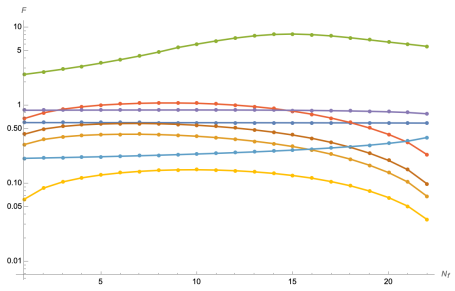

(H) Decay constants for the SU(7) theory.

FIGURE 7.5: The spectra and decay constants of the SU(N_c) gauge theory with one two index symmetric rep. matter field and N_f^F fundamentals for $N_c = 3, 4, 6, 7$. ρ-mesons in blue (symmetric) and dark yellow (fundamental), σ-mesons in green (symmetric) and orange (fundamental), axials in purple (symmetric) and brown (fundamental) and pions in cyan (symmetric) and light yellow (fundamental).

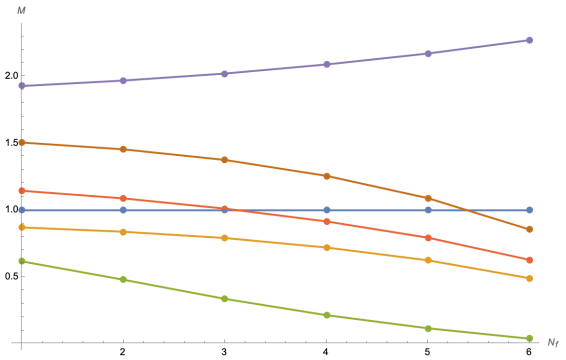

FIGURE 7.6: Meson masses for the SU(3) theory with a factor of 2 removed in (7.1): ρ-mesons in blue (symmetric) and dark yellow (fundamental), σ-mesons in green (symmetric) and orange (fundamental), axials in purple (symmetric) and brown (fundamental) and pions in cyan (symmetric) and light yellow (fundamental).

- SU(5), $N_f^F = 12$: $\frac{m_{\rho 15}}{m_{\rho F}} = 3.97$
- SU(6), $N_f^F = 16$: $\frac{m_{\rho 15}}{m_{\rho F}} = 5.18$
- SU(7), $N_f^F = 20$: $\frac{m_{\rho 15}}{m_{\rho F}} = 6.59$

The example of SU(5) with $N_f^F = 15$ though, warns that the UV of these theories might be very walking with widely separated scales. That would make analysis hard on the lattice.

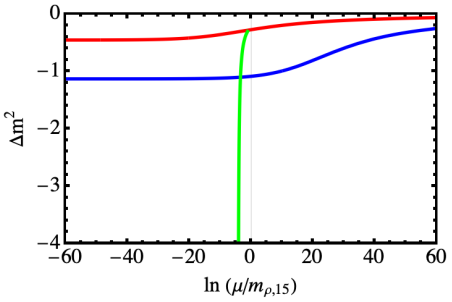

(A) SU(3) with $N_f^F = 8$: $\Delta m^2 = -1$ occurs at 9.3 for the 6 and -2.1 for the 3 with the 6 decoupled.

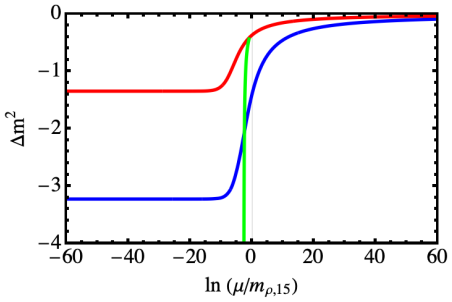

(B) SU(4) with $N_f^F = 8$: $\Delta m^2 = -1$ occurs at 2.2 for the 10 and -1.3 for the 4 with the 10 decoupled.

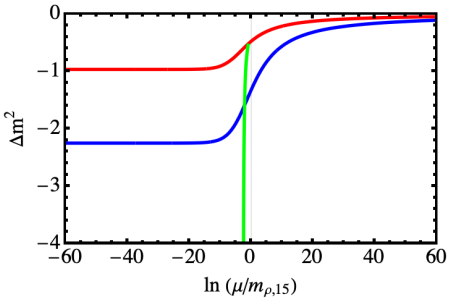

(C) SU(5) with $N_f^F = 12$: $\Delta m^2 = -1$ occurs at 3.0 for the 15 and -1.5 for the 5 with the 15 decoupled.

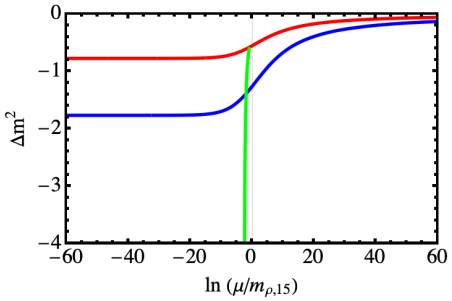

(D) SU(6) with $N_f^F = 16$: $\Delta m^2 = -1$ occurs at 3.8 for the 21 and -1.7 for the 6 with the 21 decoupled.

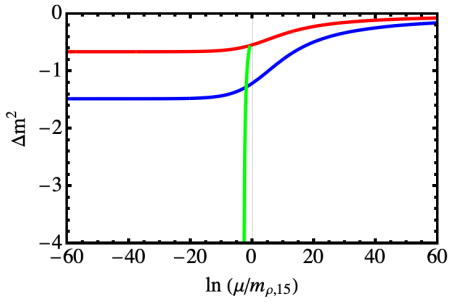

(E) SU(7) with $N_f^F = 20$:$\Delta m^2 = -1$ occurs at 4.9 for the 28 and -1.8 for the 7 with the 28 decoupled.

FIGURE 7.7: The running of Δm^2 vs $\ln \mu$, for theories with N_f^F multiples of 4 that give the largest spectral gaps, for the two index symmetric rep. (blue), fundamental (red) and for the fundamentals with the higher dim. rep. decoupled below the scale where it is on mass shell (green). The energy scales are given in units of the ρ-meson mass in the 15 sector.

In Figure 7.7, we show the running of Δm^2 for each case. In all cases the running in the UV theory is faster at the symmetry breaking scale than the case in Figure 7.1. The scales of BF bound violation in the two sectors are more compressed. In fact the SU(4) theory has the strongest running at the 15 condensation scale and so may be the easiest to study on the lattice to find a gap in scales. Of course in that case the gap is only a factor of three - but this trade off may ease the computation.

7.3 A Massive Theory

Finally, we explore briefly the dependence of the gap on the fundamental quark mass. This mass is the most crucial to keep small to maintain the gap size. We study this mass dependence in Figures 7.8 and 7.9 for the SU(3) theory with $N_f^F = 8$ showing the spectrum's dependence on the pion mass in the fundamental sector (which is proportional to the square root of the quark mass at small quark mass). Clearly to maintain the gap one will need the quark mass typically an order magnitude smaller than the chiral symmetry breaking scale of the higher representation.

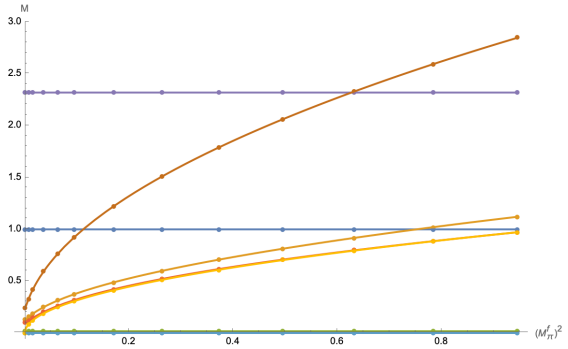

FIGURE 7.8: Mass spectra for the SU(3) theory with $N_f = 8$ and non-zero UV mass. ρ-mesons in blue (symmetric) and dark yellow (fundamental), σ-mesons in green (symmetric) and orange (fundamental), axials in purple (symmetric) and brown (fundamental) and pions in cyan (symmetric) and light yellow (fundamental).

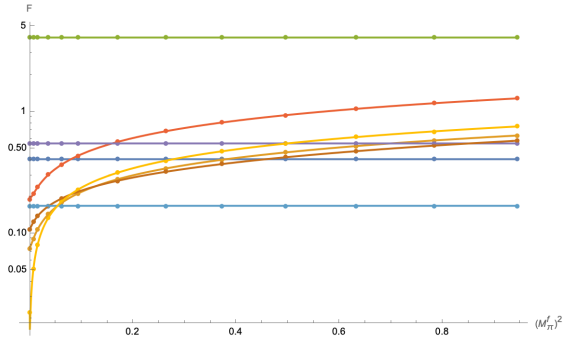

FIGURE 7.9: Decay constants for the SU(3) theory with $N_f = 8$ and non-zero UV mass. ρ-mesons in blue (symmetric) and dark yellow (fundamental), σ-mesons in green (symmetric) and orange (fundamental), axials in purple (symmetric) and brown (fundamental) and pions in cyan (symmetric) and light yellow (fundamental).

7.4 Conclusions

We have used a holographic model to study the spectrum of $SU(N_c)$ gauge theories with one Dirac fermion in the two index symmetric representation and N_f^F Dirac fermions in the fundamental representation. The model predicts the chiral symmetry breaking scale and meson spectrum once the dynamics is included through a running anomalous dimension. We have extrapolated

the perturbative two loop runnings into the non-perturbative regime to provide estimates of these running γ. We have identified a number of theories with spectral gaps between the two ρ-mesons made of fundamental and two index symmetric matter. These gaps could potentially be larger than an order of magnitude. Even in the case where we used a very pessimistic ansatz for the critical coupling value the gaps were still discernible and as large as a factor of two. It would be interesting to study these theories on the lattice to confirm these gaps and to realize theories at finite temperature with chiral symmetry breaking but potentially no confinement. Many of the theories with the largest gaps are quite walking with separated scales but we have identified less walking theories that have a gap that may be easier to study. For example, SU(4) gauge theory with $N_f^F = 8$ may be a candidate with the smaller gap of three but more QCD-like running.

Chapter 8

Holography for QCD(Adj) and QCD(Adj)+F

8.1 Holography for QCD(Adj)

The fundamental mechanisms by which strongly coupled gauge theories, such as QCD, break chiral symmetries and confine remain to be clearly understood. The literature has split into two sectors. One group view chiral symmetry breaking as occurring due to the running coupling driving the anomalous dimension of the quark anti-quark operator through $\gamma = 1$ (see for example [89, 90, 67, 66, 91, 92, 83, 82, 68, 69, 61] and the lattice papers measuring γ with reference to this language such as [74, 70]). In this picture, confinement is a property of the low energy glue theory below the scale where the quarks have been integrated out. The alternative group have sought models where confinement is isolated and associated with non-perturbative monopole configurations [93, 94, 95, 96]. Here, as one moves back towards QCD, the monopole vacuum expectation value (vev) through effective Yukawa terms is responsible for chiral symmetry breaking. In QCD, these scales are presumably very close, and in reality it may be a mixture of these scenarios that occurs. It is interesting to continue to find theories in which the phenomena are separated. Here we will use holographic models of the two scenarios to contrast them and to look for separation mechanisms.

The "$\gamma = 1$" construction was first motivated by Schwinger-Dyson truncation (gap equation) methods [89, 90, 67, 66, 82]. It is natural that an instability switches on when the running coupling grows enough to make the dimensions of the quark mass and condensate equal at $\Delta = 2$. This picture has separately emerged in holography [68, 69, 61], where the dimension of scalar operators is dual to the mass of a scalar in the AdS_5 bulk ($M^2 = \Delta(\Delta - 4)$)[14]. In rigorous top-down models, chiral symmetry breaking is triggered when the mass squared becomes radially dependent and passes in the IR through $M^2 = -4/R$ (where R is the AdS radius) - the Breitenlohner-Freedman instability bound [57]. Models in which supersymmetry and conformality are broken by a magnetic field or running coupling display this mechanism [71, 72]. The

$\gamma = 1$ criteria is often used to determine where the edge of the Conformal Window is for gauge theories as a function of the number of fermion flavours [66, 91, 92]. Here it is believed that the Banks-Zaks fixed point, when N_f lies close to the boundary for the loss of asymptotic freedom, gives way to a chiral symmetry breaking phase at lower N_f where the IR fixed point coupling rises. Lattice studies of the conformal window often concentrate on the value of γ to argue that a theory is IR conformal [74, 70, 97, 98, 99]. Inherent in this world view is that instanton or monopole configurations appear in the deep IR below the chiral symmetry breaking scale.

On the other hand, there have been some very impressive pieces of work in which the confinement mechanism has taken centre stage [93, 94, 95, 96]. The Seiberg-Witten theory of $\mathcal{N} = 2$ supersymmetric Yang Mills (SYM) theory [93] is an example where chiral symmetry breaking is forbidden by the supersymmetry, and non-perturbative monopole configurations manifest. Breaking to $\mathcal{N} = 1$ supersymmetry leads to their condensation and confinement. The gauginos acquire a mass via a Yukawa term to the monopole vev. Another impressive construction is the work in compactified SU(N_c) theories with fermions in the adjoint representation (QCD(Adj)) [94, 95, 96]. When this theory is compactified on a small circle (relative to the inverse strong coupling scale), confinement by instanton configurations, which appear as a monopole density in the 3 dimensional IR theory, occurs at weak coupling. It is natural to speculate from these cases that non-perturbative configurations are potentially key to both confinement and chiral symmetry breaking.

In this chapter, we wish to make a first step in bringing these pictures together. We will use holographic model building to attempt to unify the ideas. In particular, the condensation of monopoles and quarks must each be driven by a BF bound violation in the theory. Here we will build a very simple model of QCD(Adj) on a compact circle whose radius is close to the inverse strong coupling scale. The IR theory is expected to be strongly coupled and holography may be a sensible tool to study the spectrum. We will produce an AdS/QCD style model that describes the monopole condensate as forming due to a BF bound violation and the resulting bound state spectrum. Here we will just model theories with massive fermions (although below the strong coupling scale).

The model allows us to estimate the scale at which the instability sets in by extrapolating from the perturbative regime. Of course, this is very naïve. The perturbative exponential suppression of instanton configurations hints that this scale is somewhat lower than the equivalent one for chiral condensation (from looking at where $\gamma = 1$ from one gluon exchange). However, the theory with a single massless Weyl fermion in the adjoint representation is $\mathcal{N} = 1$ SYM, where the gaugino condensate and the glueballs are bound into a single supermultiplet [100]. This theory is likely an example where the mechanisms maximally converge, so whether they can be separated in other cases is unclear.

To play Devil's advocate it is interesting to try to conceive of theories where chiral symmetry breaking is separated from confinement. We have argued previously [83], that this might be

supported in the $\gamma = 1$ paradigm (see also [82]). In theories with fermions in multiple representations, higher dimension representations than the fundamental typically couple more strongly to gluons, and reach the $\gamma = 1$ criteria ahead of the fundamental representation. If they condense and are integrated from the theory, then a gauge theory with just fundamentals is left in the IR, which presumably behaves like QCD (for sufficiently low N_f^F flavours). If one can include sufficient fundamentals to slow the running between the higher representation condensing and the fundamental condensing, then presumably confinement is also separated. One needs to be careful however, not to push the theory into the conformal window by adding too much matter.

In chapter 7, we built a holographic model of SU(N_c) theories with two-index symmetric matter and fundamentals which displayed such gaps [1]. The model has no confinement mechanism because it is assumed to happen at or below the chiral symmetry breaking scale of the fundamental matter. Here we use the same model for SU(N_c) with a single Weyl adjoint fermion and N_f^F fundamentals - we pick a single Weyl adjoint to allow the maximum additional number of fundamentals to slow the running below the adjoint IR mass scale. We observe mass gaps for some choices of N_c and N_f^F as large as an order of magnitude. The gap size does depend on the extrapolations used for the running of the anomalous dimensions from the perturbative to non-perturbative regime as we investigated in [1]. We also neglect interactions between the two fermionic sectors (and potentially the instanton/monopole sector) - condensation in one could trigger condensation in the other, for example, undoing the conclusions. It would be interesting in the future to study such mutual interactions. For the moment, the model presented is intended as a challenge to lattice studies to seek such phenomena.

The current state of lattice simulations for gauge theories with adjoint matter is as follows. The SU(2) gauge theories with both $N_f^{Adj} = 1$ and 2 appear to lie in the conformal window (i.e. they do not break chiral symmetry) with anomalous dimensions around $0.2 - 0.3$ [97, 98, 99]. $\mathcal{N} = 1$ super Yang-Mills theory with $N_c = 2$ and $N_c = 3$ is known to break chiral symmetry and confine [101, 102, 103, 104]. There has been one initial study of an SU(2) gauge theory with a single Weyl fermion and two Dirac fundamental fermions [105], which indeed shows a gap between the ρ-mesons made of adjoint and fundamental matter (the adjoint ρ is reported as being about 1.6 the mass of the fundamental ρ - see Table 3 in [105]) and is consistent with our holographic model using the $\gamma = 1$ criteria. A key future test of the separation of the confinement and chiral symmetry breaking mechanisms would be to check if they occur at different thermal transitions.

8.1.1 The Gauge Theories

We will consider $SU(N_c)$ gauge theories with fermionic matter in the adjoint and, later, the fundamental representations. The two loop running of the gauge coupling in QCD for arbitrary representation is given by Eq. (5.25), where we use the notation N_f^F for the number of fundamental fermions and N_f^{Adj} for the number of adjoint fermions. For $SU(N_c)$ theories $C_2(G) = N_c$; $T(Adj) = N_c$ and $T(F) = 1/2$.

To extract the running we must choose initial conditions for the RG equation. For example, $\alpha(Log(\Lambda_{UV} = 5)) = 0.1393$, for $N_c = 2, N_f = 0$, gives a Landau pole at $Log(\Lambda) = 0; \Lambda = 1$. A more accurate way to set the strong coupling scale, is to set a bound state mass (we will take the ρ-meson made from the adjoint fermions) in any theory at zero fermion mass to be the strong coupling scale. We therefore, when comparing the spectra of theories, write all masses and couplings in units of the adjoint m_ρ at $m_f = 0$.

The two-loop ansatz for the running includes IR fixed point behaviour - the so-called conformal window [66, 91, 92]. As N_f is lowered, the IR fixed point coupling grows and at some point is expected to trigger chiral symmetry breaking and or confinement - this is the edge of the conformal window. We will use our holographic models to estimate these critical couplings below. When we predict the spectra of the Weyl adjoint plus fundamentals theory, we will show plots over a range of N_f^F up to the edge of the conformal window (from below) - the position of the edge in each case can therefore be seen on those plots to come.

8.1.2 Confinement in Compact SU(2)(Adj) Gauge Theory

For simplicity, we will initially restrict our discussion to the case of $N_c = 2$ with adjoint fermions. Here, the review [96] is very useful. We will first review the results for confinement in the theory on a small compact direction [94, 95, 96]; then we will write a holographic model for the intermediate regime where the IR theory is strongly coupled; we finally briefly discuss the extension to SU(N_c). We will then be able to consider the interplay between chiral symmetry breaking and confinement in section IV.

8.1.2.1 Summary of the SU(2)(Adj) theory on $R^3 \times S^1$

There has been considerable work [94, 95, 96] on understanding four dimensional SU(2) gauge theory with N_f Weyl fermions in the adjoint representation on a compact circle of radius L. At the scale $1/L$ we can rewrite the 4d gauge field as a 3d gauge field and a real, adjoint scalar, a_4. The classical potential for the scalar, inherited from the 4d TrF^2 commutator term, allows a vev that breaks SU(2) to U(1) and leaves a massless U(1) gauge field and a massless, chargeless scalar. One expects the vev to lie at the scale $1/L$ when loop corrections are included. Any charged adjoint fermions speak to the scalar vev through a Yukawa term (generated from the 4d covariant derivative) and are massive. The charge zero fermions survive in the IR theory. The (naïvely) non-interacting IR theory has a characteristic coupling $g_4^2(1/L)$.

The consistency of this picture can be checked by computing the Coleman-Weinberg effective potential from the gauge and fermion fields (including their KK towers) and confirming that it is minimized at the vev $2\pi/L$. The potential for the vev v is given by

$$V = -\frac{(N_f - 1)}{L^3}\frac{1}{12\pi^2}[vL]^2(2\pi - [vL])^2, \tag{8.1}$$

where $[vL] = vL(\mathrm{mod} 2\pi)$. Note v is the vev of A_4^3, and a_4 is the fluctuation about the vev, i.e. $A_4^3 = v + a_4$

For $N_f^{Adj} = 1/2$ (SYM) the potential vanishes and one must argue that non-perturbative effects will stabilize the vev. For $N_f > 1$, the minimum is at $v = 2\pi/L$. Note that the fluctuation of the scalar about the minimum has a mass of order g/L and the a_4 can thus be integrated from the IR theory. In fact even if the adjoint fermions have masses $m \leq 1/L$ they still act to stabilize the vev and can then be neglected in the deep IR - we will work in this theory here for simplicity.

One can use electromagnetic duality in 3d to rewrite the IR U(1) electric and magnetic fields in terms of a single (dimensionless) scalar potential σ:

$$F^{\mu\nu} = \begin{pmatrix} 0 & E_x & E_y \\ -E_x & 0 & B \\ -E_y & -B & 0 \end{pmatrix} \leftrightarrow \partial_\mu \sigma = \frac{4\pi L}{g_4^2} (-B, E_y, -E_x). \tag{8.2}$$

The kinetic term for σ is

$$\mathscr{L}_\sigma = \frac{1}{2} \frac{g_4^2}{(4\pi)^2 L} (\partial_\mu \sigma)^2. \tag{8.3}$$

The interesting aspect of the theory is that SU(2) instanton dynamics above the breaking scale generate confinement in the low energy theory. The mechanism is the 3d version of the dual Meissner effect. In particular, note that the natural charges for a 0-form potential are pseudo-particles (as a vector couples to point particles and a two-index field to strings, etc.) So, for example, a constant density of magnetically charged pseudoparticles at some time $t = 0$ emits field lines into the time direction in analogy to a charged plane emitting field lines in the perpendicular spatial direction in 3+1d. The solution, using Gauss' law, is $\sigma = Bt$ and there is a constant magnetic field in the space. This motivates the idea that the instantons of the SU(2) theory are suitable candidates to play the role of such magnetic charges. Indeed, explicit construction shows that the instantons do indeed radiate magnetic field lines asymptotically. These computations have been done in detail [106, 107] - there are two types of instantons: M and KK instantons, which are both magnetically charged.

We would expect the instanton and anti-instanton distributions to be uniform on average at all x, y, t, so there is no net magnetic field from their presence. They do though, generate a potential for σ. If we stick to the theory where the fermions have a small mass, then a potential is generated directly by the M and KK instantons. It is given by

$$V = \frac{4e^{-S_0}}{L^3}(1 - \cos\sigma) \tag{8.4}$$

where $S_0 = \frac{4\pi^2}{g_4^2(1/L)}$ is the action of the instanton configuration, which is minimized at $\sigma = 0$ and the σ field has an effective mass

$$m_\sigma^2 = \frac{64\pi^2 e^{-S_0}}{g_4^2 L^2}$$

Note, the theories with massless fermions are more complicated since they possess a remnant of the anomalous $U(1)_A$ symmetry that acts as a Z_{4N_f}, under which σ shifts by π. This shows that the M and KK contributions to the potential must vanish in these theories. It is then possible to consider dyons made of bound M and KK states and argue that magnetic charge two dyons play the important role of condensing and causing confinement [94]. Let us stay in the massive theory for simplicity though.

Confinement can be seen directly because there are excited states of the vacuum that correspond to electric flux tubes. Here, one finds solutions for σ that traverse from 0 to 2π as one moves across a line in the $x-y$ plane - for example, in x in a y-independent solution. The solution of the classical equation of motion for σ is

$$\sigma(x) = 4\arctan e^{-m_q x} \tag{8.5}$$

Asymptotically at large x, this solution's action returns to that of the vacuum. In the central region, the solution lies at the top of the potential where the σ mass falls to zero (here the instanton density has fallen to zero) and $\partial_x\sigma = E_y \neq 0$. The flux tube's energy will be proportional to the length of the tube in y (neglecting end effects where the electric charges attach).

8.1.2.2 From Weak to Strong Coupling with Holography

One of the strengths of the work performed on the adjoint theory is that when the compact radius is small - so $1/L$ is large compared to the strong coupling scale of the field theory - one can see the confinement dynamics at weak coupling. Nevertheless, it is interesting to consider the transition to strong coupling. As the compactification length rises and the scale $1/L$ falls, eventually $g_4(1/L)$ will become large and perturbation theory will break down. In this regime, one can propose a holographic description of the strongly coupled σ-instanton bath system. This description will hold until the field vevs grow to $1/L$, when one should return to a purely 4d description.

The natural starting point is to place the effective IR action into AdS_4 space

$$ds^2 = \rho^2 dx_{2+1}^2 + \frac{d\rho^2}{\rho^2} \tag{8.6}$$

(here x_{2+1} are the Minkowski directions of the field theory, and ρ is the radial direction that becomes the renormalization group scale). We include a dimension 3 field I, that will correspond to the instanton density, and a dimensionless field $\hat{\sigma}$ which is the holographic partner to the field theory σ operator.

Our action is

$$S^{AdS_4} = \int d\rho d^3x \ \frac{1}{2}\frac{\rho^3}{r^2}\frac{\mathscr{C}}{L}G^{MN}\partial_M\hat{\sigma}\,\partial_N\hat{\sigma} + \frac{I}{r}2\sin^2\frac{\hat{\sigma}}{2} + \frac{1}{2}\left(\frac{1}{\rho^2}\frac{1}{r^2}G^{MN}\partial_M I\,\partial_N I + M_I^2\frac{I^2}{r^4}\right) \tag{8.7}$$

Note here we use symbols r and ρ, which for the moment are the same (we will distinguish them when we come to discuss fluctuations below). The constant $\mathscr{C} = \frac{g_4^2}{(4\pi)^2}$ is taken from the field theory action normalization (8.3). The field $\hat{\sigma}$, assuming $I \to 0$ in the UV, has UV solution

$$\frac{1}{L}\partial_\rho(\rho^3\partial_\rho\hat{\sigma}) = 0, \qquad \hat{\sigma} = c + \frac{c'}{\rho^2} \tag{8.8}$$

$\hat{\sigma}$ is dimensionless. We interpret c as the dimensionless field vev and c'/L as the dimension 3 source for the field.

M_I^2 is a mass term for I, which if zero in the UV (and $\hat{\sigma} \to 0$ in the UV), ensures the UV equation of motion and solution for I is

$$\partial_\rho(\frac{1}{\rho^2}\partial_\rho I) = 0, \qquad I = k + k'\rho^3 \tag{8.9}$$

I has dimension 3. Here we interpret k as the vev of the dimension 3 field and k' as its dimensionless source. We will pick an example form for M_I^2 shortly.

The interaction term is that in (8.4), where we need the field I to acquire a vev $4E^{-S_0}/L^3$. To enforce that, consider the action that controls the vacuum, where we assume that the fields do not depend on the spatial or time directions but only on ρ. The bulk Lagrangian density reduces to

$$\mathscr{L}^{AdS_4} = \frac{1}{2}\rho^3\frac{\mathscr{C}}{L}(\partial_\rho\hat{\sigma})^2 + \frac{1}{2}\left(\frac{1}{\rho^2}(\partial_\rho I)^2 + M_I^2\frac{I^2}{r^4}\right) + \frac{I}{r}2(\sin\frac{\hat{\sigma}}{2})^2 \tag{8.10}$$

In fact, the interaction term pins $\hat{\sigma} = 0$ in the vacuum solutions with non-zero I. We must solve

$$\partial_\rho(\frac{1}{\rho^2}\partial_\rho I) - M_I^2\frac{I}{\rho^4} - \frac{I^2}{2\rho^4}\frac{\partial M_I^2}{\partial I} = 0 \tag{8.11}$$

The IR boundary conditions follow the general prescription in 5.3.2, thus for I we solve using

$$I(\rho_{IR}) = \rho_{IR}^3, \qquad \partial_\rho I|_{\rho_I R} = 3\rho_{IR}^2 \tag{8.12}$$

The first condition is an on mass-shell condition for the field below which it should be integrated from the dynamics. The second condition ensures that the solution tends to a constant, dynamically generated source value at the on mass-shell point.

For $\hat{\sigma}$ and its fluctuations we will use the - similarly justified - IR boundary conditions

$$\hat{\sigma}(\rho_{IR}) = 1/\rho_{IR}^2, \qquad \partial_\rho \hat{\sigma}|_{\rho_I R} = -2/\rho_{IR}^3 \tag{8.13}$$

and require in the UV

$$\rho^3 \partial_\rho \hat{\sigma} = 0 \tag{8.14}$$

Now we must decide on a form for the mass squared for I. We want a running mass (i.e. a ρ dependent mass) that will violate the BF bound in the IR causing condensation of I - we will adjust the BF bound violation point so that the condensation occurs to match that expected in the field theory model. Note that with the chosen dimension for I, $M_I^2 = -9/4$ is the BF bound violation point where $\Delta = 3/2$. A simple choice we can make is

$$M_I^2 = -\frac{\mathcal{H}}{r} \tag{8.15}$$

at low r (for the moment ρ), this will violate the BF bound. If one were to set purely $r = \rho$, then there would be no stable IR solution since the BF bound is violated for all I vevs. A simple resolution, that occurs naturally in the D3/probe D7 system [58, 55, 52] for example, and which is dimensionally consistent is to use

$$r^2 = \rho^2 + I^{2/3}. \tag{8.16}$$

Now, if I acquires a vev, it can move to a value where the BF bound is not violated and it becomes stable. At this point, we also replace occurrences of r in the action with ρ as shown in (8.10) - here, again as in the D3/probe D7 system, the replacements feed the presence of the vev to the fluctuations, but are introduced so as not to change the UV asymptotic solutions. Although this choice looks a little arbitrary, the D3/probe D7 system artfully enables this from first principles - we follow it's example.

The constant $\mathcal{H}$ is the first introduction of a scale into the action for I (L does not enter when $\hat{\sigma} = 0$). Numerically, we have solved (8.11) with (8.15) to find the value of $\mathcal{H}$ so that the solution in the UV tends to $I = 1$ with vanishing source (derivative). We find $\mathcal{H} = 7.82498$, $\rho_{IR} =$

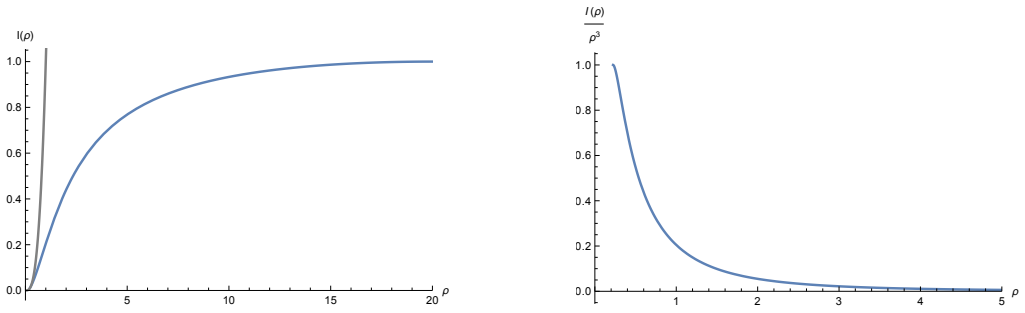

FIGURE 8.1: Left: The blue line is the numerical result for the vacuum solution $I(\rho)$. The grey line represents the function $y = x^3$ which sets the IR boundary. Right: The blue line shows the plot $\frac{I(\rho)}{\rho^3}$ against ρ. (Set-up: $\mathscr{K} = 7.82498$, $\rho_{IR} = 0.223527$, $\rho_{UV} = 20$ such that $I(\rho_{UV}) = 1$ and $I'(\rho_{UV}) = 0$).

0.223527. We plot the solution in Figure 8.1 (and also the form of I/ρ^3 which displays the solution as a running source term more analogous to the familiar D7 probe embeddings in the D3/D7 system).

Next, we consider the fluctuation around the vacuum solutions: $\bar{I}(\rho) + \epsilon I(\rho, x)$ and $\hat{\sigma}(\rho) = 0 + \epsilon\hat{\sigma}(\rho, x)$, expanding the action, Eq. (8.7), to $\mathcal{O}(\epsilon^2)$. We seek perturbations of the form $I(\rho, x) = f_1(\rho)e^{ik_1\cdot x}$ and $\hat{\sigma}(\rho, x) = f_2(\rho)e^{ik_2\cdot x}$, with $k_1^2 = -M_1^2$ and $k_2^2 = -M_2^2$ (those being the masses of the bound states). With some algebra, the equations of motion for the fluctuations are

$$\frac{\bar{I}f_2(\rho)}{\sqrt{\bar{I}^{2/3} + \rho^2}} - \partial_\rho\left(\frac{\mathscr{C}}{L}\rho^3\partial_\rho f_2(\rho)\right) - \frac{\rho^3}{(\rho^2 + \bar{I}^{2/3})^2}\frac{\mathscr{C}}{L}M_2^2 f_2(\rho) = 0 \tag{8.17}$$

$$-\frac{k\left(-19\rho^2\bar{I}^{2/3} - 2\bar{I}^{4/3} + 18\rho^4\right)}{18\left(\bar{I}^{2/3} + \rho^2\right)^{9/2}}f_1(\rho) - \partial_\rho\left(\frac{1}{\rho^2}\partial_\rho f_1(\rho)\right) - \frac{M_1^2}{\rho^2(\rho^2 + \bar{I}^{2/3})^2}f_1(\rho) = 0, \tag{8.18}$$

which implies that the fluctuations f_1, f_2 decouple. And the coefficient $\mathscr{C}/L = \frac{g_4^2}{L(4\pi)^2}$ will affect the spectrum of the dual photon.

The equations of motion for the instanton fluctuation are solved with boundary conditions $f_1(\rho_{IR}) = \rho_{IR}^3, f_1'(\rho_{IR}) = 3\rho_{IR}^2$. The meson masses are obtained by fine-tuning M_1^2 so that $f_1'(\rho_{UV}) \to 0$. The mass spectrum, in the theory with $I \to 1$ in the UV, for the instanton density fluctuation is $M_I^2 = 1.56, 4.36, 9.52$, with corresponding excitation number $n = 0, 1, 2$, and the corresponding solutions are presented in Figure 8.2.

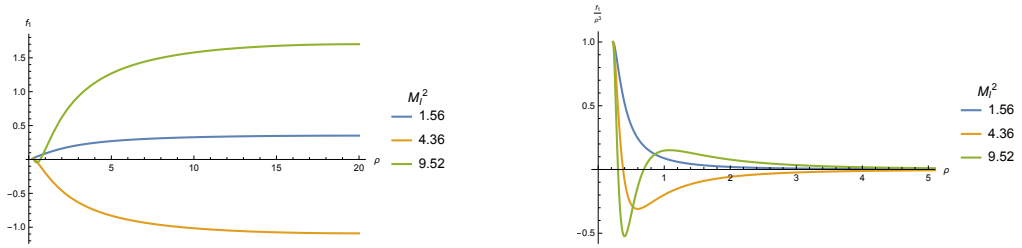

FIGURE 8.2: Left: The regular solutions for the fluctuation of the instanton density f_1 against ρ. Right: $\frac{f_1}{\rho^3}$ against ρ.

Next, we compute the meson modes for $\hat{\sigma}$. The boundary conditions used are $f_2(\rho_{IR}) = \frac{1}{\rho_{IR}^2}$, $f_2'(\rho_{IR}) = \frac{-2}{\rho_{IR}^3}$, and $\rho_{UV}^3 f_2'(\rho_{UV}) = 0$, which make the condensate vanish in the IR, and the source vanish in the UV. The results depend on the value of $\mathscr{C}/L$. Here we rewrite that scale in terms of the I vev as

$$\langle I \rangle = \frac{4e^{-S_0}}{L^3}, \quad S_0 = \frac{4\pi^2}{g_4^2} \tag{8.19}$$

$$\frac{\mathscr{C}}{L} = \frac{g_4^2}{(4\pi)^2 L} = \sqrt[3]{\frac{\langle I \rangle}{4e^{-S_0}}}\,\frac{g_4^2}{(4\pi)^2} \tag{8.20}$$

Now we compute the $\hat{\sigma}$ spectrum as a function of g_4 which directly controls $\mathscr{C}/L$ at $\langle I \rangle = 1$. The masses can be directly compared to those in Figure 8.2 for the I fluctuations. This suppresses the I dependence on L, or equivalently g_4. The $\hat{\sigma}$ masses are plotted in Figure 8.3.

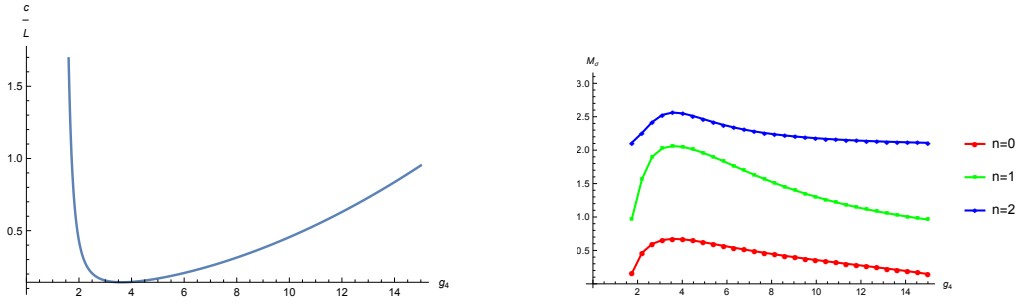

FIGURE 8.3: Left: $\mathscr{C}/L$ against g_4 in Eq. (8.20); There is a minimum $\mathscr{C}/L = 0.143$ at $g_4 = \frac{2\pi}{\sqrt{3}} = 3.7$. Right: M_σ against g_4.

It is worth noting that when $\mathscr{C}/L$ is large (when $g_4 < 1.72$ or $g_4 > 15$), there is a tachyon mode, i.e, $m_\sigma^2 < 0$. This follows from computing the spectrum using (8.17) neglecting the first term, when $M_\sigma^2 = -0.298$. These regimes correspond to parameter choices where the holographic model should not be applied. When the gauge theory is weakly coupled, the holographic dual should become strongly coupled. Equally, when the theory has $g_4 > 4\pi$, the four dimensional theory will hit strong coupling before reaching the IR compactification scale and there should never be a three dimensional description. It is interesting that the holographic model becomes aware of these regimes where it fails.

8.1.2.3 The SU(N_c) Theory

The SU(N_c) theory with adjoint matter (which we again assume is massive, but with those masses below the compactification scale) shows similar behaviour [94, 95]. The A_3 component of the gauge field again becomes an adjoint scalar on compactification and its vev breaks the theory to $U(1)^{N_c-1}$ - there are σ_i fields ($i = 0..N_c-2$). The instanton monopoles are now "bi-fundamental" fields with charge $(+1,-1)$ under the adjacent U(1)s one would obtain from breaking U(N_c) (one can just switch off the coupling of the extra U(1) to reduce to SU(N_c)).

For example, for SU(3) the resulting potential for the two σ_i are

$$V = \frac{4e^{-S_0}}{L^3}\left(\sin^2\frac{\sigma_0}{2} + \sin^2\frac{\sigma_1}{2} + \sin^2\frac{\sigma_0-\sigma_1}{2}\right) \tag{8.21}$$

with $S_0 \to 8\pi^2/g_4^2N_c$.

At the level of the holographic model, one includes three copies of the monopole field I and an appropriate potential. The holographic model for SU(3) is

$$\begin{aligned} S^{AdS_4} = &\int d\rho\, d^3x\ \frac{1}{2}\frac{\rho^3}{r^2}\frac{\mathscr{C}}{L}G^{MN}\partial_M\sigma_i\partial_N\sigma_i \\ &+ \frac{1}{2}\left(\frac{1}{\rho^2}\frac{1}{r^2}G^{MN}\partial_M I_i\partial_N I_i + M_I^2\frac{I_i^2}{r^4}\right) \\ &+ \frac{I_1}{r}\sin^2(\frac{\hat{\sigma}_1}{2}) + \frac{I_2}{r}\sin\left(\frac{\hat{\sigma}_2}{2}\right) + \frac{I_3}{r}\sin\left(\frac{\hat{\sigma}_1-\hat{\sigma}_2}{2}\right) \end{aligned} \tag{8.22}$$

where we chose the M_I^2 so that $I = 4e^{-S_0}/L^3$, and $\mathscr{C} = (\frac{g}{4\pi})^2$. The vacuum solutions for the I fields lead to the same vev solutions, and there is a multiplicity of the same excitation states as we saw in SU(2). For the $\hat{\sigma}_i$ fluctuations the potential can be diagonalized by writing

$$\tilde{\sigma}_\pm = \frac{1}{\sqrt{2}}(\hat{\sigma}_1 \pm \hat{\sigma}_2) \tag{8.23}$$

This leads to two mass eigenstates $(\hat{\sigma}_0 \pm \hat{\sigma}_1)$. We show the resultant mass spectrum in Figure 8.4.

8.1.3 Comparison of Instabilities

The BF bound violating scale [57] marks the onset of the instability to condensation of an operator in the holographic context.

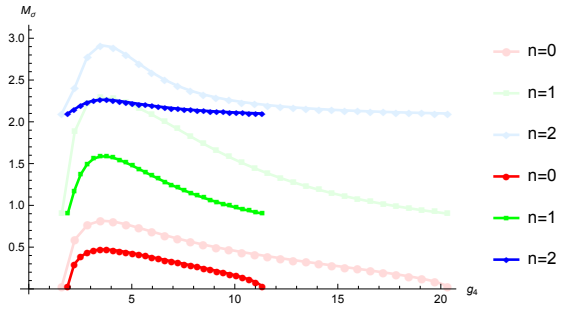

FIGURE 8.4: The mass spectrum of dual photons σ_1 and σ_2 for SU(3). The darker colours represent σ_1; The lighter colours represent σ_2.

In the SU(2) model where the instanton density vev was 1 we needed $\mathcal{H} = 7.82498$. The BF bound violation occurred (in AdS_4) when $\mathcal{H}/\rho = 9/4$, i.e., when $\rho_{BF} = 3.47$. We should rescale this scale so that the instanton density fits field theory predictions - $I = 4e^{-S_0}/L^3$ so then the model gives the BF bound violation scale as

$$\rho_{BF} = 3.47 \left(\frac{4e^{-S_0}}{L^3} \right)^{1/3} \tag{8.24}$$

The instanton condensation scale rises to $1/L$ when $g_4^2 = 7.7$ - at higher g_4 values at the scale $1/L$ the three dimensional theory no longer has any applicability. For larger N_c values $S_0 \to 8\pi^2/g_4^2 N_c$ and eg for $N_c = 3$ we find $g_4^2 = 5.2$.

In competition with this instanton-driven gap formation mechanism is the mechanism deduced from gap equations [89, 90, 67, 66, 82] and the study of chiral symmetry breaking in holography [68, 69, 61]. Here one follows the running anomalous dimension of the adjoint fermion bi-linear in the four dimensional theory above the scale $1/L$. One can write a holographic model here also with the dimension one field $\hat{\lambda}$ dual to the fermion bilinear mass and condensate

$$S_{AdS_5} = \int d^4x d\rho \;\; \rho^3 (\partial\hat{\lambda})^2 + \rho^2 \Delta M^2 \hat{\lambda}^2. \tag{8.25}$$

Here the solutions of the equation of motion are

$$\hat{\lambda} = m\rho^{-\gamma} + c\rho^{2+\gamma}, \qquad \gamma(\gamma - 2) = \Delta M^2. \tag{8.26}$$

There is a BF bound violation that causes gaugino condensation when $\gamma = 1$, $(\Delta M^2 = -1)$. We fix the form of ΔM^2 per Eq. (5.24), where $C_2(R)$ is N_c for the adjoint representation. This BF bound violation is now predicted to occur at $g_4^2 = 6.6$ for $N_c = 2$ and $g_4^2 = 4.4$ for $N_c = 3$.

Part of our goal in this chapter was to put these two mechanisms' scales in the same holographic language of BF bound violations, which we have done. In principle, one can now ask does adjoint fermion condensation or instanton condensation occur earlier? The above estimates slightly

favour adjoint fermion condensation to occur first. However, one can't really deduce any such thing, since both estimates are based on wildly extrapolating the perturbative results to the non-perturbative regime. The fact that $\mathcal{N} = 1$ super Yang-Mills theory ties the gaugino bound states and glueballs into a single multiplet suggests that the two mechanisms might merge in that theory and hence possibly all theories with adjoint matter. Holographic models are not going to resolve this fundamental question about the dynamics (first principle holographic constructions might of course).

Thus, whether the dynamics of these theories are set at a single scale by instanton condensation or whether there are two scales, one for chiral symmetry breaking ($\gamma = 1$) and one for confinement (instanton condensation) remains to be discovered. If there are two scales, one could hope to separate them. In 7, we explored this phenomenon in a theory with fundamental representation and two-index symmetric representation fermion flavours [1]. The idea is to let the theory trigger $\gamma = 1$ for the higher dimension representation, and then run as slowly as possible (by adjusting the number of fundamentals) to a new trigger scale for fundamental representation condensation. That scale, which is in a theory similar to QCD, one posits has instanton condensation near the fundamental condensation scale. In the next section, we will repeat this method to model a theory with fundamentals and adjoint fields (neglecting instanton condensation). It is a straw-man model for the $\gamma = 1$, and hence the separated scales, hypothesis which we hope will inspire first principles lattice simulations to seek the phenomena (or disprove this world view).

8.2 Holography of QCD(Adj) + Fundamentals

Here we present a holographic model of an SU(N_c) gauge theory with a single Weyl fermion in the adjoint representation and in addition N_f fundamental representation Dirac fermions. The model does not include the instanton sector so lives in the "$\gamma = 1$ paradigm" - that is, we simply use the perturbative running of the anomalous dimensions for the bi-fermion operator in each representation to predict where they condense. By adjusting N_f, we can weaken the running between the scale where the adjoint condenses and that where the fundamental condenses to try to exhibit a gap. We assume here that instanton condensation (and hence confinement) occurs below the scale of the fundamental condensation. Likely these scales are very close as in QCD because when the fundamentals are integrated out at that condensation scale one is already at very strong coupling and the pure Yang-Mills theory in the IR will run to its pole fast. Our model is a straw-man, intended to provoke lattice simulations to look for the gap in scales. The gaps we see depend on the extrapolations of perturbative results, and so of course come with large errors, the idea is intriguing though. The analysis mimics our previous study of these theories with two index symmetric matter rather than the adjoint where the model also predicts large gaps [1].

8.2.1 The Holographic Model

The holographic model is simply a refinement of the discussion in 8.25 above, as first presented in [60]. Note that we have already discussed specific extra concerns in 7.1 and the same apply here, substituting only that our higher dimensional representation is now the adjoint, rather than the symmetric.

The sole difference between the following adjoint+fundamental calculations and those prior, is that we do not explore the 'more pessimistic ansatz' as was done in [1]: here we simply show that large gaps seem possible.

As with the symmetric case, the adjoint representation always condenses at a higher ρ_R^{IR} than the fundamental representation. At that scale we integrate out the adjoint representation fermions and remove their contribution to the beta function at lower scales. We show an example running of Δm_R^2 for the two representations in the case of $N_c = 5$ and $N_f^F = 17$ in Figure 8.5.

The mesons of the theory are fluctuations of this vacuum configuration that satisfy the appropriate boundary conditions, matching those of the vacuum in the IR and consisting of just fluctuations of operators in the UV. The resulting Sturm-Liouville problems fix the meson masses. Decay constants obtained by substituting these solutions and those for a background source back into the action and integrating over the radial direction. The full equations can be found in [1].

8.2.2 N_c and N_f^F Dependence In The Massless Theory

We will now discuss the predictions of the holographic model, starting with the case that has the largest gap in the spectrum between the adjoint and fundamental fermion bound states.

8.2.2.1 $N_c = 5$ Theory

The most extreme theory makes a good example. We take $N_c = 5$ and a single Weyl fermion in the adjoint representation plus N_f^F Dirac fundamental flavours. In [83] this model was identified as having a maximum gap between the condensation scales of the representations at $N_f^F = 17$. There, the adjoint sector is eliminated from the running at the scale of the BF bound violation (i.e. at $\gamma_{Adj} = 1$) and the $\gamma_F = 1$ BF bound violation scale is then computed from the running, resulting in a separation of 22.

We implement this theory in our holographic model. We show the running of Δm_{Adj}^2 against the log of the RG scale in Figure 8.5. We set scales with the ρ-meson mass composed of adjoint fermions. In fact, the edge of the conformal window for this theory is slightly above $N_f^F = 17$, but calculations for 17 flavours are numerically intractable, 16.9 was used as a near approximation. Already at $N_f^F = 16.9$, the IR fixed point value of the adjoint sector is exceedingly close to 1, with Δm_{Adj}^2 in the IR being -1.04. We can extrapolate that for $N_f^F = 17$, given that the IR fixed

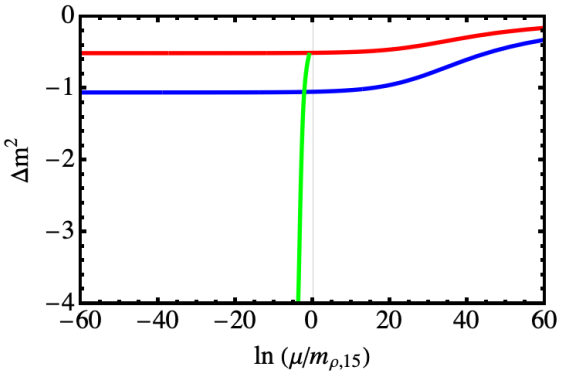

FIGURE 8.5: SU(5) gauge theory with one Weyl adjoint field and $N_f^F = 16.9$ (as an approximation to $N_f = 17$): The running of Δm^2 for the adjoint rep. (blue), fundamental (red), and for the fundamentals with the higher dim rep. decoupled below the scale where it is on mass-shell leaving the fundamental running (green). The energy scales are given in units of the ρ-meson mass in the adjoint sector. BF bound violation occurs at 13.9 for the adjoint and -2.2 for the fundamental with the adjoint decoupled.

point is even closer to 1, the violation point will be increased further and the mass gap will be slightly larger, i.e. a continuation of the trend that we will see across the range of N_f^F in this section.

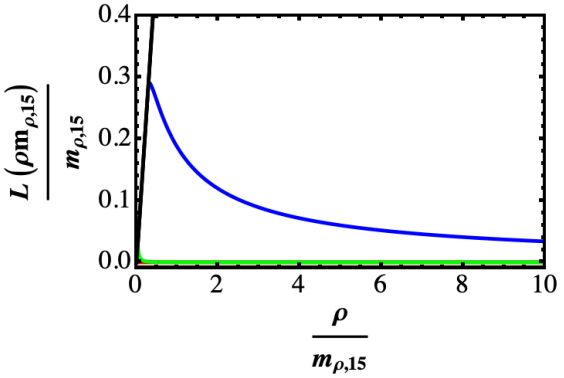

FIGURE 8.6: SU(5) gauge theory with $N_f^F = 17$ (approximates by $N_f^F = 16.9$): The $L_R(\rho)$ functions for the adjoint (blue) and 5 (green) representations with $m_{IR,A} \approx 0.29$ and $m_{IR,F} \approx 0.025$ respectively in units of the ρ-meson mass in the adjoint sector.

Figure 8.6 shows the vacuum configuration $L_{Adj}(\rho)$ in the holographic model (blue line). It corresponds to the effective fermion mass as a function of ρ, the RG scale. We see chiral symmetry breaking, with the line bending away from $L = 0$ in the IR. The value of the lower IR value of the mass is significantly lower than the scale of BF bound violation.

Returning to Figure 8.5 we next consider the fundamental sector. The red and green lines show the running of Δm_F^2, the red being the running with the presence of the adjoint sector, and thus valid only above the scale where the adjoint goes on shell at the IR value $L_{Adj}(\rho) = \rho$. The green line then shows the results of integrating out the adjoint sector. We use an interpolation function to transition between the two runnings. BF bound violation for the fundamentals occurs

at $\ln \mu = -2.2$ in units of the ρ mass in the adjoint rep (compared to the value for the adjoints of $\ln \mu = 13.9$).

As with the adjoint, we solve for the embedding function $L(\rho)$ for the fundamental representation, which can be seen as the green line in Figure 8.6. There is an IR mass gap between the two representations of 11.6. This is smaller than the factor of 22 from [83] but nevertheless substantial.

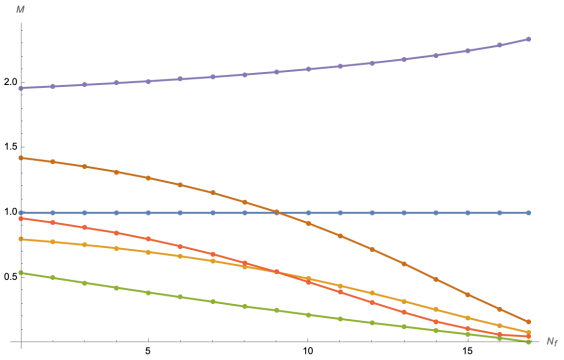

FIGURE 8.7: Mass spectra for the SU(5) theory, ρ-mesons in blue (adjoint) and dark yellow (fundamental), σ-mesons in green (adjoint) and orange (fundamental), axials in purple (adjoint) and brown (fundamental). The pions in both sectors are massless at zero fermion mass.

We can use the holographic model to compute the spectrum and decay constants of the theory for all N_f^F from 1 to 16.9 (with integer N_f^F excepting the last case), beginning by computing the equivalent embedding for each value. The mass-spectrum results are shown in Figure 8.7. For each theory, the spectrum is normalized in terms of the adjoint representation ρ-meson mass, hence the blue line for the adjoint ρ is a flat line at precisely 1. The decay constants are shown in Figure 8.8. One can see that the adjoint ρ-meson decay constant is also relatively unaffected by N_f^F.

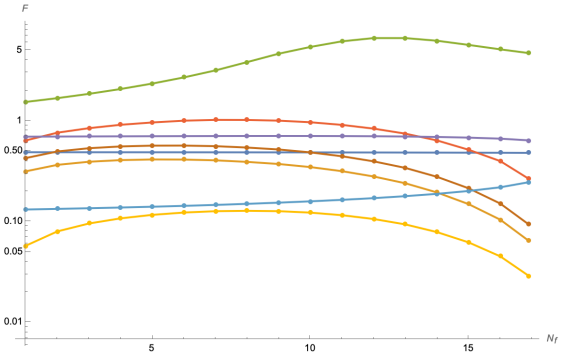

FIGURE 8.8: Decay constants for the SU(5) theory, ρ-mesons in blue (adjoint) and dark yellow (fundamental), σ-mesons in green (adjoint) and orange (fundamental), axials in purple (adjoint) and brown (fundamental) and pions in cyan (adjoint) and light yellow (fundamental).

For the other mesons, in the adjoint sector we see that the axial-mesons (purple) have a larger mass than the ρ-mesons, slightly increasing with N_f^F and their decay constant is slightly larger and decreases with N_f^F, though both changes are marginal.

The adjoint σ-mesons (green) are the lightest state, reflecting the walking in the high energy theory. The mass spectrum decreasing to essentially zero by the edge of the conformal window. The adjoint sigma decay constant is the largest at all N_f^F, with an initial rise followed by a tail off at large N_f^F. Finally we have the adjoint pions which are of course, massless in the massless theory but whose decay constant (cyan) is $\sim 2/3$ that of the ρ-meson and only slightly affected by the increasing N_f^F.

In the fundamental sector, we see the ρ-meson (dark yellow) mass decreases strongly relative to the adjoint ρ mass, with the mass gap for $N_f^F = 16.9$ being ~ 12.38. This gap should be expected to increase marginally at the actual final, non-conformal integer value of $N_f^F = 17$. Meanwhile, the decay constant for the fundamental ρ initially rises, before falling at large N_f^F as the scale of the gap decreases. The fundamental axial-mesons (brown) begin with a larger mass than the adjoint ρ-meson, before falling sharply with increasing N_f^F, approaching the scale of the fundamental ρ-meson at high N_f^F, while the decay constant for the fundamental axials has the same shape as that of the fundamental ρ-mesons, though larger at every N_f^F.

The fundamental σ-mesons (orange) behave similarly to their adjoint counterpart, albeit, starting at a higher mass and falling more sharply before levelling off at high N_f^F as they approach the mass scale of the adjoint σ-meson. The decay constant however, along with that of the fundamental pions, displays behaviour more similar to the fundamental ρ and axial-mesons, with a smooth initial rise followed by fall.

8.2.2.2 Other N_c

We additionally investigated the N_c dependence of the spectrum, looking at the cases $N_c = 2, 3, 4$. For each we retained the single adjoint representation Weyl fermion and N_f^F fundamental Dirac fermions, computing all N_f^F up to the edge of the conformal window (as per our ansatz for the running of γ). The results are shown in Figure 8.9. As with the SU(5) case, we computed the maximum mass gap for each theory (the ratio of the adjoint and fundamental ρ-meson mass spectra) which are:

SU(2), $N_f^F = 6$: 5.26;
SU(3), $N_f^F = 10$: 10.63;
SU(4), $N_f^F = 13$: 8.50.

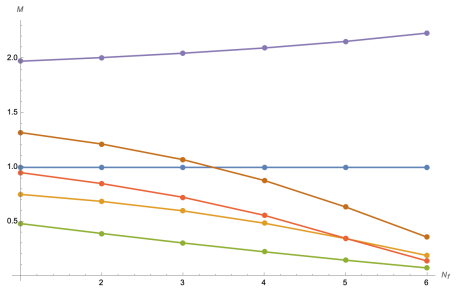

(A) Mass spectra for the SU(2) theory.

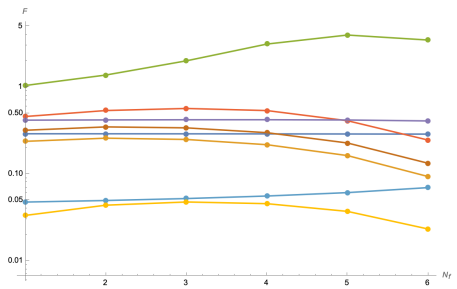

(B) Decay constants for the SU(2) theory.

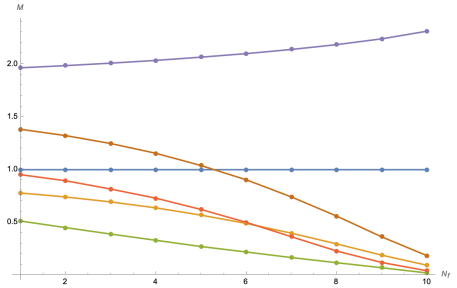

(C) Mass spectra for the SU(3) theory.

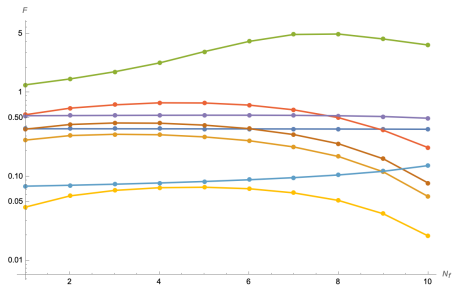

(D) Decay constants for the SU(3) theory.

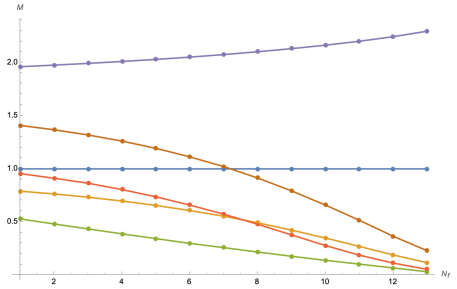

(E) Mass spectra for the SU(4) theory.

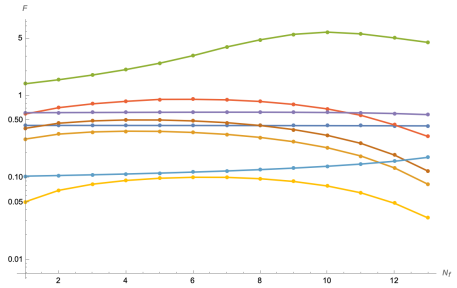

(F) Decay constants for the SU(4) theory.

FIGURE 8.9: The spectra and decay constants of the SU(N_c) gauge theory with one adjoint representation matter field and N_f^F fundamentals for $N_c = 2, 3, 4$. ρ-mesons in blue (adjoint) and dark yellow (fundamental), σ-mesons in green and orange (fundamental), axials in purple (adjoint) and brown (fundamental) and pions in cyan (adjoint) and light yellow (fundamental).

8.2.3 Conclusions

Gauge theories with fermions in the adjoint representation could potentially shed light on the origins of confinement and chiral symmetry breaking. When compactified on a small circle, such that the theories are weakly coupled, they display low energy confinement by the formation of a background density of magnetically charged instantons [94]. Chiral symmetry breaking has been understood to set in when the anomalous dimension of the fermion bilinear operator becomes equal to one [89, 90, 67, 66]. Here we have made a first step to model these two mechanisms together by presenting holographic models of both phenomena. Both the condensation of instantons and fermions are associated to BF bound violations in holographic models. A very naïve extrapolation of perturbative results suggests that the fermion condensation may occur first, but

this is very far from clear cut. If the two mechanism are separable, then it is interesting to try to grow the gap between the scales. We have proposed doing this by adding additional fermions in the fundamental representation that condense at higher coupling values and slow the gauge running. A simple holographic model suggests gaps as big as an order of magnitude might be possible, although this again depends on the extrapolation of running results from the perturbative regime. Our results are intended to provoke first principle lattice simulations of such theories (in the spirit of [105]) which could shed light on the mechanism(s) of confinement and chiral symmetry breaking.

Chapter 9

Surveying the Theory Space of Pion Dark Matter

9.1 Introduction

An interesting possibility is that dark matter is the pseudo-Nambu Goldstone bosons (pNGB) (or pions) of a dark sector strongly coupled gauge theory. Such theories provide a new relic density mechanism by means of the $3\pi \rightarrow 2\pi$ Weiss-Zumino-Witten process. They also generate a large enough self-interaction cross-section that might explain the core versus cusp problem in astrophysical data. These theories are collectively known as strongly-interacting massive particle (SIMP) theories [108].

The original SIMP models have a spectrum where all bound states (ρ, σ etc) are heavier than twice the π mass and so decay in the strongly coupled sector leaving purely a theory of pions in the infra-red (IR). These models though need a large value of M_π/f_π to reconcile relic density by $3\pi \rightarrow 2\pi$ processes and self-interaction cross-section constraints. Depending on the theory details, the SIMP models may also feature additional relic density mechanisms, where heavier states such as ρ or σ play an important role [109, 110, 111, 112, 113]. These extra annihilation channels alleviate the tensions between relic density and self-interaction limits in the basic SIMP model. In this paper we seek to more systematically analyse the space of possible infra-red effective models. We will concentrate here on SU(N_c) gauge theories with mass-degenerate fermions in the fundamental representation and a chiral symmetry breaking pattern SU$(N_f)_L\times$ SU$(N_f)_R \rightarrow SU(N_f)_V$. Throughout this paper we will use the mass of the ρ meson, M_ρ, at $m_Q = 0$ as a measure of the strong coupling scale - we denote it M_ρ^0. Our analysis concentrates on the π which are light as pNGB of the chiral symmetry breaking, the scalar singlet σ since it potentially becomes light as a pNGB of conformal symmetry breaking in theories with a walking gauge coupling, and the ρ as the lightest vector state which can be phenomenologically relevant. Our aim is here is to establish the properties of light states that will be important for possible

dark matter scenarios, rather than carrying out full cosmological analyses or attempting strongly-interacting dark matter model building.

The main obstruction to simply enumerating SIMP scenarios is their inherent non-perturbative nature. The low energy properties of the theory, which emerge from the strongly coupled theories, such as the pion masses and decay constants can not be directly calculated using any known perturbative methods. This means, the low energy parameters of the theory, although controlled by high energy inputs, need to be determined using methods beyond ordinary perturbation theory. Ideally one would use lattice gauge theory, a first principle approach, but the computational time and expense is huge. Even in the presence of lattice data, practical computation of all phenomenological implications needs to be done using low energy effective field theories, which need to be constructed. There is current work on determining the form of the effective theories particularly at large number of flavours (N_f) to colours (N_c) ratio, taking the theory in the walking regime [114, 65].

We will make use of a holographic model to explore these theories [60, 87]. The model works well for the lightest meson sector of QCD (at the 20% level quantitatively [63]) and incorporates the dynamics through an input running coupling for a theory as a function of N_c, N_f. For a fixed number of colours (N_c), the model incorporates the approach to the conformal window at some N_f^c critical value of the number of flavours. The model displays a light σ "dilaton" in the walking regime - the more conformal symmetry is restored near the chiral symmetry breaking scale the lower the σ mass is [64]. The model has simple N_f, N_c scalings for the decay constants of the theory compatible with the UV theory. The model also includes arbitrary quark masses (m_Q). Whilst the model is not a first principles computation it does allow us to explore possible behaviours in the space of N_f, N_c, m_Q and identify possible low energy effective theories and estimate the tuning needed to achieve them. The holographic model can also be used to describe quarks in higher dimension representations [86, 87, 1, 3] but here we concentrate on the fundamental representation - the main change resulting from using higher dimension representations would be that the decay constants grow with the dimension of the representation which would not aid raising M_π/f_π.

In total we identify seven different possible IR regimes which are summarized in Figure 9.1 (left panel). In Figure 9.1 (right panel) we show the results of the holographic model revealing where in the N_f/N_f^c versus M_π^2 plane each phase is likely to be found. As we will see this is largely N_c independent. Note that M_π^2 is a measure of the quark mass, at least at small m_Q.

We will begin by presenting the holographic model (sec. 9.2) that can describe the strongly coupled phases (Regions 1-6,9 in Figure 9.1 (left panel)). In sec. 9.3 we will determine and present fits for the σ, π and ρ masses and decay constants across the N_f, M_π^2 plane at $N_c = 3$. We will discuss the simple N_c scaling the model holds to allow extrapolation of these results to higher N_c. These results then lead to the phase space depicted in Figure 9.1(right panel). Regions 1–6 have an IR sector made from some or all of the fields π, ρ, σ. The regions 7 and 8 in Figure 9.1 can not be realised since we know of no mechanism to parametrically lower the ρ

mass. Region 9 is expected to describe the meson sector of gauge theories where m_Q lies near or above the strong coupling scale of the theory. If the quark mass is very large one expects the gauge dynamics to be weakly coupled at the mass scale. The meson masses will lie close to $2m_Q$. However, we also expect at these large m_Q that the gauge dynamics will survive below m_Q going on to become strong in the deeper IR. It will generate light glueballs so these are not pionic dark matter models - we do not study such glueball dark

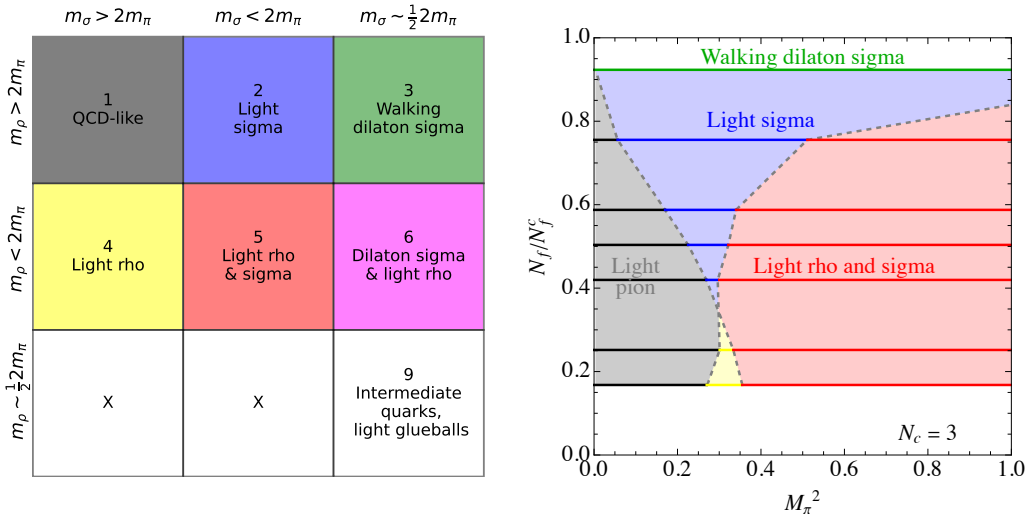

FIGURE 9.1: Left panel: The regions of parameter space denoted by their low energy spectrum. Right panel: the classification of the $N_c = 3$ theory, using the colours from the left in the N_F/N_F^c versus m_Q plane. The horizontal lines are for integer N_F where we compute. Regions 1-5 are present at these M_π (in units of M_ρ^0). Regions 6 and 9 lie to the right of the right panel where the gauge theories are transiting to weak coupling and holography is less reliable.

matter models here. Region 9 is therefore intended as the transition regime where the pions are light but the glueballs are also playing a role in the IR dynamics.

Having obtained these results for the spectrum we will then return to discuss the phenomenology of the different types of IR theory in sec. 9.5. We stress here that in this work, we are only introducing this space of theories and our observations are initial and do not include relic density calculations which we hope to perform in the future led by this survey.

The highlights of these analyses include the following. First, consider QCD-like models in which the low-energy spectrum contains only pions, while all other states lie above the $2M_\pi$ threshold and can therefore spontaneously decay within the strong-sector. These models struggle to generate a large enough M_π/f_π value to be viable and need extra pion relic density generation modes such as through mediators with the Standard Model (SM). Our results suggest higher values of this ratio may be possible in very walking models. The largest space of models we find are those with an intermediate quark mass and they have both the σ and the ρ lying below $2M_\pi$. These states may aid the pion depletion rate in the cosmological evolution as needed for valid theories. They are largely unexplored in the literature so far and we plan to return to them to determine relic abundances. Regions with just one of the ρ or σ light are possible in constrained parameter

regions (obtaining a model with only a light ρ is quite tuned in the holographic model). The σ always lies above the π mass becoming degenerate with the π in the extreme walking limit.

Finally in sec. 9.6, to be complete in our survey, we briefly address other possible strongly coupled dark matter sectors. This includes the high mass scenario discussed above that leaves glueball dark matter [115, 116, 117, 118, 119, 120]. If mesonic matter is unstable then dark baryons are possibly stable, see [121, 122] for associated reviews. For models truly in the chirally symmetric conformal window the lightest matter is an unparticle plasma [123, 124]. Finally we present some models that remove the pions from the spectrum leaving a dark matter σ although in absence of additional symmetries it likely decays too fast due to dimension 5 operators to be a sensible dark matter candidate.

9.2 The Holographic Model

This chapter applies the Dynamic AdS/QCD model (detailed in Chapter 5 5.3) to matter in the fundamental representation ($R = F$). Our goal is to use its qualitative power to elucidate what phases one can expect to find in such gauge theories as a function of N_c, N_f and a common quark mass m_Q. It is also useful to see how the various low energy parameters depend on N_c, N_f. We will briefly present the action and equations of motion which will be used to calculate meson masses and decay constants.

We employ the Dynamic AdS/QCD model detailed in Chapter 5 5.3, applying it to matter in the fundamental representation ($R = F$). The model's equations of motion, boundary conditions, and methods for computing meson spectra and decay constants are as described in Sections 5.3.2 and 5.3.3 of Chapter 5. The scaling of decay constants with N_c and N_f for the fundamental representation follows from the general formulas in Chapter 5:

$$f_\pi^2 \sim N_c N_f, \quad F_V^2 \sim \sqrt{N_c N_f}. \tag{9.1}$$

The dynamics of the gauge theory with N_c colours and N_f fundamental flavours are included through the running mass Δm^2 in Eq. (5.1), driven by the anomalous dimension $\gamma(\mu)$. We use the two-loop running coupling $\alpha(\mu)$ with beta function coefficients for the fundamental representation:

$$\begin{aligned} b_0 &= \tfrac{1}{6\pi}\left(11C_A - 4T_R N_f\right), \\ b_1 &= \tfrac{1}{24\pi^2}\left(34C_A^2 - (20C_A + 12C_F)\, T_R N_f\right). \end{aligned} \tag{9.2}$$

where $T_R = 1/2$, $C_F = (N_c^2 - 1)/2N_c$, and $C_A = N_c$.

With our definition, the running coupling has IR poles at low N_f, IR fixed points at intermediate N_f and describes the lower edge of the conformal window near $N_f = 4N_c$ (it follows the choices in [66]). The true value of $N_f = N_f^c$ corresponding to the position of the edge of the conformal window is still being investigated and lattice, functional renormalization group studies suggest it is lower than this e.g., below $N_f^c = 10$ for $N_c = 3$ [70, 125]. Our eventual phase structure diagram Figure 9.1(right panel) though is shown in N_f/N_f^c and we expect it to be broadly similar if the edge is lower. For $N_f > N_f^c$ the theory enters the conformal window and describes unparticles, which we briefly return to in sec. 9.6.

We numerically solve the equations of the holographic model using `NDSolve` in `Mathematica` for the results below. All dimensionful quantities are calculated in units of the ρ-meson mass in the chiral limit M_ρ^0, as outlined in Chapter 5.

9.3 Mass spectrum

We now present results and fits to the data from the holographic model. We begin with the SU(3) gauge theory where the results for the light meson spectrum and decay constants along with their fits are shown in Figures 9.2 – 9.8 and Tables 9.1 – 9.2. Finally, we show the N_f dependence of our fits in Figure 9.9.

9.3.1 $N_c = 3$ results

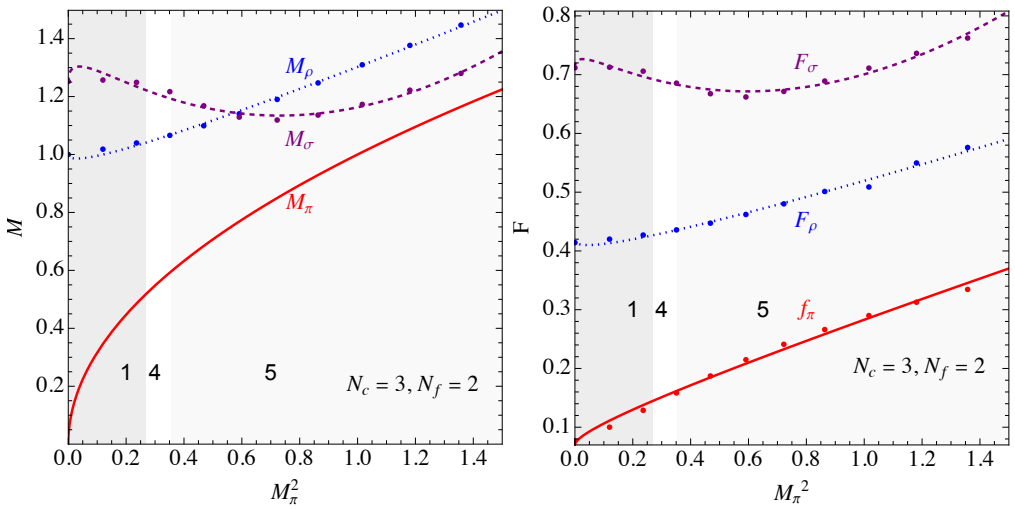

FIGURE 9.2: Mass spectrum (left) and decay constants (right) in units of M_ρ^0 for $N_f = 2$. The gray shaded areas correspond to the different regions of parameter space presented in Figure 9.1.

The left hand plots in Figure 9.2 – 9.8 show the ρ, σ and π masses as a function of M_π^2 in the unit of M_ρ^0. At low quark mass $M_\pi^2 \sim m_Q$ making M_π^2 serve as an observable proxy for the quark

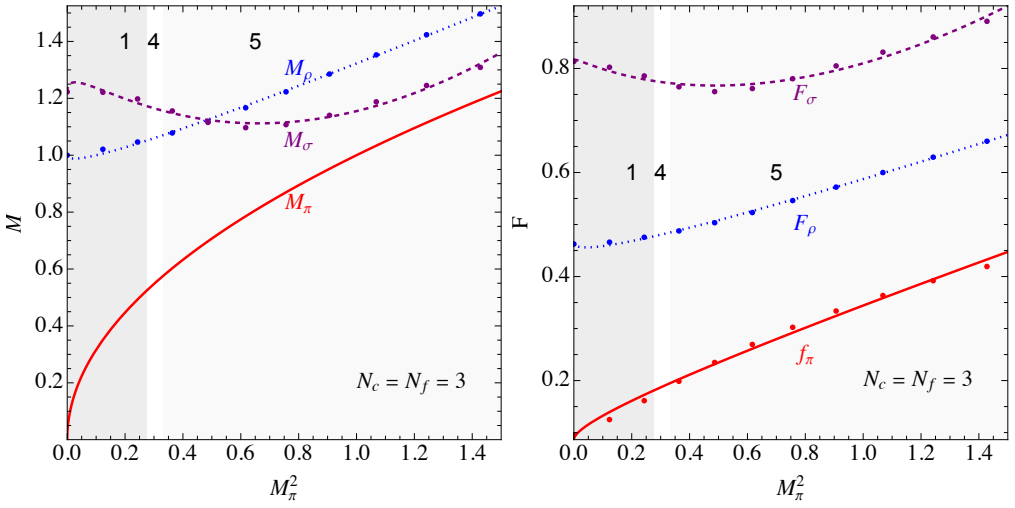

FIGURE 9.3: Mass spectrum (left) and decay constants (right) in units of M_ρ^0 for $N_f = 3$. The gray shaded areas correspond to the different regions of parameter space presented in Figure 9.1.

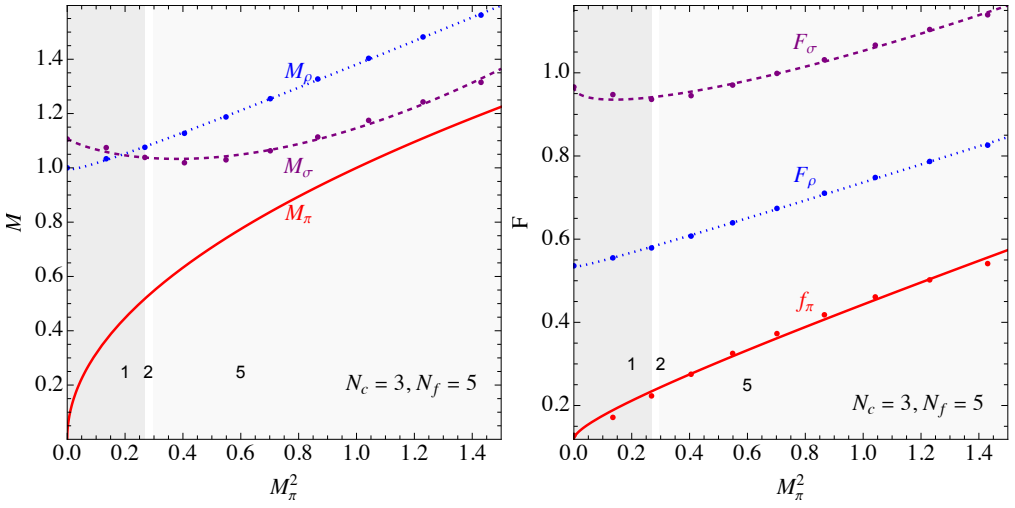

FIGURE 9.4: Mass spectrum (left) and decay constants (right) in units of M_ρ^0 for $N_f = 5$. The gray shaded areas correspond to the different regions of parameter space presented in Figure 9.1.

N_f	M_ρ/M_ρ^0	M_σ/M_ρ^0
2	$1 - 0.161m + 0.463m^2$	$1.25 + 0.604m - 1.88m^2 + 1.19m^3$
3	$1 - 0.15m + 0.472m^2$	$1.22 + 0.431m - 1.56m^2 + 1.06m^3$
5	$1 - 0.097m + 0.478m^2$	$1.11 - 0.0313m - 0.501m^2 + 0.569m^3$
6	$1 - 0.063m + 0.495m^2$	$0.988 - 0.002m - 0.488m^2 + 0.664m^3$
7	$1 + 0.00931m + 0.48m^2$	$0.814 - 0.175m + 0.482m^2 + 0.0219m^3$
9	$1 + 0.309m + 0.409m^2$	$0.384 + 0.201m + 0.846m^2 - 0.309m^3$
11	$1 + 1.09m + 0.363m^2$	$0.0736 + 0.715m + 0.431m^2 - 0.188m^3$

TABLE 9.1: Fits for M_ρ, M_σ in units of M_ρ^0 as a function of N_f for $N_c = 3$ derived within our holographic model. N.b. $m \equiv M_\pi$ for brevity.

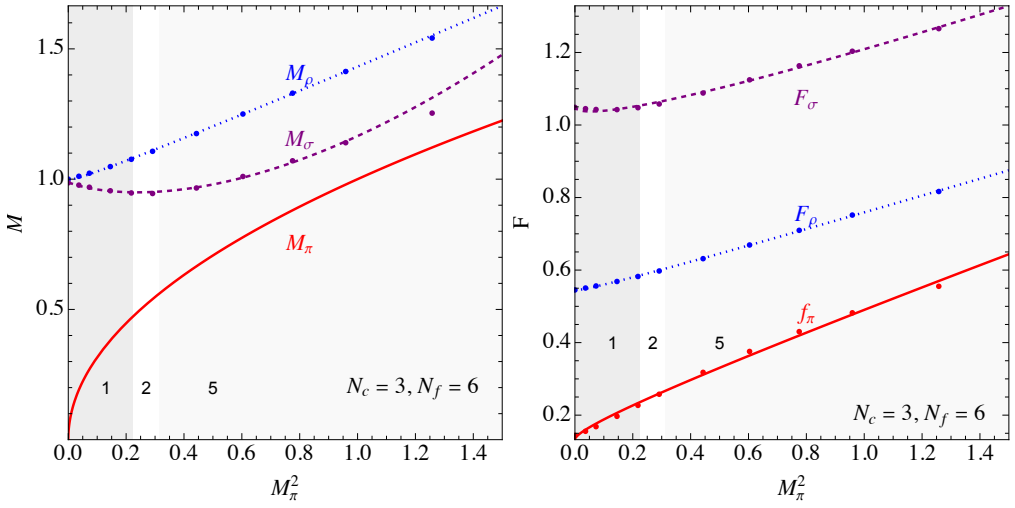

FIGURE 9.5: Mass spectrum (left) and decay constants (right) in units of M_ρ^0 for $N_f = 6$. The gray shaded areas correspond to the different regions of parameter space presented in Figure 9.1.

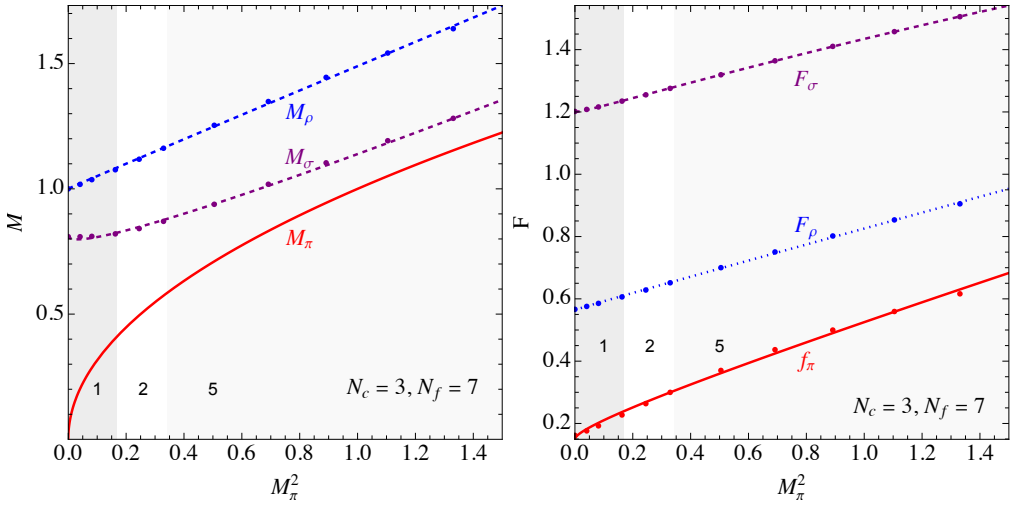

FIGURE 9.6: Mass spectrum (left) and decay constants (right) in units of M_ρ^0 for $N_f = 7$. The gray shaded areas correspond to the different regions of parameter space presented in Figure 9.1.

N_f	f_π/M_ρ^0	F_ρ/M_ρ^0	F_σ/M_ρ^0
2	$0.07 + 0.070m + 0.143m^2$	$0.418 - 0.075m + 0.176m^2$	$0.71 + 0.186m - 0.69m^2 + 0.49m^3$
3	$0.086 + 0.094m + 0.164m^2$	$0.465 - 0.086m + 0.208m^2$	$0.82 + 0.04m - 0.42m^2 + 0.37m^3$
5	$0.119 + 0.114m + 0.211m^2$	$0.535 - 0.03m + 0.231m^2$	$0.97 - 0.17m + 0.19m^2 + 0.06m^3$
6	$0.133 + 0.093m + 0.265m^2$	$0.546 - 0.035m + 0.248m^2$	$1.05 - 0.13m + 0.27m^2 + 0.018m^3$
7	$0.149 + 0.11m + 0.266m^2$	$0.564 + 0.012m + 0.25m^2$	$1.20 - 0.04m + 0.34m^2 - 0.06m^3$
9	$0.229 + 0.3m^2$	$0.63 + 0.31m^2$	$2.76 - 1.27m + 1.24m^2 - 0.25m^3$
11	$0.072 + 0.078m^2$	$0.788 + 0.735m^2$	$8.33 + 2.07m^2$

TABLE 9.2: Fits for decay constants f_π, F_ρ, F_σ in units of M_ρ^0 as a function of N_f for $N_c = 3$ obtained using our holographic model. N.b. $m \equiv M_\pi$ for brevity.

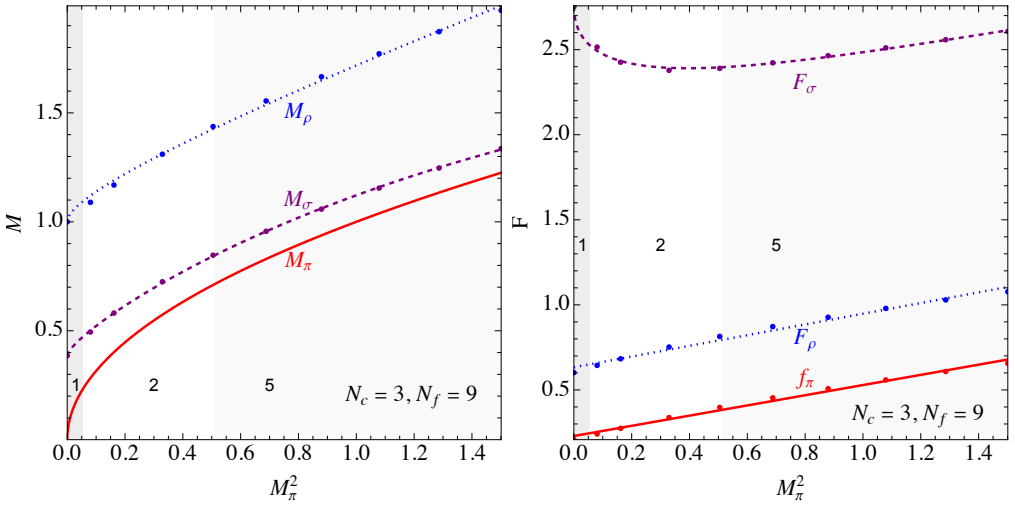

FIGURE 9.7: Mass spectrum (left) and decay constants (right) in units of M_ρ^0 for $N_f = 9$. The gray shaded areas correspond to the different regions of parameter space presented in Figure 9.1.

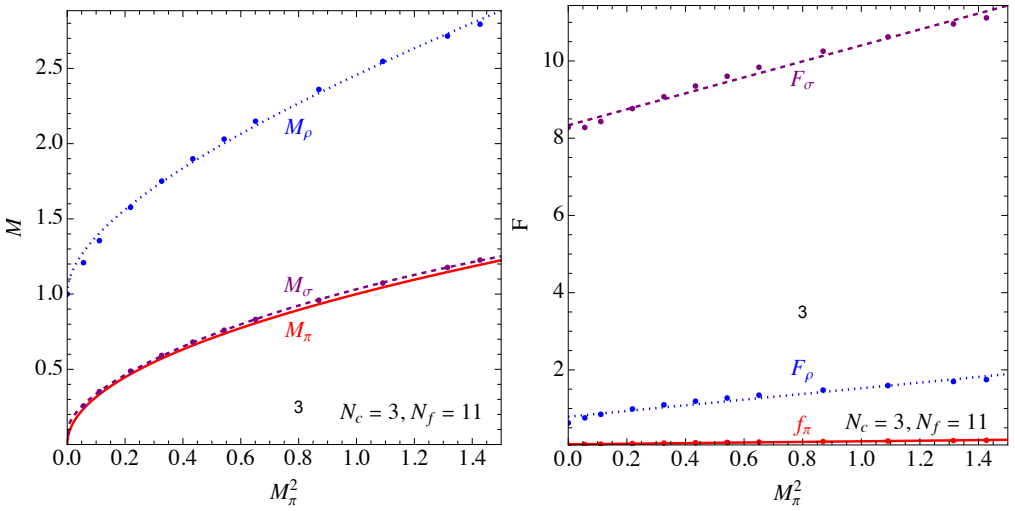

FIGURE 9.8: Mass spectrum (left) and decay constants (right) in units of M_ρ^0 for $N_f = 11$. The gray shaded areas correspond to the different regions of parameter space presented in Figure 9.1.

mass. The red π mass curve is, of course, trivial against M_π^2 but included for comparison to the other states.

We normalize the mass scales of the spectrum by setting the ρ mass at $M_\pi = m_Q = 0$ to be unity in each case. Thus $M_\rho(m_Q = 0) = M_\rho^0 = 1$ is the measure of the strong coupling scale when one compares theories. The ρ mass is well fitted as a function $a + bM_\pi + cM_\pi^2$ at all N_f and are shown in tab. 9.1. As shown in Figure 9.9 (left panel), the fits we obtain are a function of N_f, although we do not attempt to fit this dependence. The N_f dependence of the ρ mass becomes stronger as one approaches the lower edge of the conformal window at $N_f \sim 11$ (formally the edge lies at 11.9). The M_π term in the fits makes the largest difference near the edge of the conformal

window. These results clearly demonstrate the importance of establishing N_f dependence of heavier resonance properties by means of lattice simulations.

We have concentrated on the regime $M_\pi^2 < 1.5(M_\rho^0)^2$ – in the holographic model above this scale there is a transition to a linear regime where all $M, F \propto M_\pi \sim m_Q$ but in all but the most walking theories the gauge theory becomes perturbative here and holography isn't the correct description. Also in these high m_Q cases the glue dynamics separates from the quark dynamics below the quark mass scale. These theories will include glueballs that are lighter than the mesons so the models are no longer pion based dark matter models. We have not attempted to describe the glueball sector here but we note that at intermediate m_Q there will be theories with glueballs as well as light ρ, σ, π. Without being quantitative about the intermediate m_Q region, in Figure 9.1 (left panel) we show this as region 9 which corresponds to intermediate quarks where glueballs will be a relevant light degrees of freedom. This region lies at higher M_π^2 in Figure 9.1 (right panel).

The σ meson mass is much more N_f dependent than the ρ (see Figure 9.9, right panel), at least in this holographic model. The key term is the third term in Eq. (5.31) which depends on the rate of change of the running mass M_X^2. Without this term the equation becomes degenerate with the pion Eq. (5.42) (using Eq. (5.28)). Thus at the edge of the conformal window where the IR running of the coupling is negligible the σ becomes degenerate with the π. On the other hand in the low N_f theories the running is fast and the resulting σ is much heavier (heavier than the ρ for $N_f < 5$).

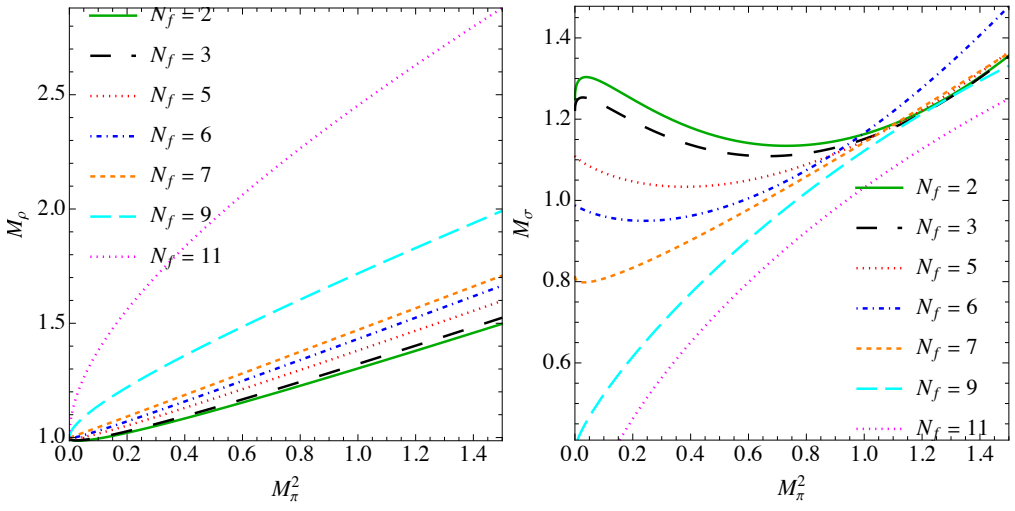

FIGURE 9.9: N_f dependence of the ρ and σ masses using the fits presented in table 9.1.

We have used the fits to determine where the IR theory lies in the space of theories described in Figure 9.1 (left panel) and this then determines the regions shown in Figure 9.1 (right panel). We will discuss Figure 9.1 (right panel) in detail below.

Finally, in Figure 9.2 – 9.8 (right panels) we also show the corresponding decay constants for the ρ, σ, π. They all grow with M_π. The main N_f scaling is that discussed in section 9.2 – $f_\pi^2 \sim N_f$ and $F_{\rho,\sigma}^2 \sim \sqrt{N_f}$. In addition there is N_f dependence through the holographic wave functions

of the particles involved. Here the biggest effect is in F_σ which grows sharply with N_f as one approaches the edge of the conformal window.

9.3.2 N_c Dependence

At large N_c, i.e. the Veneziano limit [38], the β function ansatz we use to input the dynamics of the theory is simply a function of N_f/N_c at leading order. As is frequently argued $N_c = 3$ lies close to large N_c so it is interesting to test how good an approximation this scaling is.

A natural set of theories to compare are SU(3) with $N_f = 3$, SU(4) with $N_f = 4$ and SU(5) with $N_f = 5$. We show a selection of computations at various quark mass of the meson and decay constants in Figure 9.10. To compare the decay constants we remove the explicit $\sqrt{N_c N_f}$ factors in f_π and F_ρ^2, F_σ^2. Certainly within any errors the holographic models contain, this scaling is clearly present. We have also cross checked SU(3) with $N_f = 9$, SU(4) with $N_f = 12$ and SU(5) with $N_f = 15$ where again within 10% the degeneracy is accurate. We will therefore not present further results

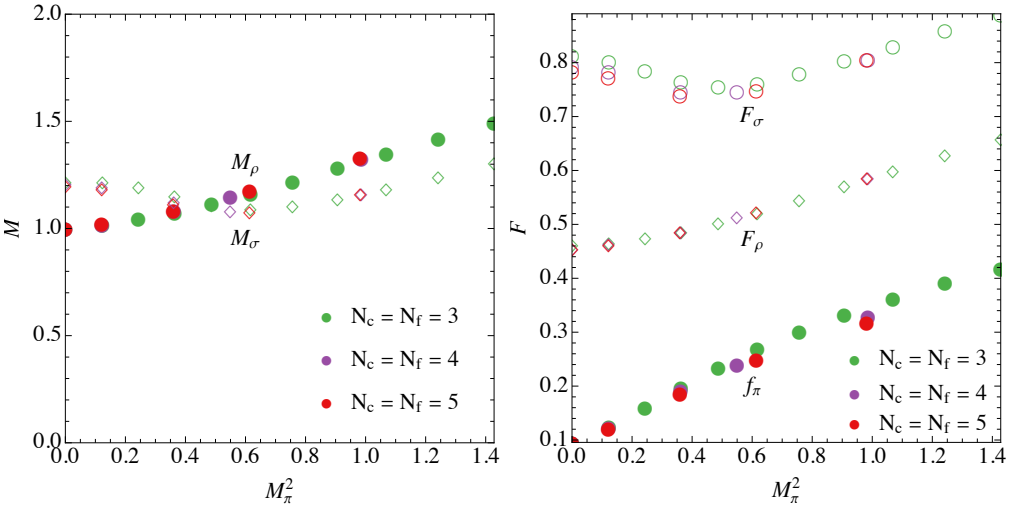

FIGURE 9.10: Comparison of the theories with $N_f = 3$ (green), SU(4) with $N_f = 4$ (Purple) and SU(5) with $N_f = 5$ (Red) Left: data for the σ and ρ meson masses Right: the decay constants f_π, F_ρ, F_σ corrected by the rude N_f, N_c scaling discussed in the text.

at higher N_c since they can be extrapolated from $N_c = 3$ and the corresponding N_f variations. Similarly Figure 9.1 (right panel) although valid for $N_c = 3$ is in fact a good description of all N_c theories.

9.4 Comparison to Lattice Data

It is worth making some comparisons of the holographic predictions to known lattice calculations. Several lattice investigations for SU(N_c) gauge group are available. Most notably, ref. [126,

127, 128] provide a comprehensive study of meson properties for large-N_c theories in the quenched approximation. We choose here data from [129] for our comparisons as it is presented in the most useful fashion for our purposes.

The mass spectrum is the most important component of our analysis. In Figure 9.11 we show a comparison to QCD functional methods analysis from [130, 131] (here we take $N_c = N_f = 3$ in the holographic model to represent the light states in the 2+1 quark theory). The quantity M_π/M_ρ is plotted as a function of M_π^2 in units of M_ρ^0. At low M_π^2 this is a plot against the quark mass. The comparison is good. There is a modest deviation at larger M_π^2, which likely stems from the fact that in holographic models the conformal, weakly coupled UV of QCD is replaced by a strongly coupled conformal UV theory. Introducing a mass scale in the UV adds additional strong interactions so heavy quarks are poorly described. The holographic description of the ρ seems very good up to $(M_\pi/M_\rho^0)^2 = 0.5$ and even above there is decent agreement to draw qualitative conclusions. The transitions between regions in Figure 9.1 (right panel) lie below this value.

The dimensionful F_ρ rises linearly with M_π^2. In the lattice review [129] they call what we call F_ρ^2, $M_V^2 F_V$. We fit their data and use our conventions. In Figure 9.11 we plot the dimensionless F_ρ/M_ρ in the holographic model against the lattice data taken from [129]. The holographic model prediction is a little lower but the weak mass dependence is reasonably consistent.

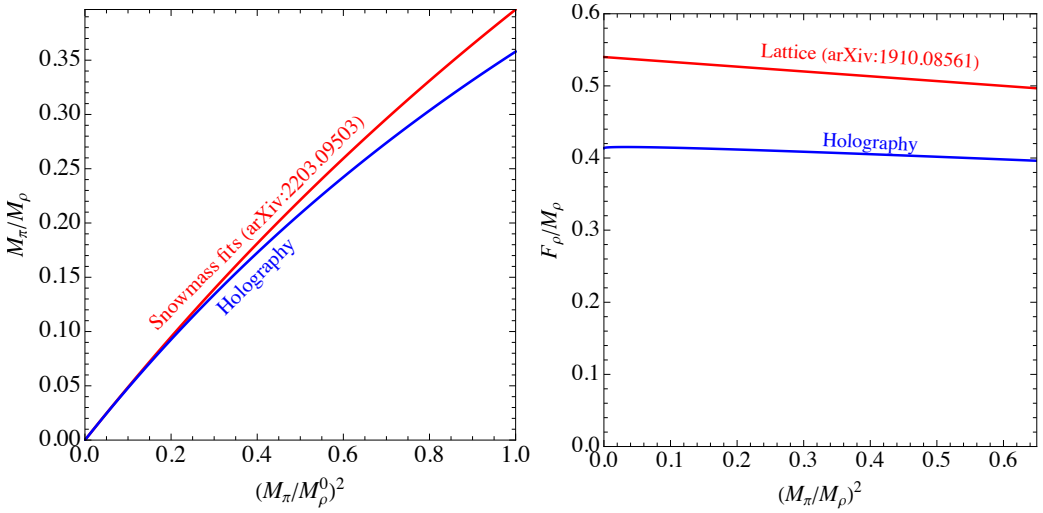

FIGURE 9.11: Left: Comparison of the holographic predictions (blue) for QCD compared to the lattice results in [130] (red) for M_π/M_ρ vs $M_\pi^2/M_\rho^{0\,2}$ in units of the ρ mass at $m_Q = 0$. Right: a comparison of the holographic results (blue) for F_ρ/M_ρ vs M_π^2 in units of the ρ mass (note not at $m_Q = 0$) and the lattice results from [129] (red).

The holographic model's prediction for f_π is more troubling. We can see in the $N_f = N_c = 3$ case in Figure 9.3 – 9.4 that f_π approximately quadruples across the M_π^2 range. If one looks at the equivalent plot in [129] f_π does not even double across this range. We believe this is again a result of the UV artifice of the holographic model. As the quark mass rises above the strong coupling scale Λ in QCD f_π is expected to scale as $\sqrt{m_Q \Lambda}$ reflecting the role of the strong coupling scale still in the bound state dynamics. On the other hand in holography there is strong coupling at the

scale m_Q and one sees $f_\pi \sim m_Q$. The physics in the holographic model is wrong and this shows up at lower quark mass with f_π rising more sharply to attain its larger UV quark mass behaviour. We nevertheless present the f_π predictions because they include interesting N_f dependence that we believe is qualitatively correct and has lessons for the QCD-like theories.

Let us immediately turn to the quantity M_π/f_π which plays an important role in SIMP models. In Figure 9.12 we plot this quantity against M_π^2/M_ρ^2 - note here that it is M_ρ in the denominator, not M_ρ^0 - the ultra heavy quark limit is at $M_\pi^2/M_\rho^2 = 1$. We plot the lattice results fitted from [129] and our holographic results for a number of choices of N_f.

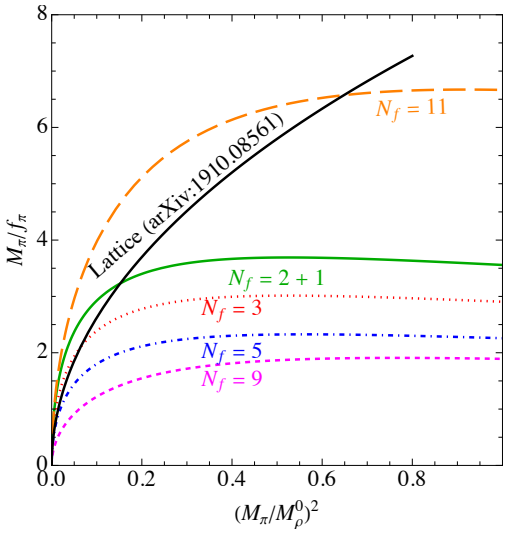

FIGURE 9.12: The ratio M_π/f_π in the holographic model as a function of M_π for $N_c = 3$, and various N_f together with the lattice data (black line) from [129].

Here one should immediately compare the $N_f = 2+1$ holographic theory (we use the $N_c = 3$ running but $N_f = 2$ in the decay constant calculation) and the lattice results. Until $M_\pi/M_\rho \sim 0.5$ one could live with the holographic model but above this mass value the spurious UV behaviour of f_π kicks in and takes the holographic model away from the true lattice data.

The lattice data shows that for $N_c = 3, N_f = 2+1$ reaching a value of M_π/f_π greater than 5-6 seems very hard [129]. The original SIMP phenomenology wanted this ratio to be 12. The higher N_f holography curves are lower reflecting the $\sqrt{N_c N_f}$ factor one expects in f_π. Raising N_c or N_f will only make things worse (M_π/f_π lower). This observation motivates our search for more complex models with additional dark matter relic density mechanisms present.

The only outlier is the $N_f = 11$ curve which does reach higher values of the ratio. This theory is very walking and lives in Region 3 which we discuss below. The effect of walking (for which the idea was invented in [132]) is to raise the quark condensate relative to f_π. This rise in the holographic model infects all other masses and decay constants and hence M_π/f_π can be larger. In the holographic model the ratio rises indefinitely as one tunes to N_f^c. This conclusion is likely to map across from the holographic model with poor UV behaviour to true walking SIMP models which therefore might have an important role to play in the SIMP paradigm.

9.5 Phenomenology

A strongly coupled dark matter sector, such as the $SU(N_c)$ gauge theories we have considered here, in principle feature an infinite tower of states. The expectation is that for most of the parameter space the IR is well described by an effective theory of a few light meson states that all other states decay to. Our main goal here has been to determine the likely states in those IR theories for SU(N_c) dynamics as a function of N_c, N_f and a common quark mass. As we have seen the spectrum is largely N_c independent at fixed N_f/N_c although the decay constants grow with N_c. We have identified 7 viable low energy theories shown in Figure 9.1. We have displayed the phase space in the N_f vs m_Q plane where each occurs in Figure 9.1 (right panel). Here one can interpret the area in the plane as indicative of how tuned the parameter space for each region is. Of course the reliability of those conclusions depends on one's trust of the holographic model. The ρ mass seems perfectly reasonably modelled (see Figure 9.11). The σ meson seems more model dependent. The holographic model places it heavier than the ρ at low N_f and low m_Q (the identification of the σ meson among the f_0 states in QCD is still uncertain) before becoming lighter for larger N_f as it moves towards a dilaton behaviour in the walking regime. Whilst this behaviour seems reasonable it is not a first principles result. At worst we view the holographic model as a guide to the types of phases that may exist.

It is worth noting the trajectory of the theories through the regions as N_f and m_Q change for a fixed N_c:

1. *Massless theories ($m_Q = 0$)*: In the chiral limit, as N_f increases one moves from theories containing only light πs (region 1) → light π, σ (region 2) → walking dilaton σ (region 3) before entering the regime of unparticles [123] in the conformal window.

2. *Increasing mass ($m_Q > 0$), small N_f*: Low N_f theories move from only light πs (region 1) → light π, ρ (region 4) → light π, ρ, σ (region 5) → light glueballs (region 9), although region 4 is rather a tuned part of the parameter space.

3. *Increasing mass ($m_Q > 0$), large N_f*: For higher N_f one sees light πs (region 1) → light π, σ (region 2) → light π, ρ, σ → light glueballs (region 9) or walking dilaton σ (region 3) → light ρ, σ (region 6) → light glueballs (region 9) at the edge of the conformal window.

4. *No Regions 7,8:* there is no mechanism we know to make the ρ anomalously light relative to the σ and π (whereas for those we can use chiral symmetry breaking or conformal symmetry breaking to make them light).

We will now turn to discuss the phenomenology, as currently known, for these seven regions featuring different mass hierarchies although we do not aim to rigorously analyse this phenomenology here. We also stress that we do not consider dark matter – SM thermalization aspects, for which an external mediator between the strong-sector and the SM is often introduced. Our aim

here is to analyse the strong sector in isolation and consider potential impact of higher dimensional effective couplings between the SM and strong sector which must arise at least at the Planck scale.

9.5.1 Region 1: only light π

Region 1 describes QCD-like theories with a strongly running coupling and light quark mass relative to the strong coupling scale. The spectrum including the σ and ρ lie above twice the pion mass at the strong coupling scale and so will decay quickly to pions. The pions are light because of their pseudo-Goldstone nature associated with the spontaneous breaking of chiral symmetry. Thus the only relevant IR dynamical degree of freedom in the system are pions which are described by a chiral Lagrangian for dark matter calculations. One expects effective dark pion - SM couplings. The lowest dimension examples are the UV dimension-7 operator $\bar{Q}\gamma_5 Q\bar{q}\gamma_5 q h$ (h is the Higgs, Q are dark quarks and q SM quarks) and the UV dimension-8 operator $h^2(\bar{Q}\gamma_5 Q)^2$. These are highly suppressed by the ultraviolet scale and pion annihilations to the SM will thus be negligible allowing strong-sector only interactions to dominate.

The relic abundance in the pion model has been computed in [108]. Famously, the presence of a Wess-Zumino-Witten term of the form

$$L_{WZ} \propto \frac{1}{f_\pi^5}\epsilon^{\mu\nu\rho\sigma}\mathrm{Tr}[\pi\partial_\mu\pi\partial_\nu\pi\partial_\rho\pi\partial_\sigma\pi] \tag{9.3}$$

generates $3 \to 2$ processes that deplete the pions and lead to lower dark matter masses than in other models. The authors traded the strong coupling scale and m_Q for M_π and the ratio M_π/f_π. The pion mass is predicted to lie in the ten-few hundred MeV for M_π/f_π up to 12 (Here again we stress we use the convention where $f_\pi = 93\mathrm{MeV}$)[1].

Equally though the model contains four point self interactions of the pions (coming from the $\mathrm{Tr}[M^\dagger U]$ type terms in the chiral Lagrangian ($U = \exp(\pi/f_\pi)$) in low energy limit where one neglects derivative interactions). The cross-section behaves as

$$\sigma_{\mathrm{scatter}} \propto \left(\frac{M_\pi}{f_\pi}\right)^4 \frac{1}{M_\pi^2} \tag{9.4}$$

so that at fixed M_π/f_π one needs a sufficiently large pion mass for the self interaction to explain but not violate the bound from the bullet cluster observations [133, 134, 135].

The conclusion was that the dark pion mass should lie in the few 100s MeV with large $M_\pi/f_\pi \sim 12+$. This value lies close to the naive perturbativity bound of the chiral Lagrangian and implies a rather large quark mass whilst maintaining the chiral Lagrangian structure [136, 137, 109]. We

[1]Note that we use a definition of f_π that differs by 2 relative to [108] – this figure is with our definition.

have seen in Figure 9.12 above that neither lattice data nor our holographic models suggest it is easy to achieve such a large value. This suggests the other regions we discuss below may be of more phenomenological interest. We note here that it may be possible to generate relic density via bound states of two pions, as demonstrated in [138]. We also note that the dark pion relic density may be generated via the misalignment mechanism [139], a possibility we do not pursue in this discussion.

9.5.2 Region 2: light π, σ

Region 2 is a substantial part of the parameter space in Figure 9.1 (right panel) at larger N_f values and intermediate quark masses. In these models the running of the coupling at the scale of the chiral condensate is weaker than in QCD (either because of the larger N_f or the quark mass scale). The holographic model then predicts a light σ meson below twice the pion mass.

The σs therefore can not decay directly to two pions and naively will form part of the final dark matter mix. However one can expect couplings between the quantum number free σ and the SM from the UV completion of the theory. For example, a $c_{\sigma hh}\sigma|h|^2$ Lagrangian term where $c_{\sigma hh}$ is the coupling to the SM Higgs. The dark matter quark anti-quark operator that forms the σ is dimension 3. Thus $c_{\sigma hh}$ will be given by the ratio of the dark sectors strong coupling scale squared to the scale at which the dark sector and SM interact. This coupling between the σ and h will induce a mixing between these particles leading to the decay of σ into two fermions. The partial widths are of the form

$$\Gamma(\sigma \to f\bar{f}) \simeq \frac{1}{8\pi m_\sigma^2} Y_f^2 \left(\frac{c_{\sigma hh}}{\lambda v}\right)^2 (m_\sigma^2 - 4m_f^2)^{3/2} \tag{9.5}$$

with Y_f the usual Yukawa couplings, λ the usual Higgs quartic coupling and v the Higgs vacuum expectation value. Due to the strong hierarchy in the Yukawa sector, the decay into the heaviest fermion kinematically allowed will determine the order of its life-time. We assume here $m_\sigma \ll m_h$. Assuming the UV completion is at the Planck scale the width is approximately $Y_f^2 m_\sigma^5/v^2\Lambda_{Pl}^2 \sim Y_f^2(1\text{GeV})^5/(246\text{GeV})^2/(10^{19}\text{GeV})^2 \sim Y_f^2\, 10^{-42}\text{GeV}$. Note, the age of the Universe is $\sim 10^{41}\,\text{GeV}^{-1}$. For a light dark σ of order 1 GeV the decay can only proceed to lighter fermions than the top and the Yukawa suppression (e.g. for decays to the strange quark $Y_f^2 \sim 10^{-7}$) will make the σ effectively stable and hence a dark matter candidate. Some avenues for dilaton dark matter have been explored in [140, 141, 142, 143].

In any model where the UV completion provides thermalization to the SM sector the UV scale is likely much lower than the Planck mass and the σ is unlikely to be stable and in fact can be expected to decay quickly. In such cases the σ can still play a significant role in the evolution of the π. Strong interactions will allow the process $(2\pi \to 2\sigma)$ during the regime where the kinetic energy of the π is sufficiently large. The $\pi\pi\sigma$ coupling together with σ decaying to the

SM effectively allow $\pi\pi \to f\bar{f}$ with a rate that depends on the UV completion scale. Overall this may provide a depletion mechanism for the π. This has been analysed in [113]. It will further be interesting to understand the N_f dependence of this annihilation channel for which holography may provide qualitative guidance, but lattice computations are necessary for more quantitative estimates. The σ meson may also alter the pion-interaction strength, therefore impacting the phenomenologically viable regions [144].

9.5.3 Region 3: walking dilaton sigma

Region 3 is the extreme walking limit of Region 2 where the running is so slow that the σ meson becomes essentially degenerate with the pions. The holographic model suggests this occurs when N_f is within approximately 10% of N_f^c. This is when the new decay channel of Region 2 ($2\pi \to 2\sigma$) becomes maximally strong.

Furthermore as we saw in Figure 9.12 it is possible to realise much large M_π/f_π values in this region. The effect of walking (for which the idea was invented in [132]) is to raise the quark condensate relative to f_π. This rise in the holographic model infects all other masses and decay constants and hence M_π/f_π can be larger.

Together, these effects should facilitate obtaining the observed relic density compared to the pure pion model, as long as the σ decays sufficiently rapidly.

9.5.4 Region 4: light π, ρ

Phenomenologically, region 4 has been assumed to be a dominant region in parameter space of strong-sector theory. Our results in Figure 9.1 show that region 4 is in fact only a small part of the parameter space. At small N_f the σ is heavy due to the strong running. As the pion mass rises it reaches half the ρ mass first, however σ quickly becomes light enough to be phenomenologically significant.

Within region 4, the ρ can be created for example by $3\pi \to \pi\rho$ processes, but cannot quickly decay back to pions. If ρ decays to the SM are rapid enough, this channel can be used to deplete the pion abundance efficiently as it destroys two pions per annihilation. This mechanism also allows one to lower the required M_π/f_π to reconcile the relic density and self-scattering cross-section. This scenario has been studied in [111]. In addition to $3\pi \to \pi\rho$ processes $\pi\pi \to \rho\rho$ processes are also a possible relic density mechanism, given that ρ decays are rapid. A possible model is presented in [110]. Additionally the ρ may also take part in the $3 \to 2$ number changing processes modifying the phenomenologically viable region [112].

9.5.5 Region 5: light ρ, σ

Region 5 is the largest region in Figure 9.1 (right panel). It occurs at all N_f and when the quark mass is sufficiently large that the π mass is more than about $0.4M_\rho^0$. Here the π is essentially heavy enough to bring the ρ and σ below $2M_\pi$. Both the ρ and σ can now provide additional annihilation channels to reduce the pion abundance. This scenario is likely to be even more successful at making a working model with low M_π/f_π. Note that here and in the next two regions other higher mass bound states such as the axial vector mesons may begin to become stable against decay to lighter states however that is beyond the scope of this work.

We have not found discussion of this case in the literature. Several competing processes such as $3\pi \to \pi\sigma, 3\pi \to \pi\rho, 3\pi \to \rho\sigma, 2\pi \to 2\rho$ and $2\pi \to 2\sigma$ may be present in this region. Depending on the model construction, this offers a rich signature space not only for relic density generation mechanisms but also for experimental analyses [2]. We do not perform the relic density calculations or signature space analysis here but one of our key findings is that this scenario is a very likely one. It would be very interesting to study it in more detail.

We also note that low $N_c, N_f = 1$ theories are also essentially region 5 theories. for these theories, the strong effect of the axial anomaly makes the pNGB heavy (as the η' is in QCD). It is therefore likely that the η', ρ and σ will all be close in mass [145].

9.5.6 Region 6: dilaton σ, light ρ

Region 6 is simply a walking variant of Region 5 where the σ is degenerate with the π and the ρ is light. It doesn't appear in Figure 9.1 (right panel) because it lies on the right hand end of the $N_f = 11$ (at $N_c = 3$) green line above $M_\pi = 2M_\rho^0$.

9.5.7 Region 9: light glueballs

Region 9 occurs in all theories when the quark mass rises to of order the strong coupling scale. The IR theory will consist of π, ρ, σ and scalar glueballs. The scalar glueballs look like extra σs and again it would be interesting to study a combined model of all these particles. This candidate is connected to the SM through operators of at least UV dimension 6 (such as TrF^2h^2) and so can have lifetimes longer than the age of the Universe. The glueballs could form part of the final dark matter mix with π. Again this mixture and its interactions remain to be explored and could provide interesting models.

[2] For a review of collider searches for strong-sector theories see [130].

9.6 Other Strongly Coupled Possibilities

In this final section we note some other lightest states in strongly coupled theories which could serve as dark matter scenarios simply for completeness. We have sought to identify the lightest hadronic states in theories. Were these unstable in some model then it is possible that baryons could remain stable as the dark matter relic - see for example [122, 121, 146].

9.6.1 Glueball Dark Matter in Pure Yang-Mills or Heavy Quark Theories

At very large quark mass the dominant scale for meson physics is m_Q and all meson masses are approximately $2m_Q$. The holographic model shows this behaviour at large quark masses but we do not show these results because the holographic approach assumes the gauge dynamics to be strongly coupled whereas the gauge theories become weakly coupled at the quark mass scale. Below the quark mass the gauge dynamics becomes a pure Yang-Mills theory. At large quark mass the glueball sector will be lightest part of the spectrum and these theories are not pionic dark matter theories. Glueball dark matter is discussed in e.g. [115, 116, 117, 118, 119, 120].

9.6.2 Unparticles

Theories with $N_f > N_f^c$ and massless quarks live in the conformal window. The IR theory is a conformal plasma known as unparticles [123]. Since the unparticle plasma is massless it can't be dark matter. As soon as a mass is introduced one enters our region 5 (if the fixed point is strongly coupled) or region 9 if more weakly coupled. A first study of these later models can be found in [124]. We note here that although the mass hierarchy in these scenarios resembles one of the regions in Figure 9.1 (left panel), their low energy effective theory may be considerably different.

9.6.3 σ Dark Matter

An interesting question that emerges from the above theory space scan is whether it is ever possible within the N_f, N_c space we consider to have a theory in which the σ meson is the lightest particle and hence a dark matter candidate. In the theories so far discussed the σ is always heavier than the π moving to degenerate in the extreme walking case. We now briefly describe two models that could possibly achieve this goal though.

As we have discussed above a σ is not a natural dark matter candidate because naively one would expect the presence of UV dimension five operators such as $\bar{Q}Q|h|^2$ that become $\sigma|h|^2$ in the IR. These likely lead to the σ being unstable relative to the lifetime of the Universe unless both the σ is light and the UV completion scale is very high as discussed above. It is possible though that some Z_2 symmetry might eliminate these terms in a more UV complete model (this is also

true in the cases with a light σ already discussed). We therefore include this discussion for completeness.

9.6.3.1 $N_f = 1 + N_X$ Theories

One possible way to achieve the σ as the lightest particle is to consider SU(N_c) theories with $N_f = 1$. Here the chiral symmetry is anomalous and the single "pion" associated with the quark condensate will be heavy due to that anomaly [145]. Our holographic model does not include the anomaly since it is based on dualities at large N_c where the anomaly vanishes. The problem in this theory though is that $N_f = 1$ theories are not walking and the σ would be heavy. This could be repaired by including N_X additional massive fermions with masses below but close to the dark sector strong coupling scale. All bound states containing the X fermions would lie near the strong coupling or X mass scale. The $N_f = 1$ sector would experience the running dynamics of the $N_f = 1 + N_X$ so in the (anomalous) U(1) sector a light σ would likely emerge made from the massless quark.

9.6.3.2 Chirally Gauged $N_f = 2 + N_X$ Theories

An alternative possibility is to remove the Nambu-Goldstone bosons from the light spectrum by having them eaten by a set of gauge bosons. Inspired by technicolour/the SM one could for example use $N_f = 2$ and gauge the $SU(2)_{L_D}$ symmetry of the massless dark matter quarks (note this is not the $SU(2)_L$ of the SM). The matter content is shown in tab. 9.3 or as a moose diagram [147] in Fig. 9.13. The massless pions will be eaten by the $SU(2)_{L_D}$ gauge fields and become part of a massive multiplet of gauge bosons with mass $g_2 f_\pi$. Note the case where one gauges an $SU(2)_{L_D}$ sub-group, rather than some SU(N_f) subgroup, is unique in that it has real representations and is anomaly free. That this dark matter sector mimics the SM structure is amusing!

	$SU(N_c)$	$SU(2)_{L_D}$	$SU(2)_{R_D}$	$SU(N_X)_V$
$q_L = \begin{pmatrix} u_L \\ d_L \end{pmatrix}$	$\square$	$\square$	1	1
$q_R^C = \begin{pmatrix} u_R^C \\ d_R^C \end{pmatrix}$	$\overline{\square}$	1	$\overline{\square}$	1
$\psi_{X,L}$	$\square$	1	1	$\square$
$\psi_{X,R}$	$\overline{\square}$	1	1	$\square$

TABLE 9.3: Matter representation for a possible σ dark matter model.

Again the problem is that the models with $N_f = 2$ do not have walking dynamics to make the σ light. As in the previous model we could solve this by including extra fermions with masses near the strong coupling scale to force a walking behaviour at the the chiral symmetry breaking scale. In Figure 9.13 we call these fermions ψ_X, they are a singlet of the $SU(2)_{L_D}$ gauge symmetry. It is likely a σ made from the massless fermions will be the lightest state.

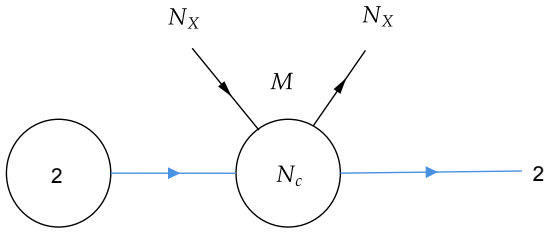

FIGURE 9.13: Matter content of the $N_f = 2 + N_X$ model as a moose diagram [147].

9.7 Conclusions

Strongly-coupled theories provide interesting dark matter candidates in the form of pions, which produce relic density through number changing interactions within the strong-sector. Together with their ability to generate large self-interaction cross-section, they form a viable class of theories resulting in new phenomenology across cosmology and experimental searches. Due to their inherent non-perturbative nature these theories demand careful attention, especially to understand possible new relic density mechanisms beyond the well known ones. In this work, we embarked on such a survey using a holography model. Our aim was to demonstrate the lightest degrees of freedom in a large part of theory parameter space and elucidate associated potential dark matter phenomenology.

In this context, working within a SU($N_c = 3$) gauge groups with N_f fermions in the fundamental representation, we sketched out seven distinct regions where qualitatively different dark matter phenomenology may appear. Regions where pions are the only relevant degrees of freedom are restricted and do not generate large enough M_π / f_π to obtain phenomenologically consistent theory space. This points to analysis of additional relic density mechanisms adhering to the theory constraints. From this point of view, the next lightest species may play an important role. An obvious example is ρ, π only theories but they appear viable only in a very small region of parameter space within our investigations. A heavier quark mass or larger number of flavours, immediately leads to a light σ which may have interesting consequences for dark matter phenomenology. Such ρ, π, σ admixed regions have not yet been analysed in the literature to the best of our knowledge. This region is in fact the most dominant region in the parameter space we study. Complementary to these we also find regions where π, σ can be simultaneously light, as one nears the conformal window.

Comparison of our results with non-perturbative calculations such as the lattice demonstrates that our mass spectrum is in good agreement with first principles calculations. Our values of decay constant are less precise due to limitations of the holographic model itself, where large quark masses reveal strong coupling in the conformal UV that is nor present in the true gauge theories. Never-the-less, the qualitative understanding is correct. Variation with respect to N_c for fixed N_f/N_c is almost trivial, wherein no change in the spectrum is observed. This leads us to conclude that we can generalise our results across large regions of parameter space.

Finally we commented on other possible dark matter candidates such as the glueballs or unparticles with mass gap. We also briefly sketch confining theories where a light σ can be obtained, keeping it as the only relevant degree of freedom in the theory. We argue that to stablise σ against potential decays to the Standard Model, additional symmetry mechanisms may be necessary.

Our investigation underlines the necessity of coupling non-perturbative understanding of strongly-interacting theories with dark matter phenomenology. Lattice studies while the best course of action for such an analysis, may not be computationally feasible. Therefore, use of holography techniques can serve as a first guiding principle in identifying interesting regions of parameter space as well as setting qualitative understanding of underlying parameters for dark matter. This understanding, followed by dark matter analysis will lead to useful feedback for the lattice community where targeted analyses may be carried out. We intend to embark on such a program in our follow up studies.

Chapter 10

Conclusion

In this thesis, we made use of the dynamic AdS/QCD framework to study several phenomena. This model, a bottom-up holographic approach, eschews ad-hoc IR cutoffs by dynamically solving for the scale of the dynamical mass generation from the equations of motion, coupled to bulk fields that encode the properties of boundary field theory operators. This approach provided us with a versatile tool for modelling the non-perturbative dynamics of strongly coupled gauge theories, including χSB and confinement.

First, in Chapter 6, we applied this model to analyse the approach to the conformal window from within the chirally broken phase. Our model provided inherent treatment of the running coupling and anomalous dimensions, which naturally generates walking behaviour near the conformal boundary. However, a problem, common to many holographic models, was the indirect connection between the bulk gravitational description and the precise scaling dimensions of boundary operators, which had to be inferred rather than directly set. Nevertheless, we were able to successfully identify a significant challenge for lattice simulations, i.e. we demonstrated that a theory with walking behaviour, and hence broken chiral symmetry, can exhibit a meson spectrum and correlation functions that closely mimic those of a genuine IR-conformal theory over a wide range of energy scales, potentially leading to misidentification of such theories.

Next, in Chapter 7, we adapted our framework to model a gauge theory containing matter in both the fundamental and the two-index symmetric (S_2) representations. Our model has the ability to incorporate the backreaction of the bulk fields representing each distinct representation on the shared dynamical geometry, capturing the dynamics of the two sectors. Our analysis showed that even when the two representations have similar underlying masses, a dramatic hierarchy emerges in the physical meson spectra, with the mesons of the higher-dimensional representation (S_2) sector being up to an order of magnitude heavier than their fundamental counterparts, a direct consequence of the different gauge interactions experienced by each type of fermion. Acknowledging the model's limitation - namely, that the gravitational bulk mass for the S_2-field (mapping to its anomalous dimension) is a phenomenological input - we also tested a theory with

a reduced bulk mass. In spite of a quantitative reduction in the observed hierarchy, the qualitative results remained consistent with our original ansatz, suggesting that our core finding of a significant mass hierarchy between representations is robust.

Following on from this result, in Chapter 8 we then developed a holographic description for a theory with only adjoint fermions, a case where the concepts of confinement and χSB may, in principle, be separated. The model was crucial for solving, in a self-consistent manner, for the IR geometry generated by the adjoint matter, providing a clear mechanism for confinement via a soft wall. We found, however, that this model had difficulty stabilising a scenario in which the confinement and χSB scales are widely separated within a single matter sector. To overcome this, we created a theory analogous to that explored in the previous chapter, substituting the S_2 sector with the adjoint (G), resulting in a theory with both adjoint and fundamental quarks. This addition dramatically amplified the separation between scales. Our analysis showed that the presence of fundamental matter can catalyse χSB at a scale much lower than the original adjoint-induced confinement scale, thereby demonstrating a robust holographic mechanism for generating a significant hierarchy between these two phenomena.

Finally, in Chapter 9 we leveraged the dynamic AdS/QCD model as a powerful spectroscopic tool for strongly-coupled dark sectors. Our model allowed an efficient, systematic survey of a vast landscape of dark gauge theories through the variation of N_c and N_f. A necessary step in this process is the mapping of holographic parameters onto real-world field theory quantities, which introduces a layer of interpretation. However, the phenomenological power of our survey lies in identifying robust, qualitative patterns - such as mass hierarchies between meson types - rather than precise numerical predictions. The results of our survey provided a comprehensive map of the light mesonic spectrum (including vector, axial, scalar and pseudoscalar mesons) across this landscape. We were then able to identify distinct phenomenological regions based on the mass relations between the meson types, and to correlate specific spectral features with the likely efficacy of different dark matter relic density generation mechanisms.

Looking ahead, the dynamic AdS/QCD framework presents several avenues for refinement. A primary goal is to improve the connection between our model and more fundamental, top-down constructions. While the bottom-up nature of our model provides excellent flexibility, a deeper string-theoretic embedding would reduce reliance on phenomenological inputs, such as our ansatz for the anomalous mass dimension, and provide a first-principles understanding of the dynamics we have explored in this thesis. Furthermore, the dramatic mass hierarchies generated between different matter representations in Chapters 7 and 8 naturally invite investigation into whether similar mechanisms could be leveraged to address the broader fermion mass hierarchy problem. It would be useful to explore whether the gauge structure of these theories alone - via their representation-dependent interactions - can generate the vast scales between different fermion masses. We would posit that this is a fascinating direction for future model-building within a holographic framework.

The conclusions we have drawn in this thesis, particularly regarding walking dynamics and mass generation, would be significantly strengthened by confirmation from other non-perturbative methods. In making our holographic predictions, we have called for direct comparisons with dedicated lattice studies, such as those investigating near-conformal theories [70]. Beyond this, the application of functional methods such as the exact renormalization group [125] could provide an independent, field-theoretic perspective on the β-function dynamics that we have modelled gravitationally. In a similar vein, the conformal bootstrap approach [148] also offers us a powerful avenue by which to constrain the operator scaling dimensions of these strongly coupled systems in a rigorous way. Convergent results between these diverse approaches and our own would mark a significant advance in our understanding of strongly coupled gauge theories.

Finally, we posit that the tools and results we have developed in this thesis are eminently suited for application in Beyond the Standard Model (BSM) phenomenology. We have demonstrated that the dynamic AdS/QCD model provides a versatile toolkit for constructing viable, complex dark sectors. The comprehensive spectroscopic survey of dark mesons which we began in this thesis should be expanded into full-fledged model building, where specific points in the N_c, N_f landscape can be chosen to yield specific dark matter phenomenology, such as correct relic density via thermal freeze-out, or self-interacting cross sections to address small-scale structure problems. The logical next step is to use these holographic spectra as inputs for detailed phenomenological studies, thereby connecting the salient qualitative patterns we identified to potential experimental signatures in direct and indirect detection experiments, as well as at colliders.

References

[1] Anja Alfano and Nick Evans. Mass hierarchies in gauge theory with two-index symmetric representation matter. *Phys. Rev. D*, 111(2):026001, 2025.

[2] Anja Alfano and Nick Evans. Scale separation, strong coupling UV phases, and the identification of the edge of the conformal window. *Phys. Rev. D*, 111(5):054003, 2025.

[3] Anja Alfano, Nick Evans, and Wanxiang Fan. Holography for QCD(Adj) and QCD(Adj)+F. 6 2025.

[4] Anja Alfano, Nick Evans, Suchita Kulkarni, and Werner Porod. Surveying the theory space of pion dark matter. 9 2025.

[5] David J. Gross and Frank Wilczek. Ultraviolet Behavior of Nonabelian Gauge Theories. *Phys. Rev. Lett.*, 30:1343–1346, 1973.

[6] H. David Politzer. Reliable Perturbative Results for Strong Interactions? *Phys. Rev. Lett.*, 30:1346–1349, 1973.

[7] Kenneth G. Wilson. Confinement of Quarks. *Phys. Rev. D*, 10:2445–2459, 1974.

[8] Joseph Polchinski. Dirichlet Branes and Ramond-Ramond charges. *Phys. Rev. Lett.*, 75:4724–4727, 1995.

[9] Edward Witten. Bound states of strings and p-branes. *Nucl. Phys. B*, 460:335–350, 1996.

[10] Juan Martin Maldacena. The Large N limit of superconformal field theories and supergravity. *Adv. Theor. Math. Phys.*, 2:231–252, 1998.

[11] Gerard 't Hooft. Dimensional reduction in quantum gravity. *Conf. Proc. C*, 930308:284–296, 1993.

[12] Leonard Susskind. The World as a hologram. *J. Math. Phys.*, 36:6377–6396, 1995.

[13] S. S. Gubser, Igor R. Klebanov, and Alexander M. Polyakov. Gauge theory correlators from noncritical string theory. *Phys. Lett. B*, 428:105–114, 1998.

[14] Edward Witten. Anti de Sitter space and holography. *Adv. Theor. Math. Phys.*, 2:253–291, 1998.

[15] Tadakatsu Sakai and Shigeki Sugimoto. Low energy hadron physics in holographic QCD. *Prog. Theor. Phys.*, 113:843–882, 2005.

[16] Joshua Erlich, Emanuel Katz, Dam T. Son, and Mikhail A. Stephanov. QCD and a holographic model of hadrons. *Phys. Rev. Lett.*, 95:261602, 2005.

[17] Andreas Karch, Emanuel Katz, Dam T. Son, and Mikhail A. Stephanov. Linear confinement and AdS/QCD. *Phys. Rev. D*, 74:015005, 2006.

[18] Michael E. Peskin and Daniel V. Schroeder. *An Introduction to quantum field theory*. Addison-Wesley, Reading, USA, 1995.

[19] Murray Gell-Mann. Symmetries of baryons and mesons. *Phys. Rev.*, 125:1067–1084, 1962.

[20] M. Srednicki. *Quantum field theory*. Cambridge University Press, 1 2007.

[21] L. D. Faddeev and V. N. Popov. Feynman Diagrams for the Yang-Mills Field. *Phys. Lett. B*, 25:29–30, 1967.

[22] Curtis G. Callan, Jr. Broken scale invariance in scalar field theory. *Phys. Rev. D*, 2:1541–1547, 1970.

[23] K. Symanzik. Small distance behavior in field theory and power counting. *Commun. Math. Phys.*, 18:227–246, 1970.

[24] C. Becchi, A. Rouet, and R. Stora. Renormalization of Gauge Theories. *Annals Phys.*, 98:287–321, 1976.

[25] I. V. Tyutin. Gauge Invariance in Field Theory and Statistical Physics in Operator Formalism. 1975.

[26] William E. Caswell. Asymptotic Behavior of Nonabelian Gauge Theories to Two Loop Order. *Phys. Rev. Lett.*, 33:244, 1974.

[27] Tom Banks and A. Zaks. On the Phase Structure of Vector-Like Gauge Theories with Massless Fermions. *Nucl. Phys. B*, 196:189–204, 1982.

[28] H. Fritzsch, Murray Gell-Mann, and H. Leutwyler. Advantages of the Color Octet Gluon Picture. *Phys. Lett. B*, 47:365–368, 1973.

[29] Dennis D. Dietrich and Francesco Sannino. Conformal window of SU(N) gauge theories with fermions in higher dimensional representations. *Phys. Rev. D*, 75:085018, 2007.

[30] Thomas A. Ryttov and Francesco Sannino. Conformal Windows of SU(N) Gauge Theories, Higher Dimensional Representations and The Size of The Unparticle World. *Phys. Rev. D*, 76:105004, 2007.

[31] Peter W. Higgs. Broken symmetries, massless particles and gauge fields. *Phys. Lett.*, 12:132–133, 1964.

[32] F. Englert and R. Brout. Broken Symmetry and the Mass of Gauge Vector Mesons. *Phys. Rev. Lett.*, 13:321–323, 1964.

[33] Emmy Noether. Invariant Variation Problems. *Gott. Nachr.*, 1918:235–257, 1918.

[34] Yoichiro Nambu. Quasiparticles and Gauge Invariance in the Theory of Superconductivity. *Phys. Rev.*, 117:648–663, 1960.

[35] J. Goldstone. Field Theories with Superconductor Solutions. *Nuovo Cim.*, 19:154–164, 1961.

[36] S. Navas et al. Review of particle physics. *Phys. Rev. D*, 110(3):030001, 2024.

[37] M. Luscher. Symmetry Breaking Aspects of the Roughening Transition in Gauge Theories. *Nucl. Phys. B*, 180:317–329, 1981.

[38] G. Veneziano. Construction of a crossing - symmetric, Regge behaved amplitude for linearly rising trajectories. *Nuovo Cim. A*, 57:190–197, 1968.

[39] J. Polchinski. *String theory. Vol. 1: An introduction to the bosonic string*. Cambridge Monographs on Mathematical Physics. Cambridge University Press, 12 2007.

[40] Michael B. Green, John H. Schwarz, and Edward Witten. *Superstring Theory Vol. 1: 25th Anniversary Edition*. Cambridge Monographs on Mathematical Physics. Cambridge University Press, 11 2012.

[41] K. Becker, M. Becker, and J. H. Schwarz. *String theory and M-theory: A modern introduction*. Cambridge University Press, 12 2006.

[42] P. Goddard and Charles B. Thorn. Compatibility of the Dual Pomeron with Unitarity and the Absence of Ghosts in the Dual Resonance Model. *Phys. Lett. B*, 40:235–238, 1972.

[43] M. A. Virasoro. Subsidiary conditions and ghosts in dual resonance models. *Phys. Rev. D*, 1:2933–2936, 1970.

[44] Pierre Ramond. Dual Theory for Free Fermions. *Phys. Rev. D*, 3:2415–2418, 1971.

[45] A. Neveu and J. H. Schwarz. Factorizable dual model of pions. *Nucl. Phys. B*, 31:86–112, 1971.

[46] A. Neveu and J. H. Schwarz. Quark Model of Dual Pions. *Phys. Rev. D*, 4:1109–1111, 1971.

[47] S. Mandelstam. Interacting String Picture of the Neveu-Schwarz-Ramond Model. *Nucl. Phys. B*, 69:77–106, 1974.

[48] F. Gliozzi, Joel Scherk, and David I. Olive. Supersymmetry, Supergravity Theories and the Dual Spinor Model. *Nucl. Phys. B*, 122:253–290, 1977.

[49] N. Seiberg and Edward Witten. Spin Structures in String Theory. *Nucl. Phys. B*, 276:272, 1986.

[50] Jack E. Paton and Hong-Mo Chan. Generalized veneziano model with isospin. *Nucl. Phys. B*, 10:516–520, 1969.

[51] Gary T. Horowitz and Andrew Strominger. Black strings and P-branes. *Nucl. Phys. B*, 360:197–209, 1991.

[52] Johanna Erdmenger, Nick Evans, Ingo Kirsch, and Ed Threlfall. Mesons in Gauge/Gravity Duals - A Review. *Eur. Phys. J. A*, 35:81–133, 2008.

[53] Mariana Grana and Joseph Polchinski. Gauge / gravity duals with holomorphic dilaton. *Phys. Rev. D*, 65:126005, 2002.

[54] M. Bertolini, P. Di Vecchia, M. Frau, A. Lerda, and R. Marotta. N=2 gauge theories on systems of fractional D3/D7 branes. *Nucl. Phys. B*, 621:157–178, 2002.

[55] Martin Kruczenski, David Mateos, Robert C. Myers, and David J. Winters. Meson spectroscopy in AdS / CFT with flavor. *JHEP*, 07:049, 2003.

[56] Martin Ammon and Johanna Erdmenger. *Gauge/gravity duality: Foundations and applications*. Cambridge University Press, Cambridge, 4 2015.

[57] Peter Breitenlohner and Daniel Z. Freedman. Stability in Gauged Extended Supergravity. *Annals Phys.*, 144:249, 1982.

[58] Andreas Karch and Emanuel Katz. Adding flavor to AdS / CFT. *JHEP*, 06:043, 2002.

[59] Neil R. Constable and Robert C. Myers. Exotic scalar states in the AdS / CFT correspondence. *JHEP*, 11:020, 1999.

[60] Timo Alho, Nick Evans, and Kimmo Tuominen. Dynamic AdS/QCD and the Spectrum of Walking Gauge Theories. *Phys. Rev. D*, 88:105016, 2013.

[61] Raul Alvares, Nick Evans, and Keun-Young Kim. Holography of the Conformal Window. *Phys. Rev. D*, 86:026008, 2012.

[62] Leandro Da Rold and Alex Pomarol. Chiral symmetry breaking from five dimensional spaces. *Nucl. Phys. B*, 721:79–97, 2005.

[63] Will Clemens and Nick Evans. A Holographic Study of the Gauged NJL Model. *Phys. Lett. B*, 771:1–4, 2017.

[64] Nick Evans and Kimmo Tuominen. Holographic modelling of a light technidilaton. *Phys. Rev. D*, 87(8):086003, 2013.

[65] Roman Zwicky. QCD with an infrared fixed point and a dilaton. *Phys. Rev. D*, 110(1):014048, 2024.

[66] Thomas Appelquist, John Terning, and L. C. R. Wijewardhana. The Zero temperature chiral phase transition in SU(N) gauge theories. *Phys. Rev. Lett.*, 77:1214–1217, 1996.

[67] Andrew G. Cohen and Howard Georgi. Walking Beyond the Rainbow. *Nucl. Phys. B*, 314:7–24, 1989.

[68] Matti Jarvinen and Elias Kiritsis. Holographic Models for QCD in the Veneziano Limit. *JHEP*, 03:002, 2012.

[69] David Kutasov, Jennifer Lin, and Andrei Parnachev. Conformal Phase Transitions at Weak and Strong Coupling. *Nucl. Phys. B*, 858:155–195, 2012.

[70] Anna Hasenfratz, Ethan T. Neil, Yigal Shamir, Benjamin Svetitsky, and Oliver Witzel. Infrared fixed point of the SU(3) gauge theory with Nf=10 flavors. *Phys. Rev. D*, 108(7):L071503, 2023.

[71] J. Babington, J. Erdmenger, Nick J. Evans, Z. Guralnik, and I. Kirsch. Chiral symmetry breaking and pions in nonsupersymmetric gauge / gravity duals. *Phys. Rev. D*, 69:066007, 2004.

[72] Tameem Albash, Veselin G. Filev, Clifford V. Johnson, and Arnab Kundu. Finite temperature large N gauge theory with quarks in an external magnetic field. *JHEP*, 07:080, 2008.

[73] Anna Hasenfratz, Yigal Shamir, and Benjamin Svetitsky. Taming lattice artifacts with Pauli-Villars fields. *Phys. Rev. D*, 104(7):074509, 2021.

[74] T. Appelquist et al. Lattice simulations with eight flavors of domain wall fermions in SU(3) gauge theory. *Phys. Rev. D*, 90(11):114502, 2014.

[75] T. Appelquist et al. Nonperturbative investigations of SU(3) gauge theory with eight dynamical flavors. *Phys. Rev. D*, 99(1):014509, 2019.

[76] Anna Hasenfratz, Claudio Rebbi, and Oliver Witzel. Gradient flow step-scaling function for SU(3) with Nf=8 fundamental flavors. *Phys. Rev. D*, 107(11):114508, 2023.

[77] Anna Hasenfratz. Emergent strongly coupled ultraviolet fixed point in four dimensions with eight Kähler-Dirac fermions. *Phys. Rev. D*, 106(1):014513, 2022.

[78] Nouman Butt, Simon Catterall, and Anna Hasenfratz. Symmetric Mass Generation with Four SU(2) Doublet Fermions. *Phys. Rev. Lett.*, 134(3):031602, 2025.

[79] Georg Bergner, Gernot Münster, and Stefano Piemonte. Exploring Gauge Theories with Adjoint Matter on the Lattice. *Universe*, 8(12):617, 2022.

[80] Zoltan Fodor, Kieran Holland, Julius Kuti, Santanu Mondal, Daniel Nogradi, and Chik Him Wong. The running coupling of the minimal sextet composite Higgs model. *JHEP*, 09:039, 2015.

[81] Venkitesh Ayyar, Thomas Degrand, Daniel C. Hackett, William I. Jay, Ethan T. Neil, Yigal Shamir, and Benjamin Svetitsky. Baryon spectrum of SU(4) composite Higgs theory with two distinct fermion representations. *Phys. Rev. D*, 97(11):114505, 2018.

[82] William J. Marciano. Exotic New Quarks and Dynamical Symmetry Breaking. *Phys. Rev. D*, 21:2425, 1980.

[83] Nick Evans and Konstantinos S. Rigatos. Chiral symmetry breaking and confinement: separating the scales. *Phys. Rev. D*, 103:094022, 2021.

[84] Johanna Erdmenger, Nick Evans, and Marc Scott. Meson spectra of asymptotically free gauge theories from holography. *Phys. Rev. D*, 91(8):085004, 2015.

[85] Alexander Belyaev, Azaria Coupe, Nick Evans, Daniel Locke, and Marc Scott. Any Room Left for Technicolor? Dilepton Searches at the LHC and Beyond. *Phys. Rev. D*, 99(9):095006, 2019.

[86] Johanna Erdmenger, Nick Evans, Werner Porod, and Konstantinos S. Rigatos. Gauge/-gravity dynamics for composite Higgs models and the top mass. *Phys. Rev. Lett.*, 126(7):071602, 2021.

[87] Johanna Erdmenger, Nick Evans, Werner Porod, and Konstantinos S. Rigatos. Gauge/-gravity dual dynamics for the strongly coupled sector of composite Higgs models. *JHEP*, 02:058, 2021.

[88] Johanna Erdmenger, Nick Evans, Yang Liu, and Werner Porod. Holography for Sp($2N_c$) gauge dynamics: from composite Higgs to technicolour. *JHEP*, 07:169, 2024.

[89] V. A. Miransky. Dynamics of Spontaneous Chiral Symmetry Breaking and Continuum Limit in Quantum Electrodynamics. *Nuovo Cim. A*, 90:149–170, 1985.

[90] Thomas W. Appelquist, Dimitra Karabali, and L. C. R. Wijewardhana. Chiral Hierarchies and the Flavor Changing Neutral Current Problem in Technicolor. *Phys. Rev. Lett.*, 57:957, 1986.

[91] Thomas A. Ryttov and Francesco Sannino. Supersymmetry inspired QCD beta function. *Phys. Rev. D*, 78:065001, 2008.

[92] Francesco Sannino. Conformal Windows of SP(2N) and SO(N) Gauge Theories. *Phys. Rev. D*, 79:096007, 2009.

[93] N. Seiberg and Edward Witten. Electric - magnetic duality, monopole condensation, and confinement in N=2 supersymmetric Yang-Mills theory. *Nucl. Phys. B*, 426:19–52, 1994. [Erratum: Nucl.Phys.B 430, 485–486 (1994)].

[94] Mithat Unsal. Magnetic bion condensation: A New mechanism of confinement and mass gap in four dimensions. *Phys. Rev. D*, 80:065001, 2009.

[95] Mithat Unsal. Abelian duality, confinement, and chiral symmetry breaking in QCD(adj). *Phys. Rev. Lett.*, 100:032005, 2008.

[96] Erich Poppitz. Notes on Confinement on R3 × S1: From Yang–Mills, Super-Yang–Mills, and QCD (adj) to QCD(F). *Symmetry*, 14(1):180, 2022.

[97] Jarno Rantaharju. Gradient Flow Coupling in the SU(2) gauge theory with two adjoint fermions. *Phys. Rev. D*, 93(9):094516, 2016.

[98] Andreas Athenodorou, Ed Bennett, Georg Bergner, Pietro Butti, Julian Lenz, and Biagio Lucini. SU(2) gauge theory with one and two adjoint fermions towards the continuum limit. 7 2024.

[99] Ed Bennett, Andreas Athenodorou, Georg Bergner, Pietro Butti, and Biagio Lucini. Towards the β function of SU(2) with adjoint matter using Pauli-Villars fields. *PoS*, LATTICE2024:432, 2025.

[100] G. Veneziano and S. Yankielowicz. An Effective Lagrangian for the Pure N=1 Supersymmetric Yang-Mills Theory. *Phys. Lett. B*, 113:231, 1982.

[101] K. Demmouche, F. Farchioni, A. Ferling, I. Montvay, G. Munster, E. E. Scholz, and J. Wuilloud. Simulation of 4d N=1 supersymmetric Yang-Mills theory with Symanzik improved gauge action and stout smearing. *Eur. Phys. J. C*, 69:147–157, 2010.

[102] Sajid Ali, Georg Bergner, Henning Gerber, Pietro Giudice, Istvan Montvay, Gernot Münster, Stefano Piemonte, and Philipp Scior. The light bound states of $\mathcal{N} = 1$ supersymmetric SU(3) Yang-Mills theory on the lattice. *JHEP*, 03:113, 2018.

[103] Sajid Ali, Georg Bergner, Henning Gerber, Istvan Montvay, Gernot Münster, Stefano Piemonte, and Philipp Scior. Numerical results for the lightest bound states in $\mathcal{N} = 1$ supersymmetric SU(3) Yang-Mills theory. *Phys. Rev. Lett.*, 122(22):221601, 2019.

[104] Marc Steinhauser, André Sternbeck, Björn Wellegehausen, and Andreas Wipf. $\mathcal{N} = 1$ Super-Yang-Mills theory on the lattice with twisted mass fermions. *JHEP*, 01:154, 2021.

[105] Georg Bergner and Stefano Piemonte. Lattice simulations of a gauge theory with mixed adjoint-fundamental matter. *Phys. Rev. D*, 103(1):014503, 2021. [Erratum: Phys.Rev.D 107, 019902 (2023)].

[106] Ki-Myeong Lee and Piljin Yi. Monopoles and instantons on partially compactified D-branes. *Phys. Rev. D*, 56:3711–3717, 1997.

[107] Thomas C. Kraan and Pierre van Baal. Periodic instantons with nontrivial holonomy. *Nucl. Phys. B*, 533:627–659, 1998.

[108] Yonit Hochberg, Eric Kuflik, Hitoshi Murayama, Tomer Volansky, and Jay G. Wacker. Model for Thermal Relic Dark Matter of Strongly Interacting Massive Particles. *Phys. Rev. Lett.*, 115(2):021301, 2015.

[109] Joachim Pomper and Suchita Kulkarni. Low energy effective theories of composite dark matter with real representations. 2 2024.

[110] Elias Bernreuther, Felix Kahlhoefer, Michael Krämer, and Patrick Tunney. Strongly interacting dark sectors in the early Universe and at the LHC through a simplified portal. *JHEP*, 01:162, 2020.

[111] Elias Bernreuther, Nicoline Hemme, Felix Kahlhoefer, and Suchita Kulkarni. Dark matter relic density in strongly interacting dark sectors with light vector mesons. *Phys. Rev. D*, 110(3):035009, 2024.

[112] Soo-Min Choi, Hyun Min Lee, Pyungwon Ko, and Alexander Natale. Resolving phenomenological problems with strongly-interacting-massive-particle models with dark vector resonances. *Phys. Rev. D*, 98(1):015034, 2018.

[113] Thomas Appelquist, James Ingoldby, and Maurizio Piai. Dilaton Forbidden Dark Matter. 4 2024.

[114] Luigi Del Debbio and Roman Zwicky. Dilaton and massive hadrons in a conformal phase. *JHEP*, 08:007, 2022.

[115] Roldao da Rocha. Dark SU(N) glueball stars on fluid branes. *Phys. Rev. D*, 95(12):124017, 2017.

[116] Pierluca Carenza, Roman Pasechnik, Gustavo Salinas, and Zhi-Wei Wang. Glueball Dark Matter Revisited. *Phys. Rev. Lett.*, 129(26):261302, 2022.

[117] Pierluca Carenza, Tassia Ferreira, Roman Pasechnik, and Zhi-Wei Wang. Glueball dark matter. *Phys. Rev. D*, 108(12):123027, 2023.

[118] Austin Batz, Timothy Cohen, David Curtin, Caleb Gemmell, and Graham D. Kribs. Dark sector glueballs at the LHC. *JHEP*, 04:070, 2024.

[119] David McKeen, Riku Mizuta, David E. Morrissey, and Michael Shamma. Dark matter from dark glueball dominance. *Phys. Rev. D*, 111(1):015044, 2025.

[120] Amarjit Soni and Yue Zhang. Hidden SU(N) Glueball Dark Matter. *Phys. Rev. D*, 93(11):115025, 2016.

[121] James M. Cline. Dark atoms and composite dark matter. *SciPost Phys. Lect. Notes*, 52:1, 2022.

[122] Graham D. Kribs and Ethan T. Neil. Review of strongly-coupled composite dark matter models and lattice simulations. *Int. J. Mod. Phys. A*, 31(22):1643004, 2016.

[123] Howard Georgi. Unparticle physics. *Phys. Rev. Lett.*, 98:221601, 2007.

[124] Tatsuru Kikuchi and Nobuchika Okada. Unparticle Dark Matter. *Phys. Lett. B*, 665:186–189, 2008.

[125] Florian Goertz, Álvaro Pastor-Gutiérrez, and Jan M. Pawlowski. Gauge-Fermion Cartography: from confinement and chiral symmetry breaking to conformality. 12 2024.

[126] Gunnar S. Bali, Francis Bursa, Luca Castagnini, Sara Collins, Luigi Del Debbio, Biagio Lucini, and Marco Panero. Mesons in large-N QCD. *JHEP*, 06:071, 2013.

[127] Gunnar S. Bali and Francis Bursa. Mesons at large N(c) from lattice QCD. *JHEP*, 09:110, 2008.

[128] Luigi Del Debbio, Biagio Lucini, Agostino Patella, and Claudio Pica. Quenched mesonic spectrum at large N. *JHEP*, 03:062, 2008.

[129] Thomas DeGrand and Ethan T. Neil. Repurposing lattice QCD results for composite phenomenology. *Phys. Rev. D*, 101(3):034504, 2020.

[130] Guillaume Albouy et al. Theory, phenomenology, and experimental avenues for dark showers: a Snowmass 2021 report. *Eur. Phys. J. C*, 82(12):1132, 2022.

[131] Christian S. Fischer. Infrared properties of QCD from Dyson-Schwinger equations. *J. Phys. G*, 32:R253–R291, 2006.

[132] Bob Holdom. Raising the Sideways Scale. *Phys. Rev. D*, 24:1441, 1981.

[133] David Wittman, Nathan Golovich, and William A. Dawson. The Mismeasure of Mergers: Revised Limits on Self-interacting Dark Matter in Merging Galaxy Clusters. *Astrophys. J.*, 869(2):104, 2018.

[134] Scott W. Randall, Maxim Markevitch, Douglas Clowe, Anthony H. Gonzalez, and Marusa Bradac. Constraints on the Self-Interaction Cross-Section of Dark Matter from Numerical Simulations of the Merging Galaxy Cluster 1E 0657-56. *Astrophys. J.*, 679:1173–1180, 2008.

[135] Andrew Robertson, Richard Massey, and Vincent Eke. What does the Bullet Cluster tell us about self-interacting dark matter? *Mon. Not. Roy. Astron. Soc.*, 465(1):569–587, 2017.

[136] Martin Hansen, Kasper Langæble, and Francesco Sannino. SIMP model at NNLO in chiral perturbation theory. *Phys. Rev. D*, 92(7):075036, 2015.

[137] Pieter Braat and Marieke Postma. SIMPly add a dark photon. *JHEP*, 03:216, 2023.

[138] Xiaoyong Chu, Marco Nikolic, and Josef Pradler. Even SIMP miracles are possible. 1 2024.

[139] Stephon Alexander, Humberto Gilmer, Tucker Manton, and Evan McDonough. π-axion and π-axiverse of dark QCD. *Phys. Rev. D*, 108(12):123014, 2023.

[140] Sungwoo Hong, Gowri Kurup, and Maxim Perelstein. Conformal Freeze-In of Dark Matter. *Phys. Rev. D*, 101(9):095037, 2020.

[141] Sungwoo Hong, Gowri Kurup, and Maxim Perelstein. Dark matter from a conformal Dark Sector. *JHEP*, 02:221, 2023.

[142] Y. M. Cho and J. H. Kim. Dilatonic dark matter and its experimental detection. *Phys. Rev. D*, 79:023504, 2009.

[143] Y. M. Cho and Y. Y. Keum. Dilatonic dark matter: A new paradigm. *Mod. Phys. Lett. A*, 13:109–117, 1998.

[144] Dan Kondo, Robert McGehee, Tom Melia, and Hitoshi Murayama. Linear sigma dark matter. *JHEP*, 09:041, 2022.

[145] F. Farchioni, I. Montvay, G. Munster, E. E. Scholz, T. Sudmann, and J. Wuilloud. Hadron masses in QCD with one quark flavour. *Eur. Phys. J. C*, 52:305–314, 2007.

[146] J. M. Butterworth, L. Corpe, X. Kong, S. Kulkarni, and M. Thomas. New sensitivity of LHC measurements to composite dark matter models. *Phys. Rev. D*, 105(1):015008, 2022.

[147] R. Sekhar Chivukula, H. Georgi, and Lisa Randall. A Composite Technicolor Standard Model of Quarks. *Nucl. Phys. B*, 292:93–108, 1987.

[148] Yifei He and Martin Kruczenski. The Gauge Theory Bootstrap: Predicting pion dynamics from QCD. 5 2025.